



Well Testing and Power Plant Scenario Analysis for Hverahlid Geothermal Field

Mesay Fekadu Biru



Faculty of Industrial Engineering, Mechanical
Engineering and Computer science
University of Iceland
2020

Well Testing and Power Plant Scenario Analysis for Hverahlid Geothermal Field

Mesay Fekadu Biru

60 ECTS thesis submitted in partial fulfillment of a
Magister Scientiarum

MS Committee
Benedikt Steingrímsson
Halldór Pálsson
Magnús Þór Jónsson

Master's Examiner
Guðni Axelsson

Faculty of Industrial Engineering, Mechanical Engineering and Computer
Science
School of Engineering and Natural Sciences
University of Iceland
Reykjavik, 2020

Well Testing and Power Plant Scenario Analysis for Hverahlid Geothermal Field
60 ECTS thesis submitted in partial fulfilment of a *Magister Scientiarum* degree in
Mechanical Engineering

Copyright © 2020 Mesay Fekadu Biru
All rights reserved

Faculty of Industrial Engineering, Mechanical Engineering and Computer Science
School of Engineering and Natural Sciences
University of Iceland
Sæmundargötu 2
101 Reykjavik
Iceland

Telephone: 525 4000

Bibliographic information:

Biru, 2020, *Well Testing and Power Plant Scenario Analysis For Hverahlid Geothermal Field*, Master's thesis, Faculty of Industrial Engineering, Mechanical Engineering and Computer Science, University of Iceland

Printing: Háskólaprent ehf
Reykjavik, Iceland, May 2020

Abstract

In this thesis, different methods for analyzing well test data to estimate capacity of a geothermal field are evaluated, using the Hverahlid geothermal field in the Hengill geothermal system, SW-Iceland as a case study. The thesis includes analysis of data from step-rate injection tests, temperature and pressure analysis, discharge test analysis and different power plant scenario analysis. The power plant scenario analysis was conducted to determine the optimum electric power output and choose the most efficient energy conversion technology.

The computer software WellTester is used for the analysis of step-rate injection tests and the results are compared with results from other high temperature geothermal fields. Temperature and pressure profiles are analysed for each well to estimate the formation temperature and initial reservoir pressure. Total mass flow rate (kg/s), enthalpy (kJ/kg) and flow characteristics are calculated using the lip pressure method. The Engineering Equation Solver (EES) was used for modelling.

The estimated values of transmissivity (T) for wells HE-36, HE-53 and HE-61 ranges from $4.2 \cdot 10^{-8}$ to $7.2 \cdot 10^{-7}$ m³/Pa*s, from the injection test, whereas the storage coefficient values (S) range from $2.3 \cdot 10^{-8}$ to $4.3 \cdot 10^{-7}$ m/Pa. The estimated values for the skin factor are negative indicating that the wells are well stimulated and in good connection with the surrounding reservoir.

The evaluation of temperature for wells HE-36, HE-53 and HE-61 suggests that reservoir temperature is in the range of 270-320°C and reservoir pressure 132 bar at 1750 m (HE-36), 118 bar at 1500 m (HE-53) and 85 bar at 1140 m for HE-21 respectively. The evaluated fluid enthalpy for wells HE-21, HE-36 and HE-53 is in the range of 1352 to 1683 kJ/kg, with the steam flow ranging from 6 to 29 kg/s with an assumed separation pressure of 17 bar-g.

Three power plant scenarios for Hverahlid are studied. Scenario 1 is a single flash power plant. The power output of the four wells involved is 49.0 MW_e. Scenario 2 is a double flash power plant, which generates about 53.5 MW_e. Scenario 3 is single flash with bottoming binary plant. The binary working fluid is isopentane. The power generation for scenario 3 is about 57.0 MW_e.

Útdráttur

Í þessari mastersritgerð eru metnar mismunandi úrvinnsluáðferðir á gögnum úr borholum til að áætla afkastagetu jarðhitasvæða. Ritgerðin felur í sér greiningu og úrvinnslu á gögnum úr þrepaprófunum, hita- og þrýstimælingum og afkastaprófunum á borholum á jarðhitasvæðinu við Hverahlíð sem er hluti af Hengilssvæðinu. Einnig eru mismunandi sviðsmyndir varðandi nýtingu svæðisins til raforkuframleiðslu skoðaðar. Þrjár sviðsmyndirnar eru valdar í þeim tilgangi að ákvarða hámarks vinnslugetu og velja hagkvæmustu virkjunartilhögun. Þær eru skoðaðar og er þróað varmafræðilegt líkan af hverri vinnslurás og hámarksvinnsla þeirra metin.

Tölvuhugbúnaður, sem heitir WellTester, er notaður til úrvinnslu á gögnum úr þrepaprófum á holunum í lok borunar og niðurstöður bornar saman við niðurstöður þrepaprófana á borholum á öðrum háhitasvæðum. Unnið er úr tiltækum hita- og þrýstimælingum úr borholunum til að áætla berghita og upphafsþrýsting jarðhitakerfisins. Heildarmassastreymi (kg/s) og vermi (kJ/kg) vökvans úr borholunum og rennsliseiginleikar borholanna eru metnir og áætlaðir með aðferð Russel-James.

Áætluð vatnsleiðni (transmissivity, T) fyrir Hverahlíðarholurnar er samkvæmt þrepaprófunum á bilinu $4,2 \cdot 10^{-8}$ til $7,2 \cdot 10^{-7}$ m³/Pa*s, geymslustuðlar (rýmdarstuðull, storage coefficient, S) eru á bilinu $2,3 \cdot 10^{-8}$ til $4,26 \cdot 10^{-7}$ m/Pa. Neikvæður skinn-stuðull (skin) fæst fyrir allar holurnar sem bendir til þess að þær séu í góðu sambandi við jarðhitakerfið umhverfis þær.

Mat á berghita við holur HE-36, HE-53 og HE-61 bendir til þess að hiti í jarðhitakerfinu sé á bilinu 270-320°C og þrýstingur á bilinu 85-135 bar. Mælt vermi vökvans frá holum HE-21, HE-36 og HE-53 er á bilinu 1352 til 1683 kJ/kg og gufustreymi er á bilinu 6-29 kg/s miðað við áætlaðan 17 bar skiljuþrýsting.

Áætlað rafafl fyrir þrjár sviðmyndir er 49,5 MW_e fyrir sviðsmynd 1, sem er einföld eins þreps eimsvalavél. Fyrir sviðsmynd 2, tveggja þrepa eimsvalavél, fæst 53,5 MW_e en fyrir sviðsmynd 3, sem er eins þrepsvél að viðbætti lágþrýstri tvenndarvél (binary) fæst aflið 57,0 MW_e. Gert var ráð fyrir að vinnuvökvinn í tvenndarvélinni sé ísópentan.

Dedication

This thesis is dedicated to my wife Sefiya Medaso, my loving daughter Sena and my son Natoli for their patient during my absence.

Table of Contents

List of Figures	ix
List of Tables.....	xii
Abbreviations.....	xiv
Acknowledgements	xvii
1 Introduction.....	19
2 The Hengill Geothermal System.....	21
2.1 Geological and Tectonic setting.....	21
2.2 Geophysical Surveys	22
2.3 Geothermal Activity	24
2.4 Geothermal Power Plants in the Hengill Area	25
2.4.1 Nesjavellir power plant.....	25
2.4.2 Hellisheidi power plant.....	26
2.4.3 Planned power plant at Bitra.....	27
2.4.4 Power plant at Hverahlid	27
3 Basics of Injection Well Testing	27
3.1 The pressure diffusion equation	28
3.2 Dimensionless Variables	31
3.2.1 Semi-logarithmic well test analysis	32
3.3 Well test analysis and Interpretation	35
3.3.1 Injection Testing of Well HE-36.....	37
3.3.2 Injection Testing of Well HE-53.....	40
3.3.3 Injection Testing of Well HE-61.....	44
4 Temperature and Pressure	48
4.1 Analysis of T and P logs in well HE-36.....	50
Formation temperature of HE-36 and reservoir pressure in 2008	53
4.2 Analysis of T and P logs in well HE-53.....	54
Formation temperature of HE-53 and reservoir pressure in 2009	56
4.3 Analysis of T and P logs in well HE-61	58
Formation temperature of HE-61 and reservoir pressure in 2018	59
5 Analysis of Discharge Testing.....	60
5.1 James lip pressure method.....	61
5.2 Discharge Testing at Hverahlid.....	62
5.3 Discharge testing of well HE-21	63
5.4 Discharge testing of well HE-36	66
5.5 Discharge testing of well HE-53	68
5.6 Summary of selected discharge measurements	71

6 Power plants scenarios	74
6.1 Single flash power plant.....	74
6.2 Double flash power plant	78
6.3 Binary cycle power plant	80
6.4 Result and discussion for the scenarios.....	83
6.4.1 Wellhead pressure.....	84
6.4.2 Assumptions	85
6.4.3 Scenario 1: Single flash power plant	85
6.4.4 Scenario 2: Double flash power plant.....	89
6.4.5 Scenario 3: Single flash with bottoming ORC plant	91
7 Discussion and Conclusions	96
References	99
Appendix A	103

List of Figures

FIGURE 1. <i>A simplified geological and geothermal map of Iceland (white areas are glaciers) (Franzson et al., 2005).</i>	21
FIGURE 2. <i>Resistivity in the Hengill area at 0.8, 1.2, 4.5 and 6.5 km b.s.l. according to joint 1D inversion of TEM and determinant MT data. Red dots indicate geothermal surface manifestations, black dots MT soundings, thick black lines resistivity contour lines, and thin black lines topographic contour lines in m a.s.l. Distances are given in km (Arnason et al., 2010).</i>	23
FIGURE 3. <i>Measured aquifer temperatures and isolines of CO₂ gas geo-thermometers in the Hengill area (modified from Ivarsson, 1998). Geothermal surface manifestations are shown as red dots. Number of wells and average temperature in wells for the five known main subfields is shown.</i>	24
FIGURE 4. <i>Map of the Hengill area showing existing and potential geothermal power plants. Red ellipse shows the study area (VSO, 2007).</i>	25
FIGURE 5. <i>Essence of well testing and the associated pressure response.</i>	28
FIGURE 6. <i>Match between collected data and model response during pressure transient analysis (Horne, 1995).</i>	28
FIGURE 7. <i>Radial flow of a single-phase fluid in the vicinity of producing well (Haraldsdóttir, 2016).</i>	29
FIGURE 8. <i>Radial pressure profile for a normal, stimulated or damaged well (modified from Horne, 1995).</i>	34
FIGURE 9. <i>The geothermal field at Hverahlid. Well locations are shown as black dots and tracks of directional wells as red lines. Active fumaroles are in the red area but thermally altered areas are yellow. Roads in the area are black lines. The elevation lines in the background show the landscape (Tryggvason et al., 2018).</i>	38
FIGURE 10. <i>HE-36 pressure response against time in the two injection steps with at total duration of 3 hours.</i>	38
FIGURE 11. <i>Model results and recorded pressure for step 2 using a linear scale (to the left) and log-log scale (to the right).</i>	40
FIGURE 12. <i>HE-53 pressure response at 2000 m against time during three injection steps with at total duration of 7 hours.</i>	41
FIGURE 13. <i>Model results and recorded pressure for step 1 using a linear scale (to the left) and log-log scale (to the right) for well HE-53.</i>	43
FIGURE 14. <i>HE-61 pressure response against time in two injection steps with at total duration of 4 hours 15-16th (above) and 5 hours on 18th April (below).</i>	47

<i>FIGURE 15. Model results and recorded pressure for step 2 for well HE-61 using a linear scale (to the left) and log-log scales (to the right) for the 18th April 2018 injection test.</i>	48
<i>FIGURE 16. Well HE-36. Temperature logs during injection, heat-up, After a period of production</i>	52
<i>FIGURE 17. Well HE-36. Pressure logs during heat-up, after a period of production.</i>	53
<i>FIGURE 18. Estimated formation temperature and initial (2007/8) reservoir pressure for HE-36 and selected T&P logs.</i>	54
<i>FIGURE 19. Well HE-53. Temperature logs during injection, heat-up, after a period of production.</i>	55
<i>FIGURE 20. Well HE-53. Pressure logs during injection, heat-up, after a period of production.</i>	56
<i>FIGURE 21. Estimated formation temperature and initial (2009) reservoir pressure for HE-53 and selected T&P logs.</i>	57
<i>FIGURE 22. Well HE-61. Temperature logs during injection and heat-up. BPD-curve for reference.</i>	58
<i>FIGURE 23. Well HE-61. Pressure logs during injection and heat-up.....</i>	59
<i>FIGURE 24 Estimated formation temperature and initial (2018) reservoir pressure for HE-61 and selected T&P logs</i>	60
<i>FIGURE 25. Schematic representation of the Russel-James lip pressure method.</i>	61
<i>FIGURE 26. Summary of wellhead pressure (WHP), critical lip pressure and water height in the weir box during the discharge testing of well HE-21 in 2013-2014.</i>	64
<i>FIGURE 27. Summary of enthalpy and flowrates during the discharge testing of well HE-21 in 2013-2014.</i>	65
<i>FIGURE 28. Summary of wellhead pressure (WHP), critical lip pressure and water height in the weir box during the discharge testing of well HE-36 in 2014.</i>	66
<i>FIGURE 29. Summary of enthalpy and flowrates during the discharge testing of well HE-36 in 2014.</i>	67
<i>FIGURE 30. Summary of wellhead pressure (WHP) pressure, critical lip pressure and water height in the weir box during the discharge testing of well HE-53 in 2014.</i>	69
<i>FIGURE 31. Summary of enthalpy and flowrates during the discharge testing of well HE-53 in 2014.</i>	70

<i>FIGURE 32. Comparison of the enthalpy of wells HE-21, 36 and 53 at Hverahlid at different WHP during the flow test in 2013-2014.</i>	72
<i>FIGURE 33. Comparison of the output curves (total flow steam+water) for wells HE-21, HE-36 and HE-53 at Hverahlid at different WHP during the flow test in 2013-2014.</i>	72
<i>FIGURE 34. Comparison of steam flow at 17 bar-g separation pressure from wells HE-21, HE-36 and HE-53 at Hverahlid at different WHP during the flow test in 2013-2014.</i>	73
<i>FIGURE 35. Comparison of water flow at 17 bar-g separation pressure from wells HE-21, HE-36 and HE-53 at Hverahlid at different WHP during the flow test in 2013-2014.</i>	73
<i>FIGURE 36. Process flow diagram (PFD) of single flash power plant.</i>	75
<i>FIGURE 37. Temperature-entropy (T-s) diagram for single flash energy conversion system.</i>	76
<i>FIGURE 38. Double flash energy conversion system.</i>	78
<i>FIGURE 39. T-s diagram for double flash cycle.</i>	80
<i>FIGURE 40. Flow diagram for ORC cycle.</i>	81
<i>FIGURE 41. Production curves of wells in Hverahlid and can also be seen in Figures 32-35.</i>	84
<i>FIGURE 42. Modelled power plant output and steam quality vs. separator pressure</i>	86
<i>FIGURE 43. Scenario I specific power output vs. separator pressure.</i>	87
<i>FIGURE 44. Plant return temperature vs. separator pressure.</i>	88
<i>FIGURE 45. Scenario I plant PFD at baseline condition.</i>	88
<i>FIGURE 46. Optimized power output and steam quality for a low pressure steam turbine.</i>	89
<i>FIGURE 47. Specific output of the low-pressure steam turbine.</i>	90
<i>FIGURE 48. PFD result for the double flash power plant.</i>	91
<i>FIGURE 49. PFD results for single flash with ORC bottoming binary plant.</i>	92
<i>FIGURE 50. Total power output as function of plant return temperature.</i>	93
<i>FIGURE 51. Total power as function of vaporizer pressure.</i>	94
<i>FIGURE 52. Total, binary and steam power output as a function of separator pressure.</i>	95

List of Tables

<i>Table 1. Well HE-36. Drilled depths, casing depths with respect to ground surface, and casing information.</i>	37
<i>Table 2. Well HE-36. Analyses of the injection test data regarding injectivity.</i>	38
<i>Table 3. Initial parameters used in the well test analysis of HE-36 where those marked with * must be inserted by the user to get a meaningful output from the WellTester.</i>	39
<i>Table 4. Model selected for injection test analysis for well HE-36.</i>	39
<i>Table 5. Reservoir and well parameters obtained using nonlinear regression model for injection data from well HE-36,</i>	39
<i>Table 6. Depths and casing depths in well HE-53 with respect to ground surface and casing information's.</i>	40
<i>Table 7. Well HE-53. Analysis of the HE-53 injection test data regarding injectivity.</i>	41
<i>Table 8. Initial parameters used in the well test analysis of HE-53 where those marked with * must be inserted by the user to get a meaningful output from the WellTester.</i>	42
<i>Table 9. Model selected for injection test analysis for well HE-53</i>	42
<i>Table 10. Reservoir parameters obtained using nonlinear regression model for well HE-53,</i>	43
<i>Table 11. Depths and casing depths in well HE-61 with respect to ground surface and casing information's.</i>	44
<i>Table 12. The injectivity indices calculated from the pressure changes during the injection tests in April 2018 in well HE-61.</i>	45
<i>Table 13. Initial parameters used in the well test analysis of HE-61 where those marked with * must be inserted by the user to get a meaningful output from the WellTester.</i>	45
<i>Table 14. Model selected for injection tests in wells HE-61</i>	46
<i>Table 15. Summary of reservoir parameters estimated using nonlinear regression model for well HE-61 for the injection test on 15-16 April and 18 April 2018.</i>	47
<i>Table 16 Summary of production tests of the Hverahlid wells in 2013-2014.</i>	63
<i>Table 17. Measured and calculated values for well HE-21 by the James lip pressure method assuming a separation pressure of 17 bar-g.</i>	65

<i>Table 18. Measured and calculated values for well HE-36 by the James lip pressure method with separation pressure of 17 bar-g</i>	67
<i>Table 19. Measured and calculated values for well HE-53 by the James lip pressure method with separation pressure of atmospheric pressure</i>	70
Table 20. Input Data from wells.....	83
Table 21. Optimization variables and limitations for each power cycle.	84
<i>Table 22. The main characteristics of working fluids. Water is referred to for comparison</i>	93
<i>Table 23. Power output for different fluids</i>	94
<i>Table 24 Comparison of the scenarios</i>	95
Table 25. Well HE-21.....	103
<i>Table 26 Well HE-36</i>	104
<i>Table 27 Well HE-53</i>	105

Abbreviations

A = Cross-section area of the lip (cm^2);

A = total heat transfer area (m^2)

C = Wellbore storage (m^3/Pa);

C = Compressibility (Pa^{-1});

E = Heat energy (kJ);

g = Gravity (m/s^2);

H = Fluid enthalpy (kJ/kg);

h = Thickness (m);

II = Injectivity index ((L/s)/bar);

k = Intrinsic permeability (m^2)

LMTD = logarithmic mean temperature difference ($^{\circ}\text{C}$)

m = Slope of semi logarithmic straight line;

m_{wof} = Mass flow rate of the working fluid

p = Pressure (bar-g);

P_c = Lip pressure (bar-a);

p_D = Dimensionless Pressure;

p_e = Pressure at outer boundary(bar-a);

q = Volumetric flow rate (m^3/s);

q = Production or injection flow rate (kg/s)

r = Radial distance (m);

r_D = Dimensionless radius;

r_e = radius of investigation (m);

r_w = Wellbore radius (m);

S = Storage coefficient (m/Pa);

s = Skin factor;

T = Temperature ($^{\circ}\text{C}$);

T = Transmissivity ($\text{m}^3/\text{Pa s}$);

t = Time (s);

t_D = Dimensionless time based on well bore radius;

T_{pinch} = heat exchanger pinch temperature difference

U = is the overall heat transfer coefficient ($\text{W}/\text{m}^2\cdot^{\circ}\text{C}$)

V = Volume (m^3);

W = Water level (m);

x = Steam mass fraction ratio;

ϕ = Porosity;

μ = Dynamic viscosity ($\text{Pa}\cdot\text{s}$);

ρ = Fluid density (kg/m^3);

η = efficiency (%).

Δp = Pressure drop [bar]

ΔT = Temperature difference [$^{\circ}\text{C}$]

h = Enthalpy [kJ/kg]

M = Molar mass [g/mol]

m = Mass flow [kg/s]

s = Entropy [$\text{J kg}^{-1} \text{ }^{\circ}\text{C}^{-1}$]

U = Overall heat transfer coefficient [$\text{W}/\text{m}^2 \text{ K}$]

W_t = Work produced by the turbine (J)

W_g = Gross mechanical power (W)

W_e = Gross electrical power (MW)

P_v = Partial pressure of water vapour in the air (bar)

P_s = Partial pressure of water vapour that would saturate the air at its temperature (bar)

M_a = Molar mass of dry air (g/mol)

M_v = Molar mass of water (g/mol)

Subscripts

s = Steam

t = Total

w = Water

Acknowledgements

I want to express my deepest gratitude to the United Nations University Geothermal Training Programme (UNU GTP), later GRÓ Geothermal Training Programme (GRÓ GTP), and the Government of Iceland for the financial support for my studies and the Ethiopian Electric Power (EEP) for granting me study leave to pursue this MSc study. I want to thank Mr. Ludvik S. Georgsson, former director of the UNU GTP, Mr. Gudni Axelsson, the present director, Mr. Ingimar G. Haraldsson, Ms. Thorhildur Isberg, Ms. Vigdís Hardardóttir, Mr. Markus A.G. Wilde and Malfrídur Omarsdóttir. I also want to thank Reykjavík Energy for allowing publication of the data from the Hverahlid field used in this study.

My special thanks goes to my supervisors, Benedikt Steingrímsson, Magnús Þór Jónsson and Halldór Pálsson for sharing their great knowledge and experience, as well as for their patience and support during this project. I would also like to thank Mr. Kjartan Marteinnsson for his support and guidance in using software developed at ISOR. I want to thank geothermal projects manager of EEP Mr. Fikiru for supporting my MSc applications.

Finally, I would like to thank my family for their patience and support during my stay in Iceland.

1 Introduction

Geothermal resources are distributed throughout the world and can be found in most countries, even though most geothermal energy systems and the greatest concentration of geothermal energy are related to the Earth's plate boundaries. It is extremely focused in volcanic regions, but can also be found as groundwater in sedimentary formations in low-temperature regions.

Geothermal well tests play important role in geothermal research and development and for better understanding of geothermal systems. Geothermal wells allow access deep into the geothermal systems which enables different kinds of direct testing and measurements of conditions at depth. Through well testing and consequent pressure transient analysis the main reservoir parameters, such as injectivity index, transmissivity, storage coefficient and skin-factor, can be estimated along with reservoir boundary conditions, if a test is sufficiently long lasting. Such parameter estimates consequently provide key information for conceptual model development. Pressure transient analysis are carried out on the basis of the well-known Theis model, which involve model simulation of the pressure transient data collected (Axelsson, 2012). Normally well tests range from short step injection or discharge tests, pressure build-up and interference tests to long-term tests, sometimes involving several wells. Downhole tools allow measurements of temperature and pressure in the wells at different depths to estimate the formation temperature and the initial reservoir pressure during stages of drilling, injection, and warm-up and during discharge testing.

During the heat-up period after drilling, the water level in the well will gradually rise and eventually build a wellhead pressure above atmospheric pressure if the well is artesian. When the pressure at wellhead develops, a discharge test can be conducted by flowing the well through an orifice (Bödvarsson and Witherspoon, 1989). The lip pressure method (James, 1970) or Russel James method can be used to determine the total flow rate and enthalpy with a simple weir being used to measure water flow. Repeating the flow test with different sized orifices, the well productivity curve can be determined. These are called characteristic curves used for selecting operating conditions for the turbines in the power plant design (Bödvarsson and Witherspoon, 1989). Discharge testing is used to determine the flow characteristics and production capacity of wells.

To compare methods that increase power generation by utilizing the geothermal fluid, three different utilization methods are investigated in this study by constructing thermodynamic models of different power cycles and optimizing the specific net power output for each cycle. The specific net power outputs of the different cycles are compared along with the overall efficiency of the cycles.

This study uses the Hverahlid geothermal system in the Hengill volcanic region in SW-Iceland as a case study, with the objectives being:

- To analyse injection data from the injection testing period to estimate reservoir parameters such as transmissivity, storage coefficient, skin effect and injectivity index (II) that characterize the wells in question and reservoir.

- To analyse and interpret the temperature and pressure conditions of selected, representative wells, which help in understanding the overall reservoir conditions of the system.
- To locate the main feed zones (aquifers) that connect the wells to the geothermal system, mainly from the injection temperature logs.
- To estimate formation temperature and initial reservoir pressure of each of the selected wells.
- To analyse discharge data of the selected wells at Hverahlid geothermal field to estimate their production capacity.
- Three different utilization methods are investigated by constructing a thermodynamic model of different power cycles and optimizing the specific net power output for each cycle.

2 The Hengill Geothermal System

2.1 Geological and Tectonic setting

The Hengill volcanic complex is located within the southern end of the western volcanic zone (WVZ) of Iceland (Figure 1) and located about 30 km east from the capital city. It has an area of about 110 km². It is located at the junction of the WVZ, the Reykjanes Peninsula (RP), which is the landward extension of the Reykjanes spreading ridge, and the South Icelandic Seismic Zone (SISZ), which is transferring part of the crustal spreading from the WVZ to the eastern volcanic zone (Hersir et al., 2009) (Figure 1). The Hengill volcanic complex area is built up of volcanic rocks of late Quaternary and postglacial ages. The major rock formations are hyaloclastite (tuffs, breccias and pillow lava) formed sub-glacially. Basalt lavas from interglacial and Holocene periods occupy the lowlands but less in the volcanic centres. Some primitive rocks like picrites, intermediate rocks and rhyolites can be found in the Hengill area, the latter two are found as intrusives.

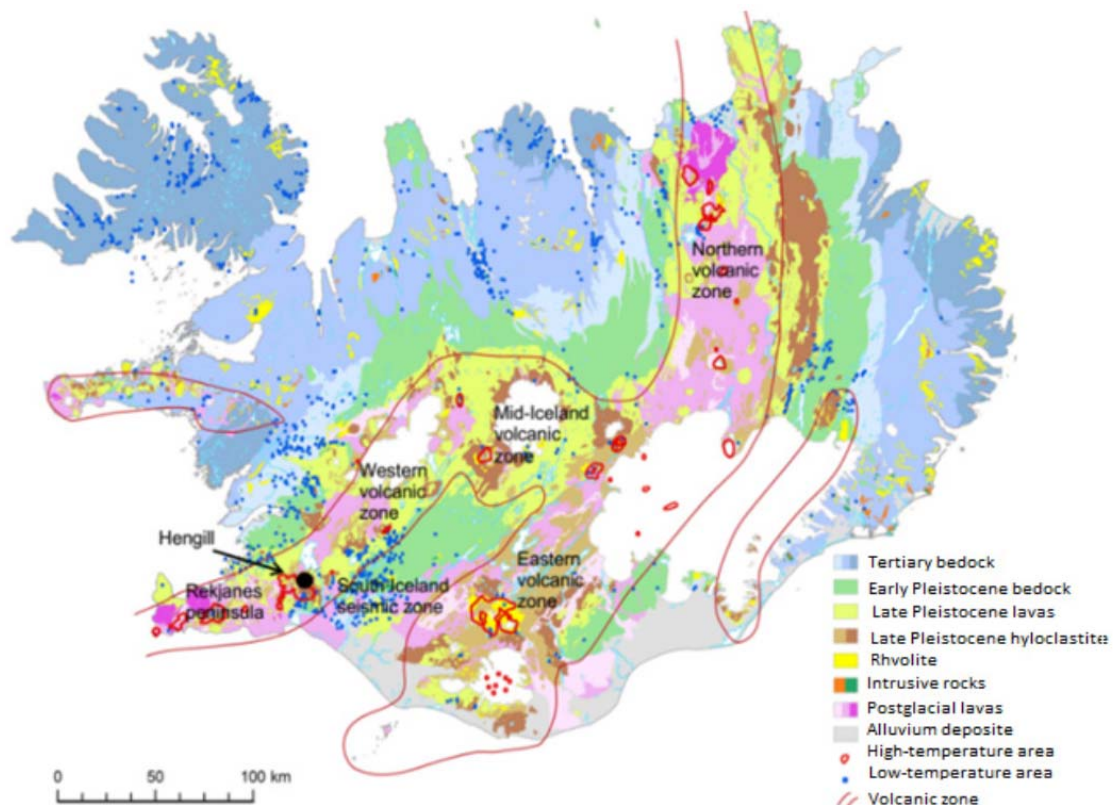


FIGURE 1. A simplified geological and geothermal map of Iceland (white areas are glaciers) (Franzson et al., 2005).

The bottom of the Hengill volcano is believed to be lava flows from the nearby Hveragerdi extinct volcano. Dating of thick lava around 900 m b.s.l suggests the age of the Hengill

volcano could be around 0.4 m.y. (Franzson et al., 2005; Helgadóttir et al, 2010). Volcanism was very intensive during the glacial period, particularly in the central Hengill and Hellisheidi area. For this reason, thick hyaloclastite formations were accumulated which were then intercalated by interglacial lava deposits (Franzson et al., 2005). The last eruptions took place after the glaciation period. Three different fissure eruptions have been identified in the Hengill area within 9, 5, and 2 thousand years (Saemundsson, 1995a; Franzson et al., 2005). The three eruptions are directly associated with 3-5 km wide and 40 km long vertical faults and fissure swarms.

2.2 Geophysical Surveys

The geophysical surveying of the Hverahlid field was part of the exploration of the Hengill geothermal system. TEM and MT resistivity surveys are presented in Arnason et al. (2010). The resistivity structure of the Hengill geothermal system at 800, 1200, 4500 and 6500 m b.s.l is presented in Figure 2. A joint inversion of TEM and MT data from 148 stations in the Hengill area shows a resistivity structure consisting of a shallow low-resistivity layer, in about the uppermost 2 km, underlain by high resistivity. At a greater depth, a second low resistivity layer occurs in most of the area, underlain by higher resistivity. The depth varies over the study area with the shallowest depth at about 3 km under and around Mount Hengill. By comparing the results from DC and TEM soundings and borehole data, the nature of the upper low resistivity layer shows a conductive hydrothermal alteration mineral formed at temperatures between 100 and 240°C. The nature of the deep conductivity layers is not clear but the reason for its high conductivity could be due to magmatic brines trapped in ductile intrusive rocks.

The 3D inversion shows deep low resistivity layer in most of the survey area. A low-resistivity anomaly, oriented NW-SE through Mount Hengill and southeast of it is also seen. The anomaly is 3.5 km wide and extends from 3-9 km depth. More to the southwest, another NW-SE oriented zone of low resistivity is observed correlating with relatively positive residual Bouguer gravity implying higher density.

The NW-SE oriented, low resistivity anomaly is found where intense seismic activity is associated with transform tectonics occurs. Since no attenuation of S-waves is observed under the Hengill area, the deep conductors are believed to reflect hot, solidified intrusions acting as a heat source for the geothermal system (Arnason et al., 2010).

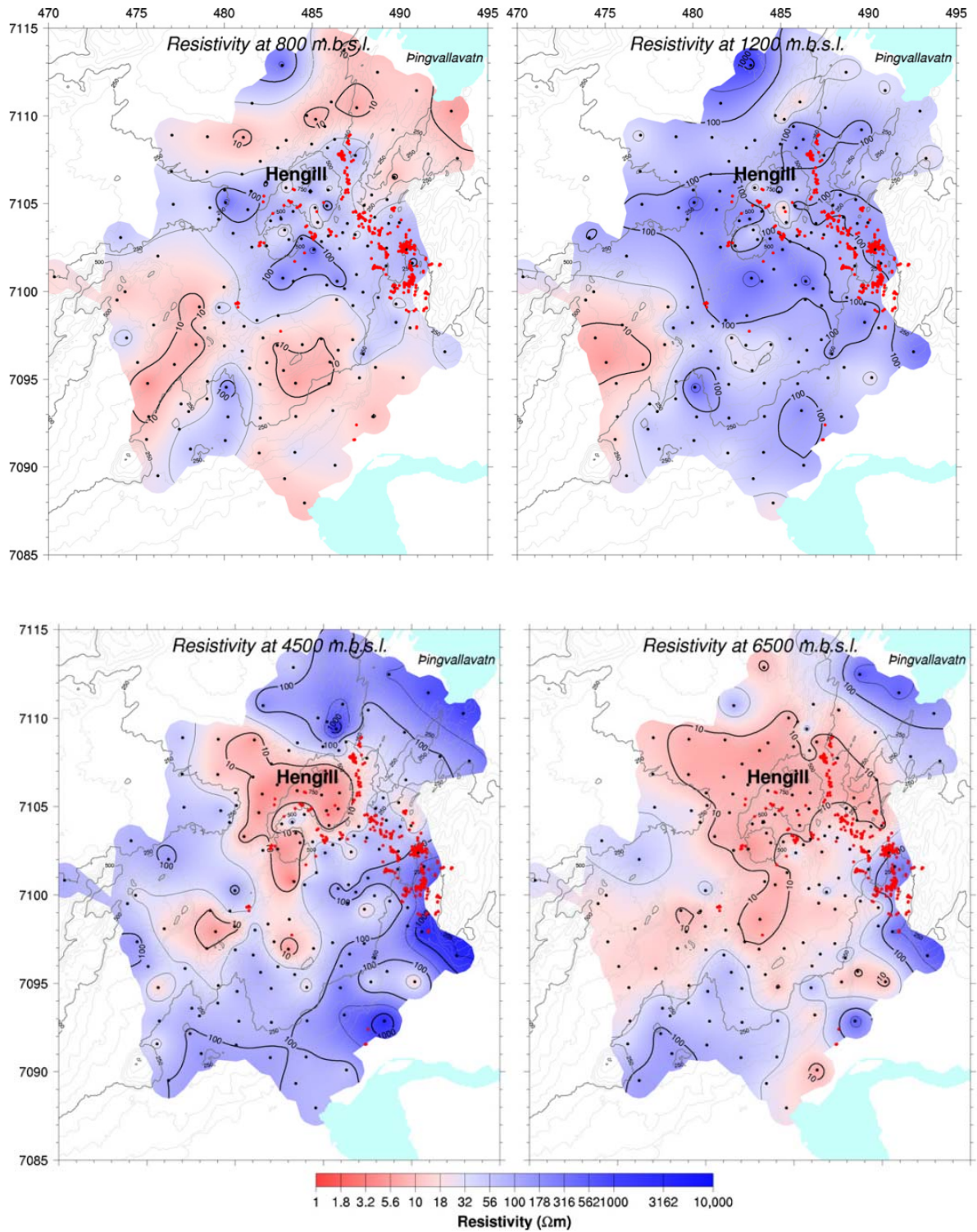


FIGURE 2. Resistivity in the Hengill area at 0.8, 1.2, 4.5 and 6.5 km b.s.l. according to joint 1D inversion of TEM and determinant MT data. Red dots indicate geothermal surface manifestations, black dots MT soundings, thick black lines resistivity contour lines, and thin black lines topographic contour lines in m a.s.l. Distances are given in km (Arnason et al., 2010).

2.3 Geothermal Activity

The geothermal surface manifestations in the Hengill area are connected to the volcanic system. Cooling magma intrusions are the main heat source of the Hengill geothermal systems within the upper crust and the heat is transported upwards by circulation of deep ground waters in highly fractured formations (Franzson et al., 2010). According to Ivarsson (1998), the CO₂ gas geo-thermometer shows three up-flow zones and the temperature seems to decrease to the southeast (Figure 3)

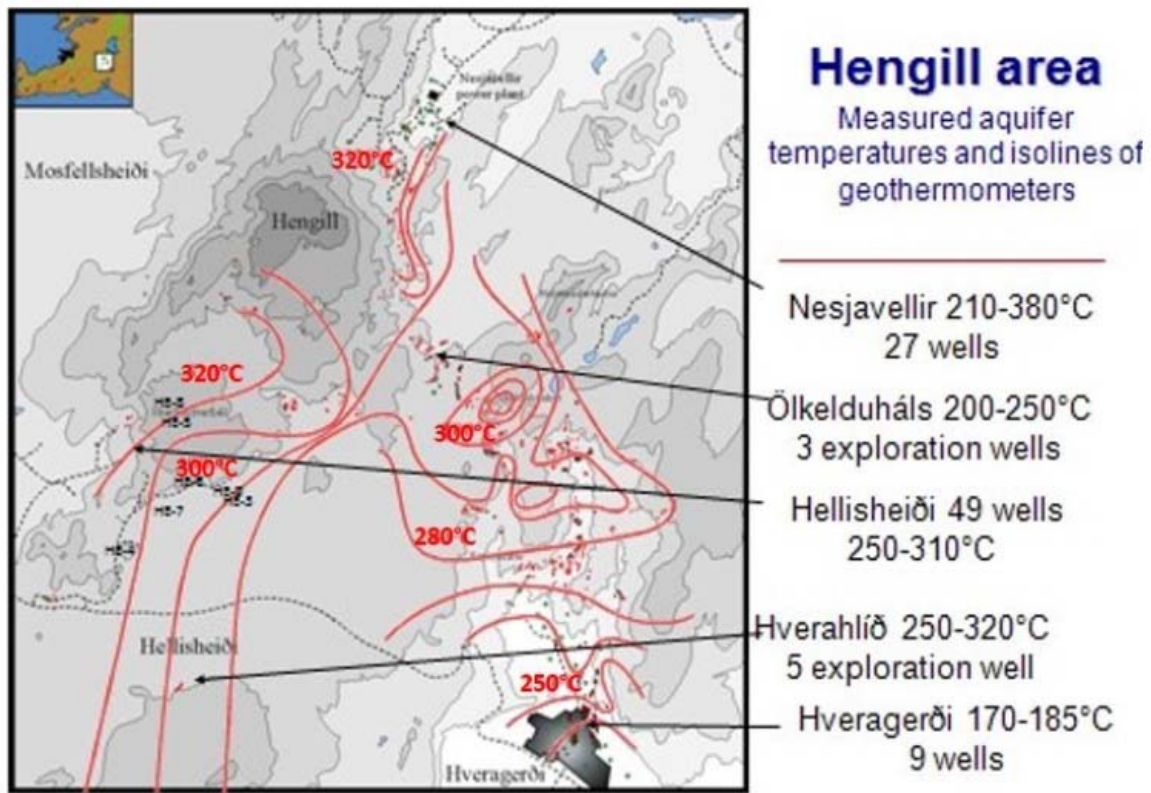


FIGURE 3. Measured aquifer temperatures and isolines of CO₂ gas geo-thermometers in the Hengill area (modified from Ivarsson, 1998). Geothermal surface manifestations are shown as red dots. Number of wells and average temperature in wells for the five known main subfields is shown.

2.4 Geothermal Power Plants in the Hengill Area

The Hengill area in south west Iceland is one of the most extensive geothermal fields in Iceland. Presently there are two geothermal power plants in operation in the Hengill area; Nesjavellir and Hellisheidi plants. Both power plants have been considered as symbols of the knowledge and tools that have been built up in the field of geothermal energy development in Iceland. Both plants play important role in producing electricity and hot water for district heating for industries and the wider community.

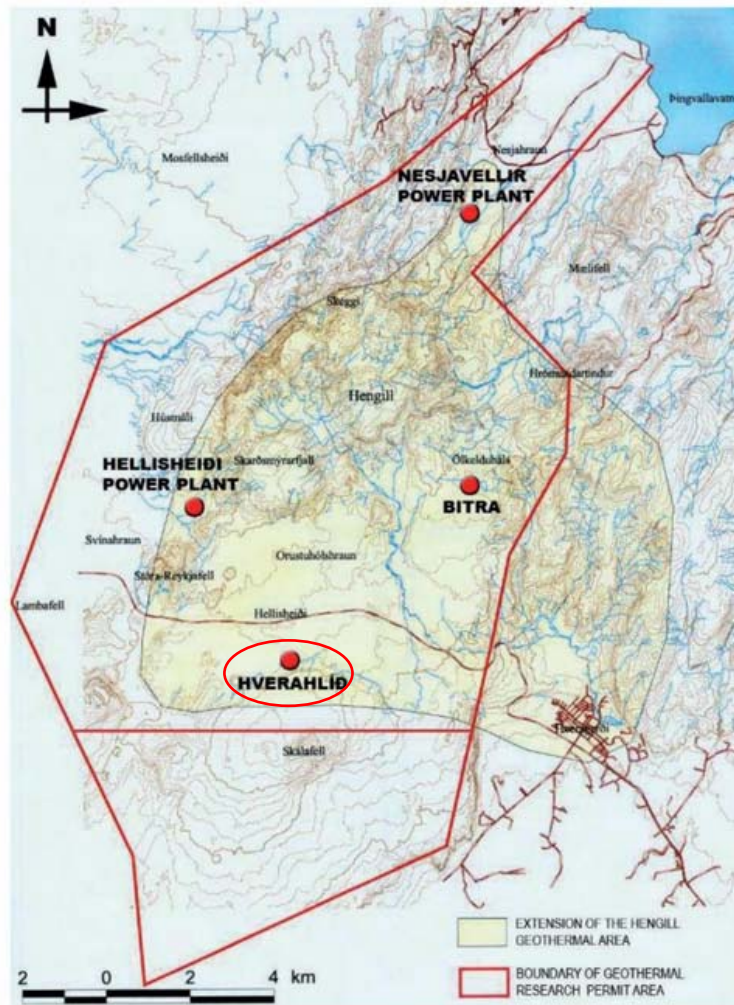


FIGURE 4. Map of the Hengill area showing existing and potential geothermal power plants. Red ellipse shows the study area (VSO, 2007).

2.4.1 Nesjavellir power plant

The Nesjavellir power plant is the first plant in the Hengill area. The construction of the plant began in 1987, with the first stage, 100 MW_{th} hot water plant, completed in September 1990. It was later expanded in several stages and 60 MW electricity generation started in 1998. The plant generates now 120 MW of electricity and 300 MW of thermal energy (hot water). It was the largest geothermal plant in Iceland at that time and is currently the second largest after Hellisheidi power plant (OR, 2007).

The production cycle at the power plant is divided into three stages: collection of steam from wells, the collection and heating of cold water and finally electricity production. Cold water is taken from six wells near Lake Thingvellir and pumped to the power plant. From there it goes to the condenser for pre-heating and then it flows through heat exchanger where the separated brine heats the water up to temperature 85°C.

About 32 wells have been drilled at Nesjavellir to a depth of 1000 to 2200 m reaching a temperature of about 380°C. Two-phase geothermal fluid is piped from the wells to the separation station, through pipelines, where the steam is separated from the water. The steam and brine are transported to the power plant via separate pipeline. The steam is led to the steam turbine for electricity generation. The separated brine passes through the heat exchanger where the final heating of the cold water takes place, as mentioned above.

The Nesjavellir powerhouse stands at a height of 177 meters above sea level. Hot water is pumped via a powerful pumping system into the tank at 400 m a.s.l on Háhyggur west of the power plant. From there the water runs by gravity to reach the hot water utility tanks at Reynisvatnsheidi in the outskirts of Reykjavik. The hot water pipeline to the capital is about 27 km long and the heat loss along the way is less than 2°C (OR, 2007).

2.4.2 Hellisheidi power plant

The construction of the Hellisheidi power plant began in late 2004 and the first turbine units, 90 MW combined, were put into operation for electricity generation in autumn 2006. With introduction of more turbines, the annual output increased steadily in the coming years. At the end of 2010, the thermal station (hot water) began operations, and in October 2011 the final phase of electricity generation started. The installed capacity of the Hellisheidi power plant is now 303 MW of electricity and 133 MW of thermal power.

The Hellisheidi power plant processes are similar to the Nesjavellir power plant. About 65 wells have been drilled at Hellisheidi with depth ranging from 2000 to 3000 meters and about 40 wells are in operation. There are six high-pressure steam turbines in the power plant each generating 45 MW. In addition, a low-pressure steam turbine generates 33 MW.

The thermal station at Hellisheidi went into operation in November 2010. The station has two heat exchanger substations, each with two serially configured heat exchangers. The installed capacity of the thermal station is 133 MW or 750 l/s of 85°C of water. The heated fresh water is used for district heating.

The hot water pipeline from Hellisheidi is roughly 20 km in length. Its diameter begins at 1000 mm and decreases to 900 mm. The pipeline runs from the hot water tank by the Hellisheidi power plant and connects with the control centre at Reynisvatnsheidi, where the water mixes with the heated water from Nesjavellir. Presently, the production rate is 750 l/s and it takes the water around 6 hours to reach Reykjavik. The pipeline is designed for a thermal station capable of producing 400 MW of thermal power which would reduce the transport time dramatically to 2.5 hours (OR, 2007).

2.4.3 Planned power plant at Bitra

The project area is located 4 km northeast of the Hellisheidi power plant, see Figure 3. The project area of the plant was reduced from its original plan size on account of environmental reasons. Because of reduction of the development area and environmental policy, the effect of the Bitra power plant on its surroundings has been minimized (VSO, 2007).

Three exploration wells have been drilled in the area. The size of the power plant was estimated from information gathered from those wells and from results from a model of the geothermal area (Björnsson, 2007). Overall estimated capacity of power plant at Bitra is 135 MWe. Further development of the Bitra has not been decided.

2.4.4 Power plant at Hverahlid

The project area is located about 3 km southeast of the Hellisheidi power plant. The development area of the power plant was also reduced from its original size because of environmental reasons. Like at Bitra, reduction of the development area and environmental policy will result in a minimal effect of the Hverahlid plant on its surroundings (Hverahlid VSO, 2007)

Six exploration/production wells have been drilled in the area. Overall estimated capacity of the power plant in that area is 90 MWe. The construction of the power plant was abandoned in 2014 and decided to connect the production wells in Hverahlid to the Hellisheidi power plant.

3 Basics of Injection Well Testing

An injection test is performed after completion of drilling by lowering a pressure tool to a selected depth close to a major feed (permeable) zone in the well. Fresh water is pumped into the well at varying pumping rates. The first pumping rate in the test is held at a constant rate to allow the pressure to stabilize. The pumping rate is then changed stepwise and each step should be long enough to allow the pressure in the well to stabilize again. This process is repeated for several pumping rates. Through all this process the well pressure is recorded as a function of time. The main purpose of injection testing is to obtain data that can be used to estimate reservoir parameters that characterize a well as well as stimulate the well (Biru, 2016).

Prior to producing a given reservoir or even financing to produce from it, we need to know its deliverability, properties and size of the reservoir. Parameters that govern the reservoir like permeability-thickness, reservoir initial pressure and the reservoir boundaries have to be determined. Wellbore conditions are also evaluated in order to determine whether the well productivity is governed by wellbore effects such as skin and storage or by the reservoir at large.

In well testing, the response of a reservoir to injection or production is monitored in the form of pressure response (Figure 5). It is possible to infer characteristics of the properties of the

reservoir from the response to a greater or lesser degree, which make well test interpretation an inverse problem. In essence well test analysis involves pressure transient analysis. The pressure transient occurs due to changes in production or injection of fluids, the flow rate transient is treated as input and the pressure transient is treated as output (Horne, 1995).



FIGURE 5. Essence of well testing and the associated pressure response.

The injection test data are prepared in the form of text file, a column containing date and a pressure column. To extract estimates of reservoir parameters, models are required to simulate the measured data, which include the reservoir properties. The pressure diffusion equation is the basis of all models in well testing and as well as the basis of pressure transient analysis founded on the models. The model depends on values selected for properties characterizing the reservoir and by iterating these values such that the modelled response fits the observed data one can infer the characteristic properties of the reservoir, see Figure 6.

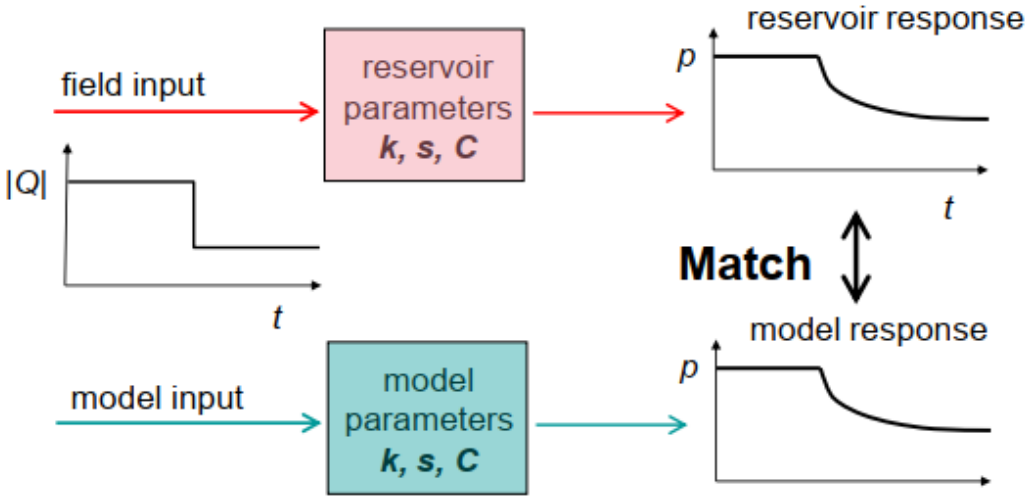


FIGURE 6. Match between collected data and model response during pressure transient analysis (Horne, 1995).

3.1 The pressure diffusion equation

Pressure transient methods have been used in evaluating groundwater and petroleum reservoirs for decades, through creating a transient condition by producing from the reservoir or injecting into the reservoir. The effects of disturbance due to production or injections are investigated at the active well or at nearby wells. Transmissivity and storage coefficient of the reservoir region affected by the pressure transients are the main parameters obtained from the tests (Bödvarsson and Witherspoon, 1989).

In this chapter we will derive the pressure diffusion equation, which is the fundamental equation in well test analysis. The approximate assumptions involved when deriving this equation, and the radial cell geometry are shown in Figure 7. These assumptions include that flow is isothermal and single phase, permeability is isotropic and independent of pressure, the fluid viscosity and compressibility is pressure independent, the fluid compressibility is low, and that the well is completed across the full formation thickness.

The pressure diffusion equation is used to calculate the pressure (p) in the reservoir at a certain distance (r) after a given time (t) and from an injection (or production) well receiving or producing fluid at specific rate (Q), starting at time t = 0. The pressure diffusion equation is derived by combining the conservation of mass law, Darcy's law and the equation of state of the fluid.

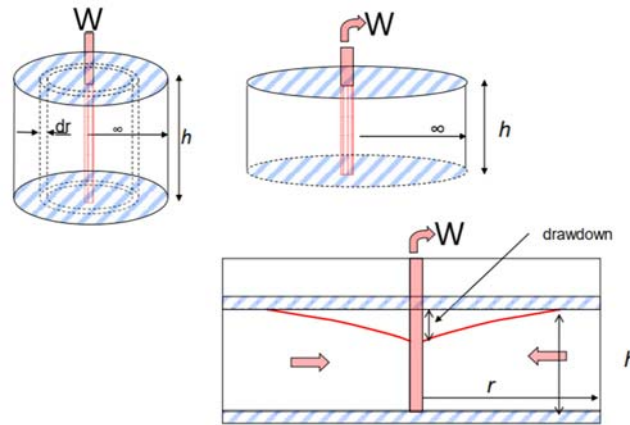


FIGURE 7. Radial flow of a single-phase fluid in the vicinity of producing well (Haraldsdóttir, 2016).

Consider the flow through a volume of thickness dr (Figure 7) situated at a distance r from the centre of the radial cell. Then applying the law of conservation mass:

$$\text{Mass flow in } (M_{in}) - \text{Mass flow out } (M_{out}) = \text{Rate of change of mass within the control volume } (\Delta M)$$

Where $2\pi r h \phi dr$ is the volume of the small element of thickness dr. The equation on the left side can be expanded as:

$$\rho q - \left(\rho q + \frac{\partial(\rho q)}{\partial r} dr \right) = 2\pi r dr \frac{\partial(\phi \rho h)}{\partial t} \quad (1)$$

Which simplifies to:

$$-\frac{\partial(\rho q)}{\partial r} = 2\pi r \frac{\partial(\phi \rho h)}{\partial t} \quad (2)$$

By applying Darcy's law, for radial, horizontal flow it is possible to substitute for the flow rate, q, in equation (2) since;

$$\left(q = -\frac{2\pi r h k}{\mu} \frac{\partial p}{\partial r} \right)$$

Giving

$$\frac{\partial}{\partial r} \left(\frac{2\pi r h k}{\mu} \rho \frac{\partial p}{\partial r} \right) = 2\pi r \frac{\partial(h\phi\rho)}{\partial t} \quad (3)$$

The time derivative of the density appearing on the right hand side of equation (2) can be expressed in terms of a time derivative of the pressure by using isothermal compressibility. Pressure transient occurs only because the reservoir fluid is compressible to certain extent and when accumulation or depletion of fluid in the reservoir occurs (Stewart, 2011).

Equation of state of the fluid of constant compressibility can be expressed as:

$$C_w = -\frac{1}{V} \frac{\partial V}{\partial p}$$

Where C_w is the fluid compressibility and V is the fluid volume. i.e., the relative change in the volume of the fluid per unit change in pressure; it has the dimensions of reciprocal pressure.

The compressibility equation can be put in terms of fluid density for a constant mass of fluid m :

$$\rho = \frac{m}{V} \text{ or } v = \frac{m}{\rho}$$

And hence

$$C_w = -\frac{\rho}{m} \frac{\partial \left(\frac{m}{\rho} \right)}{\partial p} = \frac{1}{\rho} \frac{\partial \rho}{\partial p} \quad (4)$$

The right hand side of equation (3) can then be written as

$$\frac{\partial(h\phi\rho)}{\partial t} = \rho \frac{\partial \phi}{\partial t} + \phi \frac{\partial \rho}{\partial t} \quad (5)$$

From equation (4), it can be shown that (Bear, 1979):

$$\phi \frac{\partial \rho}{\partial t} = \phi c_w \rho \frac{\partial p}{\partial t} \quad (6)$$

And,

$$\rho \frac{\partial \phi}{\partial t} = (1 - \phi) c_r \rho \frac{\partial p}{\partial t} \quad (7)$$

Where C_r is the compressibility of the rock matrix. Inserting (6) and (7) into (5)

$$\partial \frac{(\varphi\rho)}{\partial t} = \rho c_t \frac{\partial p}{\partial t} \quad (8)$$

Where C_t is the total compressibility of the system defined as $c_t = \varphi c_w + (1 - \varphi)c_r$

By inserting (8) into (3) and expanding the left-hand side of (3) assuming that the reservoir is homogeneous and therefore variations in ρ , k and μ are small, we can express the pressure diffusion equation as:

$$\frac{1}{r} \frac{\partial}{\partial r} \left(r \frac{\partial p}{\partial r} \right) = \frac{\mu c_t}{k} \frac{\partial p}{\partial t} \quad (9)$$

By introducing parameters

$$T = \frac{kh}{\mu}$$

and $S = c_t h$,

where T is transmissivity and S is the storage coefficient, the equation can be written

$$\frac{1}{r} \frac{\partial}{\partial r} \left(r \frac{\partial p}{\partial r} \right) = \frac{\mu c_t}{k} \frac{\partial p}{\partial t} = \frac{S}{T} \frac{\partial p}{\partial t} \quad (10)$$

Equation (10) is the pressure diffusion equation, the basis of well testing analysis, or the partial differential equation for the radial flow of any single phase fluid in a porous medium.

3.2 Dimensionless Variables

Well test analysis makes use of dimensionless variables. The dimensionless variables are important in that they simplify the reservoir models by including the reservoir parameters such as k , thereby decreasing the number of unknowns. They also provide model solutions that are independent of any particular system. It is an inherent assumption in the definition that permeability, viscosity, compressibility, porosity, formation volume factor and thickness are constant (Horne, 1995).

The dimensionless pressure drop is defined as:

$$p_D(r_D, t_D) = \frac{2\pi kh}{W\mu} (p_i - p(r, t)) \quad (11)$$

The dimensionless time t_D is defined as

$$t_D = \frac{kt}{\varphi\mu c_t r_w^2} \quad (12)$$

when based on wellbore radius, r_w , or

$$t_{DA} = \frac{kt}{\phi\mu c_t A} = t_D \frac{r_w^2}{A} \quad (13)$$

when based on total drainage area, A , corresponding to the reservoir area = πr_e^2 with r_e the reservoir radius (Horne, 1995).

We can also define in terms of dimensionless radius, r_D , as

$$r_D = \frac{r}{r_w} \quad (14)$$

Now we can present the differential equation (10) in dimensionless form. Substituting t_D and P_D into equation 9 gives:

$$\frac{1}{r_D} \frac{\partial}{\partial r_D} \left(r_D \frac{\partial p_D}{\partial r_D} \right) = \frac{\partial p_D}{\partial t_D} \quad (15)$$

This dimensionless diffusion equation can then be solved for the appropriate initial and boundary conditions (Kjaran and Eliasson, 1983).

3.2.1 Semi-logarithmic well test analysis

The Theis solution to the pressure diffusion equation can be approximated by:

$$-\Delta p = \frac{2.303W}{4\pi T} \left[\log(t) + \log\left(\frac{4T}{Sr^2}\right) - 0.2506 \right] \quad (16)$$

During radial flow, the pressure change is related to the logarithm of the time or if pressure is plotted against the log of time, infinite acting radial flow will give a straight line. The Theis solution plot for ΔP vs. $\log t$ results in a semi-log straight line with a slope m per log cycle

response for the infinite acting radial flow period of a well, leading to what is called a semi-log analysis (Earlougher, 1977; Horne, 1995 and Schlumberger, 1998).

$$m = \frac{2.303W\mu}{4\pi kh} \text{ (Pa/log cycle)} \quad (17)$$

Then the Transmissivity, T , is defined:

$$T = \frac{2.303W}{4\pi m} \quad (18)$$

The storage coefficient, S , can be obtained

$$S = 2.25T \left(\frac{t}{r^2}\right) 10^{-\Delta p/m} \quad (19)$$

The presence of skin effect does not alter the evaluation of the transmissivity in the semi logarithmic analysis but it does affect the storage coefficient estimates, therefore in order to calculate the skin factor s , one must re-arrange Equation 16 to get (Grant and Bixley, 2011):

$$s = 1.151 \left[\frac{\Delta p}{Lm} - \log \left(\frac{4Tt}{sr_w^2} \right) + 0.2506 \right] \quad (20)$$

Wellbore storage (C) is defined as the difference between the wellhead flow rate and the sand face flow rate (i.e. the flow into or out of the actual formation). When a well is opened, the production at surface is initially due to the expansion of the fluid in the wellbore, and the reservoir contribution is initially negligible. For many well tests, the only means of controlling the flow rate is at the wellhead valve or flow line. Hence the well may produce at constant rate at the wellhead, but the flow transient within the wellbore itself may mean that the flow rate from the reservoir into the wellbore (the "sand face" flow rate) may not be constant at all. This effect is due to wellbore storage and the flow regime may last from few seconds to a few minutes. Then the reservoir production starts and the sand face rate increases until it becomes the same as the surface rate. When this condition is achieved, the wellbore storage has no effect on the bottom hole pressure response, the data describes the reservoir behaviour and it can be used for transient analysis (Horne, 1995; Bourdet, 2002).

During shut-in periods, the wellbore storage effect is also called after flow: after the well has been shut-in, the reservoir continues to produce at the sand face and the fluid stored in the wellbore is recompressed. The same sequence with three different pressure behaviors can be observed: the pure wellbore storage effect, transition when the sand face rate declines, and the end of the wellbore storage effect then the sand face rate becomes very small and eventually zero. There is a time lag between the surface production and the sand face rate, After any change in the well flowing conditions. The pressure response is affected by the wellbore storage effect during the first test period. (Bourdet, 2002). The wellbore storage factor, C is dimensionless and is defined by:

$$C = \frac{\Delta V}{\Delta p} \quad (21)$$

Where ΔV and Δp are the change in volume and pressure inside the well, respectively.

Skin factor (s) is a variable used to quantify the permeability of the volume immediately surrounding the well and pressure transmission does not take place uniformly throughout the reservoir, since this volume is often affected by drilling operations, or completion of the well and invaded by mud filtrate. This zone may have a lower permeability than the reservoir at large, and thereby acts as a skin around the wellbore, causing higher pressure drop.

The formation volume close to the wellbore typically has altered properties compared to the surrounding reservoir. Of highest importance for well productivity is an altered permeability, and the effect of this alteration on productivity is called skin. (Bourdet, 2002 and Schlumberger, 1998).

Often there is a damaged zone in the vicinity of the wellbore, which reduces the permeability in the area. The situation is shown in Figure 8, in which r_s represents the radius of this zone.

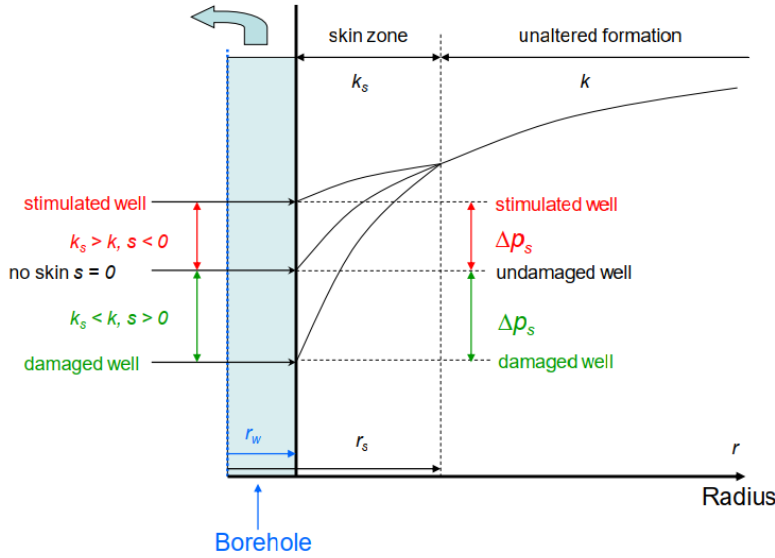


FIGURE 8. Radial pressure profile for a normal, stimulated or damaged well (modified from Horne, 1995).

If the well were undamaged, the pressure profile for $r < r_s$ would be shown as stimulated well in Figure 8, whereas due to the reduced permeability in the damaged zone, Eq. 22 implies that the pressure drop will be larger than normal, or that p_{wf} will be reduced.

The additional pressure drop close to the well is defined by:

$$\Delta p_{skin} = \frac{W\mu}{2\pi kh\rho} s \quad (22)$$

Where Δp_{skin} is a skin of reduced permeability around the well and s is a dimensionless skin factor, which can be determined from well testing methods.

Equation 22 can be expressed with the skin factor:

$$p_e - p_{wf} = \frac{W\mu}{2\pi kh\rho} \left[\ln \left(\frac{r_e}{r_w} \right) \right] + s \quad (23)$$

The productivity index of a well is defined as the mass flow divided by wellbore pressure drop:

$$PI = \frac{W}{p_e - p_{wf}} = \frac{2\pi hk\rho}{\mu \left(\ln \frac{r_e}{r_w} + S \right)} \quad (24)$$

PI is the productivity index of a well and is a measure of the well performance (Kjaraan and Eliasson, 1983). In the case of a damaged well, a flow restriction is present at the interface between the reservoir and the wellbore, producing an additional pressure drop Δp_{skin} when the fluid enters into the well. For a stimulated well, the flowing condition is improved near the well, and the pressure decline is reduced in a cylindrical near wellbore reservoir region. The same Δp_{skin} can reflect small or great damage, depending on the flow rate and the reservoir permeability. The skin factor s is a dimensionless parameter and it characterizes

the well condition: for a damaged well $s > 0$, which is a positive skin representing near-wellbore damage and $s < 0$ for a stimulated well, which is negative skin denoting stimulation, meaning that there is a smaller pressure drop close to the wellbore than would be expected in the ideal case (Bourdet, 2002; Schlumberger, 1998). Theoretically, the productivity index should correspond exactly to the injectivity index of a well.

The skin value will be seen to do more than simply influence the pressure drop during production. For instance, a high skin delays the onset of radial flow information in the pressure data and whereas negative skin brings it forward. This is due to the interdependence of skin, productivity and wellbore storage effects.

3.3 Well test analysis and Interpretation

The analysis of the injection tests at Hverahlid is performed using the software called WellTester, version 2 (Marteinsson, 2016). It is used to handle data manipulation and analysis of well tests (mainly multi-step injection tests) and presents the results both graphically and in tables. The software works in the following steps (Haraldsdóttir, 2016; Marteinson, 2016):

Initial parameters: The well temperature, rock type, porosity and wellbore radius are fed into the WellTester program. Pressure is deduced from the WellTester. These values are used to determine dynamic viscosity of the reservoir fluid and the total compressibility of the fluid and the rock matrix.

Set steps: The initial time of the injection steps is selected on the graph

Modify: In this step the data is cleaned, corrected and resampled

Model: In this step, the best model for the reservoir being investigated is selected. This is achieved using, the derivative plot along with the pressure data as a function of time on graphs with log-log scale as well as linear and log-linear scale.

The main parameters deduced from the WellTester simulation are (Júliússon et al., 2008, Marteinson, 2016):

Transmissivity describes the ability of the reservoir to transmit fluid, hence largely affecting the pressure gradient between the well and the reservoir. Represented mathematically as kh/μ , where k is permeability of the reservoir, h is a reservoir thickness and μ is the dynamic viscosity of the reservoir fluid.

Storage coefficient defines the volume of fluid stored in the reservoir, per unit area, per unit increase in pressure [$m^3 / (pa \cdot m^2)$ or m/Pa]. The storativity of the reservoir gives an indication how fast the pressure can travel. The storage coefficient is controlled by different storage mechanisms and varies greatly between reservoir types, i.e. liquid dominated, either confined or unconfined, two phase or steam dominated. In confined liquid dominated reservoirs the storage is controlled by fluid compressibility. Common values for liquid dominated geothermal reservoirs are around 10^{-8} [$m^3 / (pa \cdot m^2)$ or m/Pa] and 10^{-5} [$m^3 / (pa \cdot m^2)$ or m/Pa] for two phase reservoirs.

Skin factor (s) is used to quantify the permeability of the volume near the well. This volume is affected by drilling operations such as drill cuttings, cementing jobs etc. clogging the well. For damaged wells the skin factor is positive and for stimulated wells the skin effect is negative.

The injectivity index (II) is used as estimate of the connectivity of the well to the surrounding reservoir. Injectivity index is also evaluated during the injection well testing and predicts the performance of the well or success of the well being drilled, the bigger the value the better the performance.

$$II = \left| \frac{\Delta Q}{\Delta P} \right| \quad (25)$$

Here $\Delta Q = Q_f - Q_i$ and $\Delta P = P_f - P_i$ where i refers to the initial value and f refers to the final value.

Wellbore storage (C) is defined as the difference between the wellhead flow rate and the sand face flow rate.

Radius of investigation (r_e) is the distance at which the pressure response from the well becomes undetectable or invisible

3.3.1 Injection Testing of Well HE-36

Well HE-36 is located at Hverahlid about 1 km west of HE-21 (Figure 9). The target was to explore the presence of the geothermal reservoir related with the active fissure swarm west of HE-21. It was directed to the North West, so it intersects the NE-SW trending fissure swarm more or less perpendicularly. Drilling of well HE-36 started in August 2007 and completed in October same year. The well is drilled directionally to a measured depth of 2808 m in the direction of 295° with an inclination of 30°. The directional drilling kick off point (KOP) is at depth of 400 m (Tryggvason et al., 2018). The true vertical depth is 2527 m. The location of the well and it's well track is shown in Figure 9. The well is of a conventional diameter type with 8 ½" production part. The casing program for the well is shown in Table 1.

Table 1. Well HE-36. Drilled depths, casing depths with respect to ground surface, and casing information.

Drill bit size (inches)	Drilled depth (m)	Casing Type	Casing depth (m)	Casing diameter (inches - OD)
21	105	Surface casing	97	18 3/8
17 ½	364	Anchor casing	362	13 3/8
12 ¼	1104	Production casing	1103	9 5/8
8 ½	2808	Perforated liner	2436.5	7

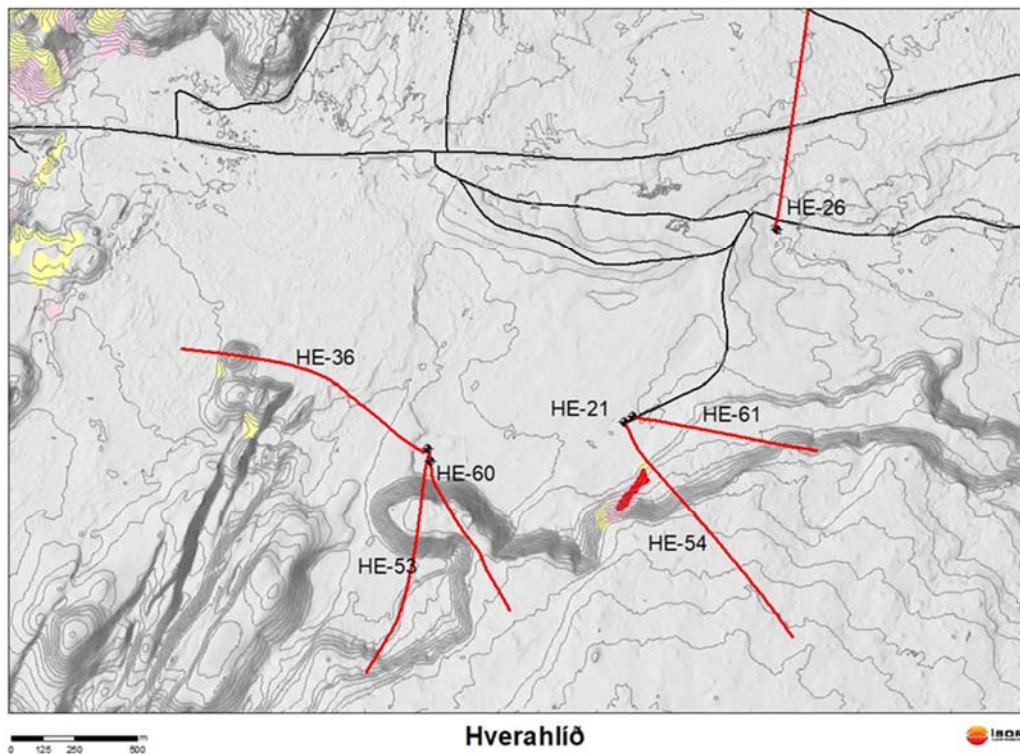


FIGURE 9. The geothermal field at Hverahlid. Well locations are shown as black dots and tracks of directional wells as red lines. Active fumaroles are in the red area but thermally altered areas are yellow. Roads in the area are black lines. The elevation lines in the background show the landscape (Tryggvason et al., 2018)

A two-step injection test was performed after completion of the drilling of the well when the liner had been lowered into the well. The pressure response in well HE-36 during the two-step injection steps, changing the injection rate from 30 to 70 L/s in the first step and back to 30 L/s in the second step. Figure 10 displays the pressure response during the injection test, which lasted for 3 hours. The pressure response was analysed and the injectivity index determined for both steps, resulting in $II = 4$ L/s/bar for the first and 5 L/s/bar for the second (Table 2).

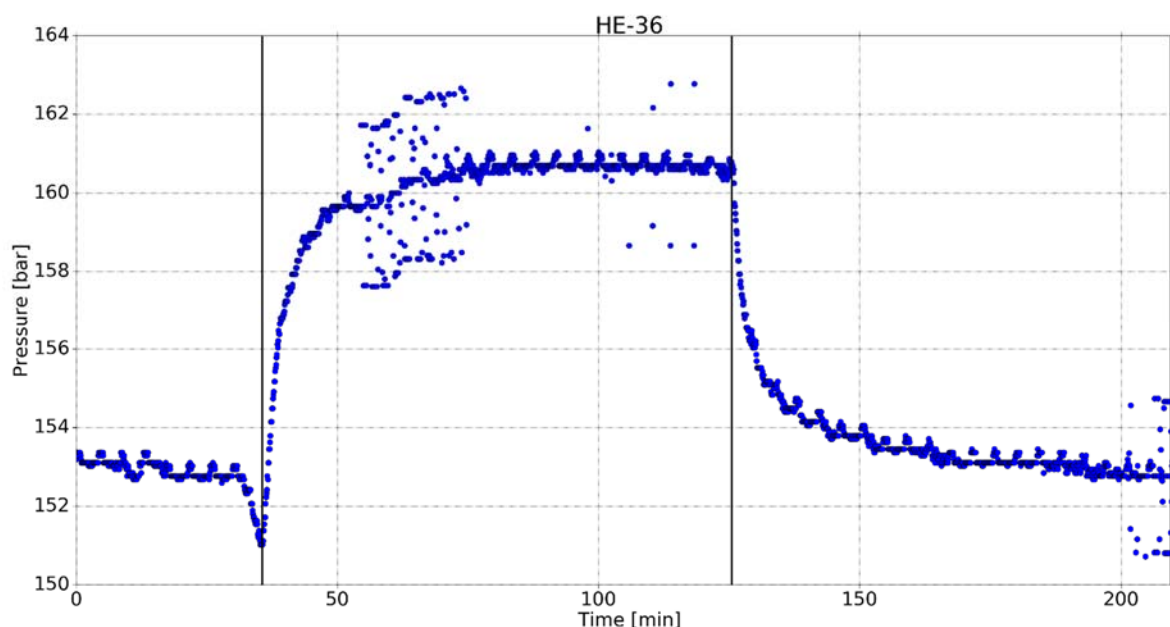


FIGURE 10. HE-36 pressure response against time in the two injection steps with at total duration of 3 hours.

Table 2. Well HE-36. Analyses of the injection test data regarding injectivity.

Step no	Time (hr)	ΔQ (L/s)	ΔP (bar)	Injectivity index (L/s)/bar
1	1.5	40	10	4.0
2	1.5	-40	8	5.0

When performing the well test analysis, many models were tested by performing a nonlinear regression in order to find the best fitting model for the measured data. Table 3 and 4 show

the selected initial parameters and the selected reservoir model for the WellTester analysis of the injection test data.

*Table 3. Initial parameters used in the well test analysis of HE-36 where those marked with * must be inserted by the user to get a meaningful output from the WellTester.*

Name of Parameters and units	HE-36
Estimated reservoir temperature [°C]*	280
Estimated reservoir pressure [bar-g]	108.6
Wellbore radius, r [m] *	0.16
Porosity, ϕ *	0.1
Dynamic viscosity of reservoir fluid, μ , [Pas]	9.5×10^{-5}
Compressibility of reservoir fluid, c_w , [Pa-1]	2.0×10^{-9}
Compressibility of rock matrix, c_r , [Pa-1]	2.4×10^{-11}
Total compressibility, C_t , [Pa-1]	2.25×10^{-10}

Table 4. Model selected for injection test analysis for well HE-36.

Reservoir	Homogeneous
Boundary	Constant pressure
Well	Constant skin
Wellbore	Wellbore storage

The WellTester results are given in Table 5 for both the steps. The second step of the injection test gives the best fit and have been used to obtain the parameters of the wellbore and the surrounding reservoir. The model results for step 2 are shown graphically in Figure 11 on both linear and log-log scales. The figure shows that the model fits the measured data fairly well.

Table 5. Reservoir and well parameters obtained using nonlinear regression model for injection data from well HE-36,

Parameter	Step 1	Step 2
Transmissivity, T ($m^3/(Pa.s)$)	5.3×10^{-8}	4.85×10^{-8}
Storage coefficient S (m/Pa)	1.1×10^{-9}	2.4×10^{-8}

Radius of investigation, r_e (m)	540	540
Skin factor, s	-0.1	-0.62
Wellbore storage, C (m^3/Pa)	8.7×10^{-6}	9.2×10^{-6}
Reservoir thickness, h (m)	5.3	175
Permeability, k (m^2)	9.6×10^{-14}	2.7×10^{-13}
Injectivity index, II ((L/s)/bar)	4.1	5.1

The results obtained indicate that well HE-36 is more open to flow during the second step than the first step of the injection test. This is clearly indicated by the injectivity index, II , as well as by the permeability, k , as both are estimated to be higher in the second step of the test (Table 3). Yet, the transmissivity values are comparable, and of the order of $10^{-8} m^3/Pa*s$, which are similar to values of Icelandic geothermal wells in general. The skin factor is negative in both steps and bigger (more negative) in the second step indicating the borehole is well connected to the surrounding geothermal reservoir.

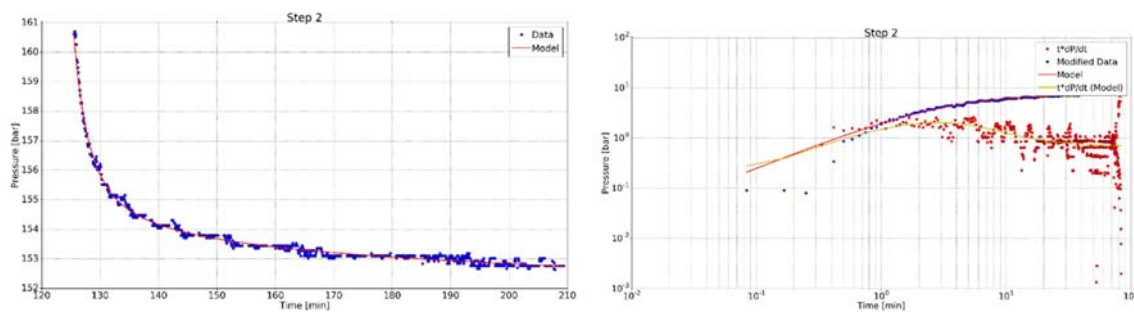


FIGURE 11. Model results and recorded pressure for step 2 using a linear scale (to the left) and log-log scale (to the right).

3.3.2 Injection Testing of Well HE-53

Well HE-53 is located on the same drilling platform as HE-36 (Figure 9). Drilling of well HE-53 started in April 2009 and it was completed in June 2009. The well is drilled directionally to a measured depth of 2507 m in the direction of 192.5° with an inclination of 30° . The directional drilling kick off point (KOP) is at depth of 450 m. The true vertical depth of the well is 2256 m. The location of the well and its well track is shown in Figure 9. The well is of a conventional diameter type with 8 1/2" production part. Well depth and casing depth information are summarized in Table 6.

Table 6. Depths and casing depths in well HE-53 with respect to ground surface and casing information's.

Bit size (inch)	Well depth (m)	Casing Type	Casing depth	Casing size (inch - OD)
21	62.5	Surface casing	61	18 3/8
17 ½	303	Anchor casing	299	13 3/8
12 ¼	959	Production casing	959	9 5/8
8 ½	2500	Perforated liner	2464	7

A three-step injection test was performed for well HE-53. The pressure response during the three steps injection test, changing the flow from 20.1 to 35.3 L/s in the first step to 45.5 L/s in the second step, reducing the flow to 20.7 L/s in third step. The first two steps lasted for 3 hours, each and the fall-off test for 4 hours. The pressure response during the test is shown in Figure 12. The pressure response was analysed and the injectivity index determined for the three steps getting $II=12.4$ for the first, 7.4 for the second and 7.9 L/s/bar for the third step (Table 7).

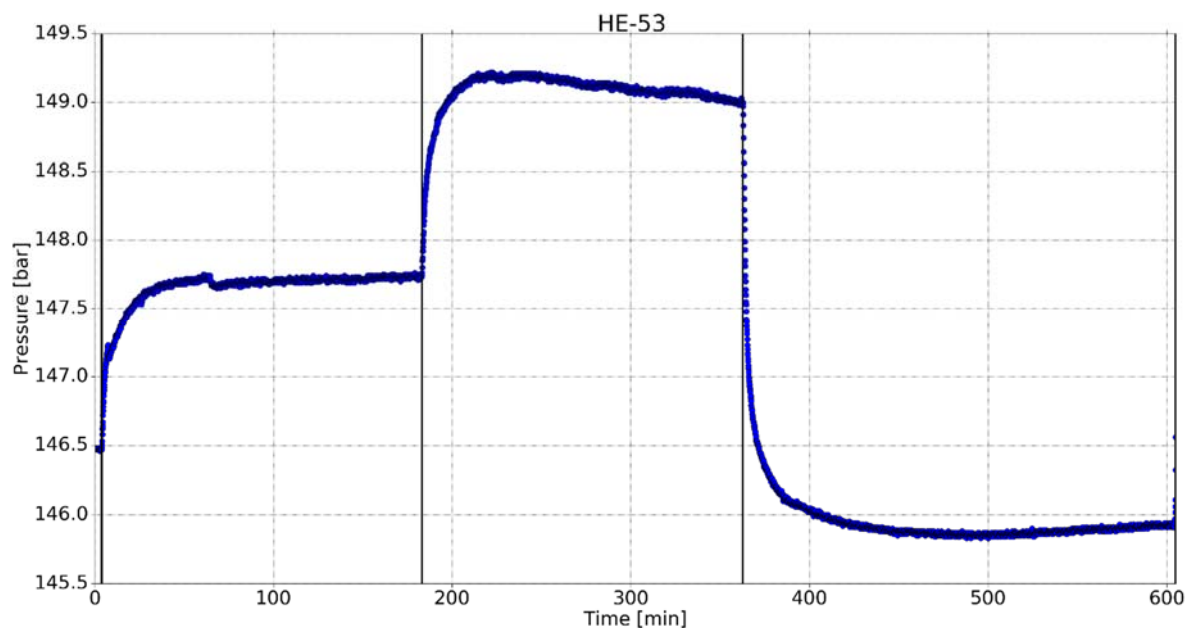


FIGURE 12. HE-53 pressure response at 2000 m against time during three injection steps with at total duration of 7 hours.

Table 7. Well HE-53. Analysis of the HE-53 injection test data regarding injectivity.

Step no	Time(hr)	ΔQ (L/s)	ΔP (bar)	Injectivity index (L/s)/bar
---------	----------	------------------	------------------	-----------------------------

1	3	15.2	1.25	12.2
2	3	10.2	1.5	6.8
3	3	24.8	3.12	8.0

When performing the well test analysis, many models were tested by performing a nonlinear regression in order to find the best fitting model for the measured data. Table 8 and 9 show the selected initial parameters and the selected reservoir model for the WellTester analysis of the injection test data.

*Table 8. Initial parameters used in the well test analysis of HE-53 where those marked with * must be inserted by the user to get a meaningful output from the WellTester.*

Name of Parameters and units	HE-53
Estimated reservoir temperature [°C]	300
Estimated reservoir pressure [bar-g]	147.7
Wellbore radius, r, [m]	0.16
Porosity, ϕ	0.1
Dynamic viscosity of reservoir fluid, μ , [Pas]	8.82×10^{-5}
Compressibility of reservoir fluid, c_w , [Pa ⁻¹]	2.7×10^{-9}
Compressibility of rock matrix, c_r , [Pa ⁻¹]	2.4×10^{-11}
Total compressibility. C_t , [Pa ⁻¹]	2.9×10^{-10}

Table 9. Model selected for injection test analysis for well HE-53

Reservoir	Homogeneous
Boundary	Constant pressure
Well	Constant skin
Wellbore	Wellbore storage

A summary of reservoir parameters estimated using nonlinear regression model for well HE-53 is presented in Table 10 and the best model fits of step 1 are shown in Figure 13.

The model results are given in Table 10 for all the steps. The first step of the injection test gives the best fit and have been used to estimate parameters of the wellbore and the surrounding reservoir, summarized in table 10 and graphically shown in Figure 13.

Table 10. Reservoir parameters obtained using nonlinear regression model for well HE-53,

Parameter	Step 1	Step 2	Step 3
Transmissivity, T (m ³ /(Pa.s))	4.21×10 ⁻⁸	4.29×10 ⁻⁸	7.9×10 ⁻⁸
Storage coefficient, S (m/Pa)	9.55×10 ⁻⁸	6.57×10 ⁻⁸	7.4×10 ⁻⁸
Radius of investigation, r _e (m)	46	33	88
Skin factor, s	-3.5	-1.7	-0.074
Wellbore storage, C (m ³ /Pa)	7.54×10 ⁻⁶	1.35×10 ⁻⁵	1.07×10 ⁻⁵
Reservoir thickness, h (m)	330	227	256
Permeability, k (m ²)	4.12×10 ⁻¹⁴	1.7×10 ⁻¹⁴	2.72×10 ⁻¹⁴
Injectivity index, II ((L/s)/bar)	12.4	7.4	7.9

The results obtained indicate that well HE-53 is more open to flow during the first step. This is clearly indicated by the injectivity index, II (L/s)/bar, as well as by the permeability, k as both are estimated to be higher in the first step of the test (Table 10). Transmissivity values are all in the order of 10⁻⁸ m³/Pa.s, which are similar to values of Icelandic geothermal wells in general. The skin factor is negative in all steps and bigger in the first step indicating the borehole is well connected to the surrounding reservoir. The injectivity index is II highest in the first step.

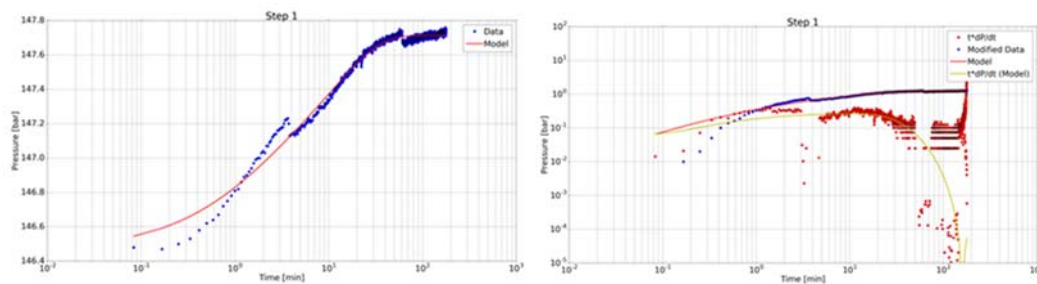


FIGURE 13. Model results and recorded pressure for step 1 using a linear scale (to the left) and log-log scale (to the right) for well HE-53.

3.3.3 Injection Testing of Well HE-61

Well HE-61 is on the same drilling platform at Hverahlid as wells HE-21, which is vertical, and the directional well HE-54, which was drilled to the southeast (Figure 9). Well HE-61 is intended as a replacement well for the Hellisheidi Geothermal Power Plant, where the production of the Hellisheidi area has decreased due to pressure draw down in the reservoir. Well HE-61 was directionally drilled in ESE direction and the aim was to explore the geothermal system to the east to intersect fracture related to fumaroles seen in the region. The drilling of HE-61 was completed in April 2018 at 1848 m depth. The well was drilled directionally to a measured depth of 1857 m in the direction of 100° with an inclination of 3°. The directional drilling kick off point (KOP) is at depth of 320 m. The true vertical depth is 1620 m. The well is of the wider type with 13 3/8" production casing to 1035 m depth and 9 5/8" liner to 1834 m depth. Other wells at Hverahlid have 9 5/8" production casings and 7" liners. The casing information is summarized in Table 11.

Table 11. Depths and casing depths in well HE-61 with respect to ground surface and casing information's.

Bit size (inch)	Well depth (m)	Casing type	Casing depth (m)	Casing size (inch - OD)
26	100	Conductor	97.5	22 ½
21	300	Surface	296.4	18 5/8
17 ½	1044	Anchor	1043	13 3/8
12 ¼	1857	Production	1844	9 5/8

Two injection tests were performed in well HE-61 after the drilling was completed on April 15-16 and on April 18. The first test on April 15-16 was a two-step test with the pressure gauge at 1350 m depth. In the first step the injection was changed from 14.5 to 40.2 L/s and in the second step the injection was reduced from 40.2 to 14.4 L/s. The duration of both steps was about 2 hours. The pressure response during the first test is shown in figure 14. It is a rather scattered response due to internal flow in the well. The response was analysed and the injectivity index determined for the steps, resulting in $II = 51.4$ L/s/bar for the first step and 54.9 L/s/bar for the second step of the first injection test (Table 12). This is very high injectivity index, suggesting that the well is in good connection with a highly permeable reservoir.

The second injection test, which was carried April 18, was also a two-step test carried out after the liner had been lowered into the well. The pressure gauge was at 1250 m during the test. The injection was increased from 20 to 44.1 L/s in the first step and reduced from 44.1 to 24.1 L/s in the second step. The first step lasted about 3 hours but the second for 2 hours. The pressure response during the second test is shown in Figure 14. It is rather scattered, as in the first injection test, due to internal flow in the well. The response was analysed and the

injectivity index determined for the steps getting $II=33.5$ for the first step and 47.6 L/s/bar for the second step (Table 12). The difference is partly because the first step is longer than the second. If using only the pressure response for the first 2 hours of step 1 an $II =40$ L/s/bar is obtained.

Table 12. The injectivity indices calculated from the pressure changes during the injection tests in April 2018 in well HE-61.

Date	Step	Depth (m)	Pressure (bar)			Injection (l/s)			II (l/s)/bar
			Before	After	dP	Before	After	dQ	
15-16.4.18	1	1350	91.7	92.2	0.5	14.5	40.2	25.7	51.4
	2	1350	92.2	91.73	0.47	40.2	14.4	25.8	54.9
18.4.18	1	1250	83.48	84.2	0.72	20	44.1	24.1	33.5
	2	1250	84.2	83.78	0.42	44.1	24.1	20	47.6

When performing the well test analysis, many models were tested by performing a nonlinear regression in order to find the best fitting model for the measured data. Table 13 and 14 show the selected initial parameters and the selected reservoir model for the WellTester analysis of the injection test data.

*Table 13. Initial parameters used in the well test analysis of HE-61 where those marked with * must be inserted by the user to get a meaningful output from the WellTester.*

Name of Parameters and units	HE-53
Estimated reservoir temperature [°C]	300
Estimated reservoir pressure [bar-g]	83.9
Wellbore radius, r, [m]	0.16
Porosity, ϕ	0.1
Dynamic viscosity of reservoir fluid, μ , [Pas]	1.95×10^{-5}
Compressibility of reservoir fluid. c_w , [Pa ⁻¹]	1.94×10^{-7}
Compressibility of rock matrix, c_r , [Pa ⁻¹]	2.44×10^{-11}
Total compressibility. C_t , [Pa ⁻¹]	1.94×10^{-8}

Table 14. Model selected for injection tests in wells HE-61

Reservoir	Dual porosity
Boundary	Constant pressure
Well	Constant skin
Wellbore	Wellbore storage

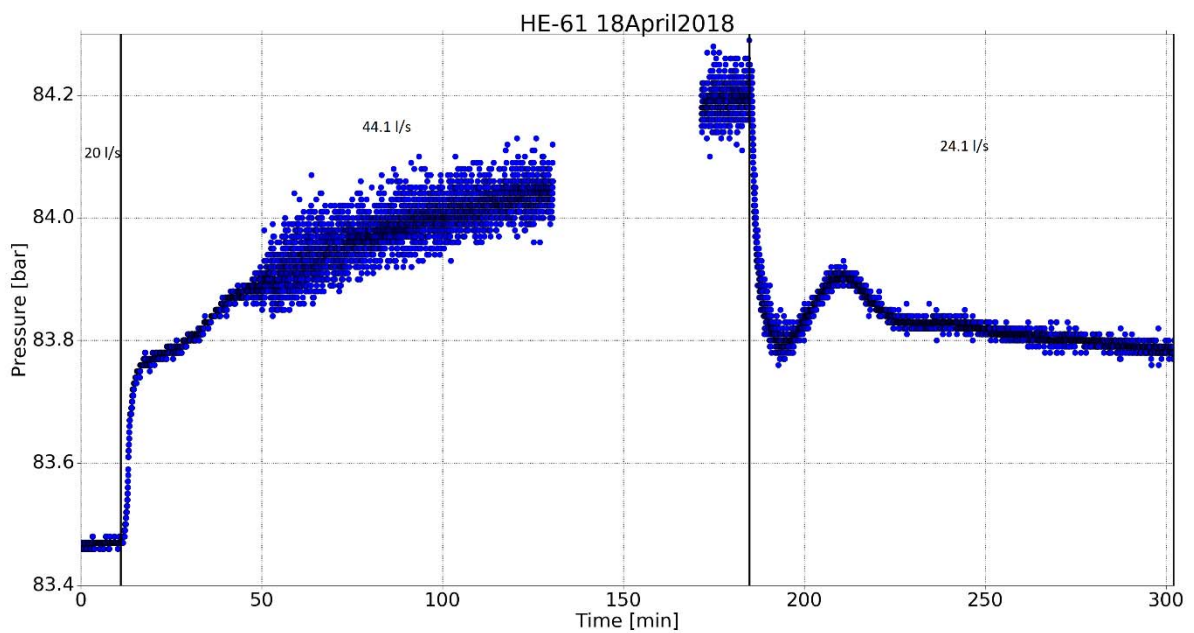
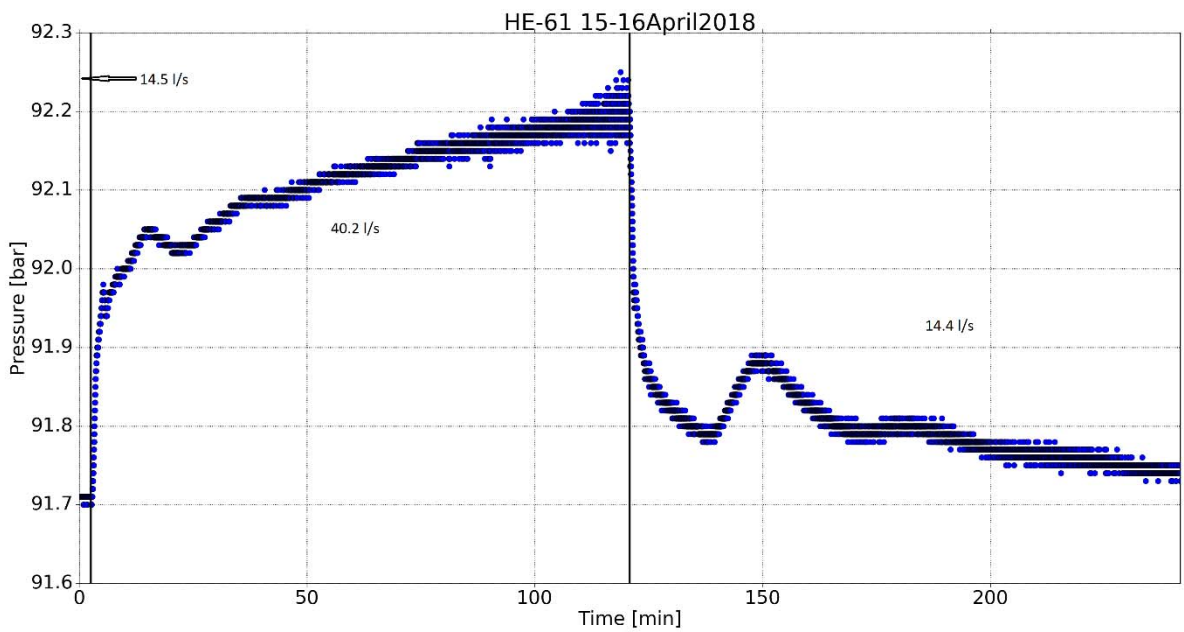


FIGURE 14. HE-61 pressure response against time in two injection steps with at total duration of 4 hours 15-16th (above) and 5 hours on 18th April (below).

The well test model selected for HE-61 assumed a dual porosity reservoir, constant pressure boundary, constant skin and a wellbore storage. The pressure gauge depth was an input into the program and the data were cleaned. Modeling was performed on both injection tests in well HE-61, i.e. the first test from 15 to 16 April and the second test from 18th of April 2018.

A summary of reservoir parameters estimated using nonlinear regression model for well HE-61 is presented in Table 15 and the best model fits of step 2 are shown in Figure 15 and summarized in Table 15. The model results are given in Table 15 for the best step. The second step of the injection test gives the best fit for both injection tests, out of the two 15-16th April 2018 injection test gives the best result and have been used to estimate parameters of the wellbore and the surrounding reservoir, summarized in table 15 and graphically shown in Figure 15.

Table 15. Summary of reservoir parameters estimated using nonlinear regression model for well HE-61 for the injection test on 15-16 April and 18 April 2018

Step 2		
Parameter	15-16th April 2018	18th April 2018
Transmissivity, T (m ³ /(Pa.s))	6.3×10 ⁻⁷	7.2×10 ⁻⁷
Storage coefficient, S (m/Pa)	2.12×10 ⁻⁷	4.26×10 ⁻⁷
Radius of investigation, r _e (m)	134	220
Skin factor, s	-0.21	-5
Wellbore storage, C (m ³ /Pa)	7.8×10 ⁻⁵	7.6×10 ⁻⁵
Reservoir thickness, h (m)	13400	1810
Permeability, k (m ²)	5.11×10 ⁻¹⁴	2.8×10 ⁻¹⁴
Injectivity index, II ((L/s)/bar)	68.2	64.4

The pressure response of the injection test on 15-16 April and on April 18 is scattered and does not reach a steady level in the first step, also showing irregular wavy behaviour in the beginning of the second step of both test and in the beginning of the first step in test 1. This behaviour is caused by internal flow in the well.

The model results obtained for the second step of the injection tests are shown in Table 15 and graphically for step 2 of the test of April 18 in Figure 15. The model results indicate that the well HE-61 is more open to flow during the first injection test (15-16 April 2018). This is clearly demonstrated by the injectivity index, II (Table 12 and 15), which is higher and suggests therefore that fractures are more open during the first test. The transmissivity values are of the order of $10^{-7} \text{ m}^3 / (\text{Pa s})$. The skin factor is negative, indicating that the well connection to the reservoir is not damaged and actually better in the second test where the skin factor -5 but -1 in the first test.

Injection Index (II) is estimated based on changes in pressure at change in the injection rate. Typically, when the pressure response to a step change in injection is theoretical, the pressure changes rapidly just after the injection step starts but the levels out reaching some pressure balance in few hours before the test is continued to the next step. This equilibrium value (or last pressure level) is usually used to calculate the injectivity index. The modeled II for step 2 of the injection tests of well HE-61 is between 64-68 (l/s)/bar (Table 15), which is a very high injection coefficient, but it should be noted that the pressure equilibrium was not reached in the steps when the measurement was stopped or the injection changed.

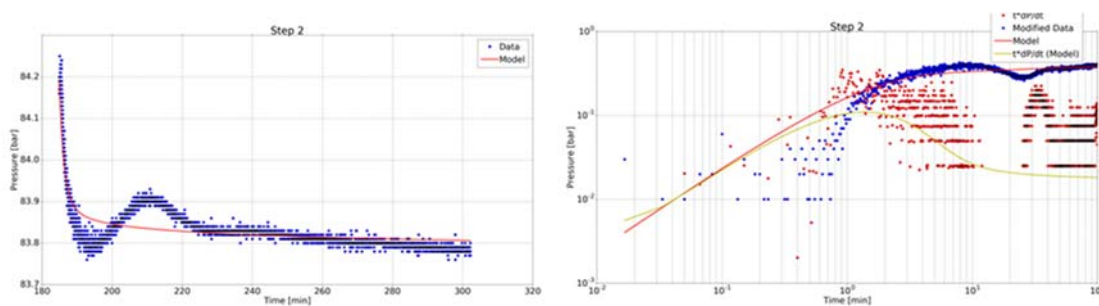


FIGURE 15. Model results and recorded pressure for step 2 for well HE-61 using a linear scale (to the left) and log-log scales (to the right) for the 18th April 2018 injection test.

4 Temperature and Pressure

In geophysics the word "log" is mainly related with continuous measurements carried out in boreholes and defined as a record of sequential data. Carrying out logs is important for two main reasons. Firstly, logs give information on well performance and design. This information is often needed during drilling when logs play important role in avoiding specific problems related to drilling. Secondly, logs provide information on structure, physical properties and performance of the geothermal system penetrated by the well (Stefansson and Steingrímsson, 1980).

The main starting task for the reservoir engineer is collection of data from geothermal wells. The data's include temperature and pressure, the most common measurements made in geothermal wells. Temperature and pressure logs are used highly in geothermal exploration and development. Their application kicks in with drilling in a green field development and

is carried throughout the life of a wellbore. Temperature and pressure logs are carried out during drilling of wells, during injection, during warm-up period after drilling and during flow testing. The downhole pressure-temperature data with downhole spinner/wellbore flow information are used to assess the condition of fluid state and flow within the wellbore and in the formation (Grant and Bixley, 2011, Steingrímsson, 2013).

Geothermal wells suffer from cooling during drilling due to circulation of cold drilling fluids to clean and cool the wells. Fluid losses into permeable fractures intersected by the well will cool the fracture zones and the geothermal reservoir surrounding the well. Temperature logs are run in wells during drilling for many purposes and rarely show the actual formation temperature drilled. In Iceland and in the geothermal world, it is a standard to log wells during drilling at casing depths and when the final depth is reached, and pressure logs are carried out when multi rate injection tests are performed at the end of drilling. Each temperature profile is evaluated and analysed to obtain information on the well. The information include (Steingrímsson, 2013):

- Location of feed zones accepting water during injection and their size.
- Evaluate internal flow (crossflow) in the wells during injection and during warm up after drilling.
- Temperature determination prior running other logging tools or drilling equipment into well, tool with limited temperature tolerance.
- Monitoring of the temperature recovery or warm up at well bottom over a period of few hours up to a day, can often be extrapolated to determine the true formation temperature at bottom.

The effect of the drilling operation on the temperature and pressure in a well during drilling will fade away through time when drilling operation stops. The well will heat-up and be in equilibrium with the surrounding in matter of several months and the well pressures will reach equilibrium with the permeable feed zones of the well. Temperature and pressure logs during the recovery period are used to estimate formation temperature and reservoir pressure. The heating of geothermal wells after drilling is monitored regularly by logging temperature and pressure tools with the aim of obtaining further information on permeable zones, to study flow between feed zones. However, the main objective in analyzing the temperature profiles after drilling is to estimate the temperature of the formations surrounding the well. Logs at later stages can improve the estimates. Generally, the aim of temperature and pressure logging in geothermal reservoir or wells is to determine formation temperature and reservoir pressure and evaluate boiling in the wells and the reservoir (Steingrímsson, 2013).

Different methods are used to determine the temperature and pressure of the formation being drilled. Formation temperature can be estimated by extrapolation of a short-term temperature data from the well logs during warm up period at selected depth for each estimation using Horner plot method. The Horner plot method is a simple analytical method used for analysing temperatures to estimate the formation temperature (Helgason, 1993). The basic criterion for the technique is the linear relationship between the measured temperature at selected depth and $\ln(\tau)$:

$$\tau = \frac{\Delta t}{\Delta t + t_0}$$

Where τ is the Horner time, Δt is the time passed since circulation (heat-up time) has stopped and t_0 is the circulation time i.e. the cooling time at the specific depth.

The formation temperature is calculated using:

$$T(\Delta t) = T_f + A * \ln(\tau) \quad (26)$$

Where $T(\Delta t)$ is the heat-up time, T_f is the final temperature = formation temperature and A is a constant.

By applying equation 26 one can plot the wellbore temperature at the selected depth from logs during the recovery period as a function of $\ln(\tau)$ and then plot a straight line through the data. Extrapolation to infinite heat-up time the Horner time (τ) will approach one and $\ln(\tau)$ become zero. This gives an estimate of the formation temperature (Helgason, 1993). A computer software from the ICEBOX package, BERGHITI, is used for estimation of formation temperature using the Horner plot method (Arason et al., 2004).

The initial reservoir pressure is estimated from data obtained during the heat-up period. The initial reservoir pressure is plotted together with the heat-up pressure profiles to determine their intersection. This intersection is known as pivot point which shows the depth and pressure at the best feed-zone in the borehole and can be considered as the actual pressure value in the reservoir at this depth. This is determined with the help of another software called PREDYP from ICEBOX (Arason et al., 2004) by feeding the obtained formation temperature values and known water level. The water level is changed in PREDYP until the pressure at the depth of the pivot point matches the pressure in the logs.

The boiling point curve was considered, to determine if there is boiling in the well and the reservoir and at what depth. The boiling point curve for a wellbore was calculated considering the initial water level and feeding it to the program called BOILCURV from ICEBOX collection.

In the following sections, the temperature and pressure state of wells HE-36, HE-53, and HE-61 are analysed and interpreted with the aim of determining their formation temperature, initial pressure and locations of aquifers and their flowing regimes.

4.1 Analysis of T and P logs in well HE-36

Drilling of well HE-36 started in August 2007 and completed in October same year. The location of the well is shown on Figure 9. The casing depth and drilled depths with respect to ground surface and casing information is shown in Table 1

The heating of the well HE-36 after drilling started on October 23rd when injection into the well was stopped and the rig moved from the site. The first T&P logs were performed on November 15th after three weeks of heating. Five days later, on November 20th, the well was stimulated with cold water for few days. The well was then left for heating. Two T&P log were carried out during the heating period on December 6th, 2007 and March 18th, 2008. After that the well was opened for flow and dynamic T&P logs were performed on April 2nd. The well was then closed and measured next on July 29, 2008. Several T&P logs have been carried out during the last 10 years to monitor changes with time.

Selected temperature logs from HE-36 are plotted against the true vertical depth of the well, plotted with the boiling point depth curve (BPD) in Figure 16, and Figure 17 shows pressure logs from similar dates. The temperature profile during injection on October 22nd, shows feed zones at around 1100 m, where loss of circulation was encountered during drilling. Most of the down flow seems to flow out of the well above 1900 m but the rest flows out of the well close to 2050 m depth. Temperature logs during the heat-up period show down flow in the well from the feed zone at 1100 m flowing down to 1750 m, where most of the down flow exits the well and very little fluid movement seems to be below 1800 where the water heats gradually by heat conduction. This suggests that the feed zones at 1100 m and 1750-1900 m depth are the main feed zones of the well. The pressure logs during heat-up on December 6th, 2007 and March 18th, 2008 show pivot point at about 1750 m suggesting that the feed zone at 1750 m is more permeable than the one at 1100 m. The pivot point pressure at 1750 m was 132 bar.

Two dynamic temperature logs are shown in figure 16. They are from April 2nd, 2008 and April 4th, 2014. They show that the inflow during production is mainly from the feed zones at 1750 and 1100 m. In general, the temperature logs show two major feed zones at 1100 m and 1750-1900 m depths. Smaller feed zones are also seen at around 1350-1400 m and 1550 m depth.

Figure 16 shows that the temperature in the well below the feed zone (1100 m) to the bottom of the well has changed little from 2010 to 2019. The highest temperature in the well is about 295°C at 1100-1200 m depth just below the feed zone at 1100 m. The temperature then declines gradually to 275°C at 1650 m where it drops to 250°C at 1660 m. Below this depth the logs show gradual heating with temperature reaching 275°C, at bottom (~2200 m). Temperature logs carried out late in the heat-up period and later, when the well was shut with no pressure on wellhead follow the BPD curve (Figure 16) from ~1200 m up to 800 and in some logs up to 400 m depth. Above 400 m, the temperature in these logs drops to 20-30°C, up towards the water level at 100-150 m depth. Temperature profile from 27-11-2009 shows an anomaly at 240-340 m depth where the temperature reaches more than 200°C. This high temperature is not linked to the true temperature in the formation at this depth but was caused by an underground blowout through ruptured production casing at 305 m depth in well HE-53, which is on the same drill pad as HE-36 only few tens of meters away (see figure 9). The underground blowout in HE-53 was immediately stopped and the casing filled temporarily with cement. Well HE-53 were repaired in August 2010 and the temperature logs in HE-36, performed after the repair, do not show the anomaly at 300 m anymore confirming successful reparation of the casing in well HE-53.

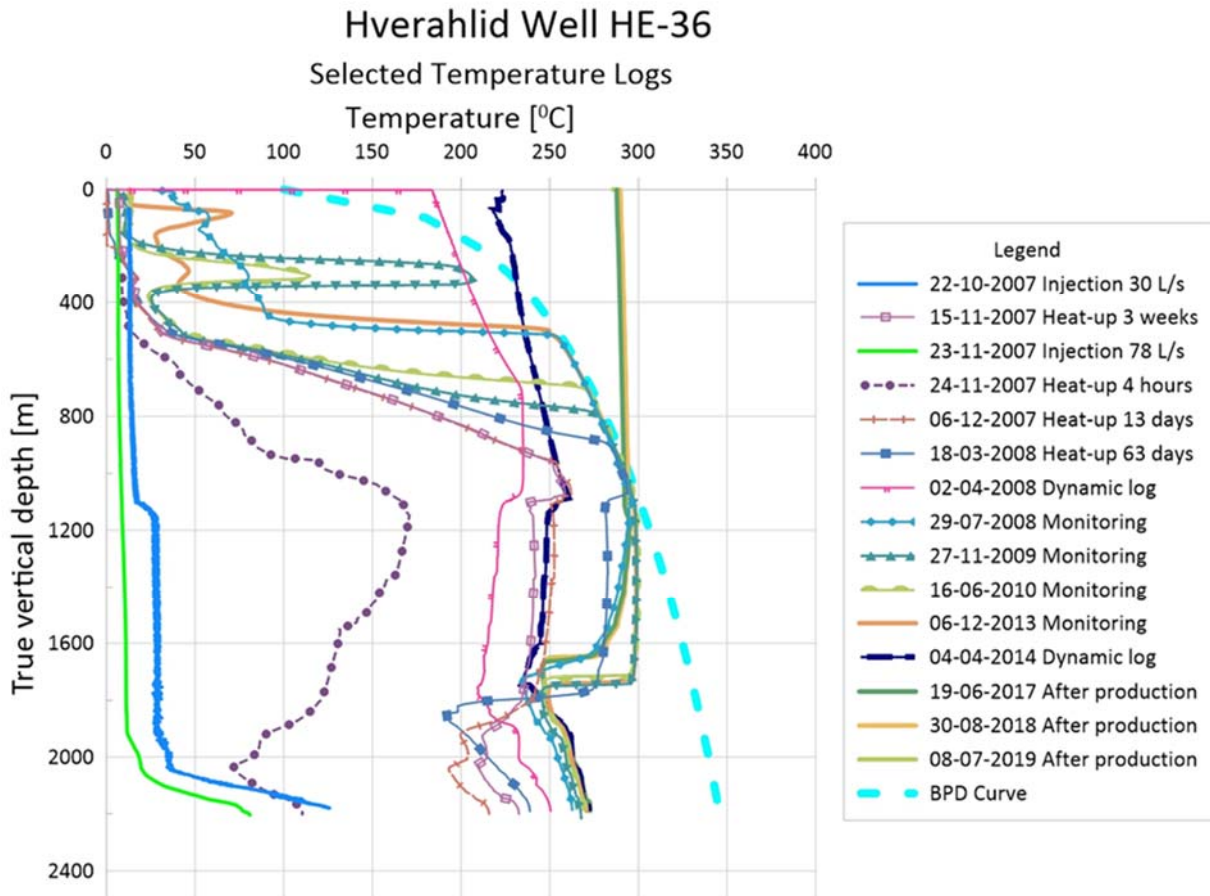


FIGURE 16. Well HE-36. Temperature logs during injection, heat-up, After a period of production

The pressure logs on Figure 17 give information on the pressure in the reservoir since the drilling of the well in 2007 and the changes up to 2019. The pressure log during the heat-up (December 2007 and March 2008) show a pivot point at 1750 m as mentioned earlier. This defines the initial reservoir pressure of the well in 2007. The pressure at 1750 m fell 1.6 bar from 2007 to 2013, probably due to production testing of the wells at Hverahlid. In 2013-2014 all the wells at Hverahlid were production tested and at the end of 2015 the field was connected to the Hellisheidi power plant and have been in production after that. The production from the field has caused continuous pressure drawdown in the reservoir. At the main feed zone in HE-36 the drawdown from 2013 to 2017 was about 7 bar and about 2 bars from 2017 to 2019. In total drawdown from 2007 to 2019 is therefore about 11 bar.

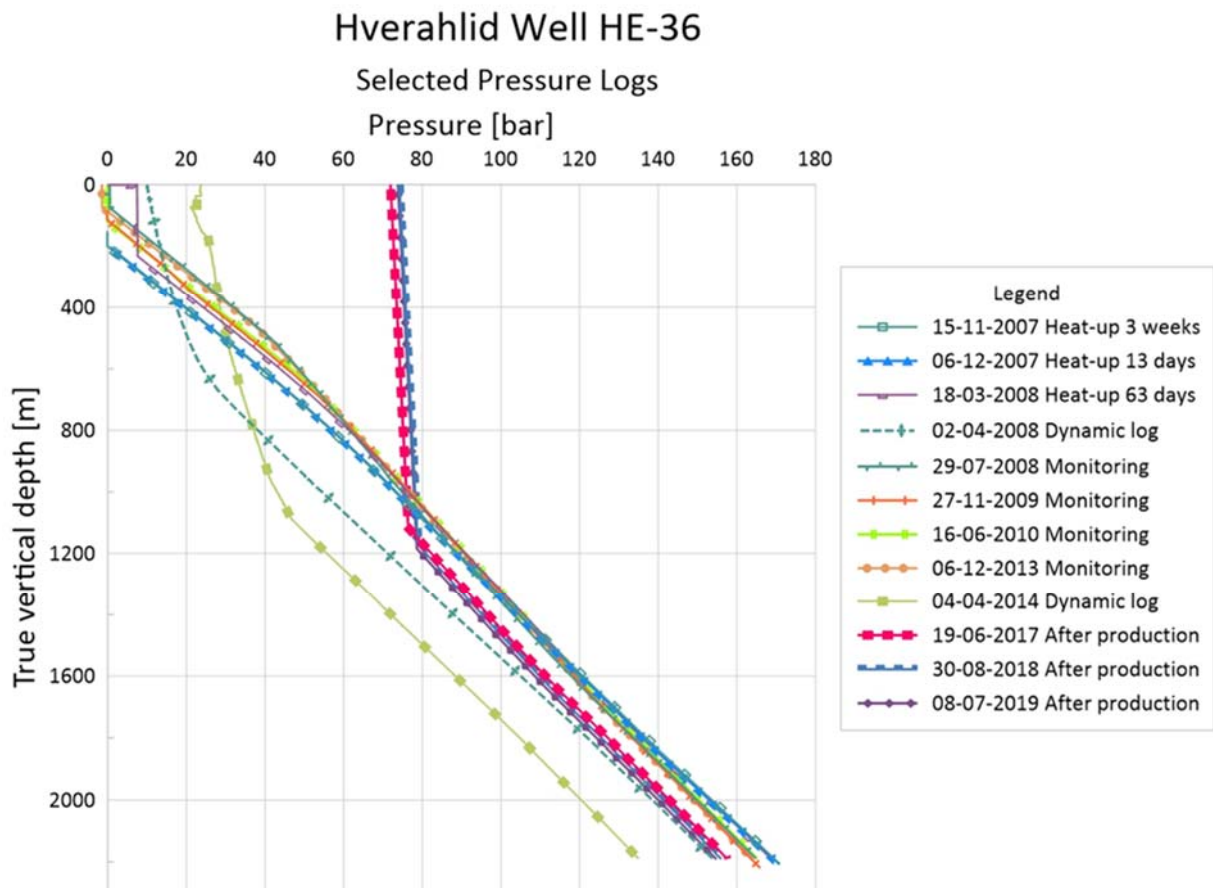


FIGURE 17. Well HE-36. Pressure logs during heat-up, after a period of production.

Formation temperature of HE-36 and reservoir pressure in 2008

The temperature logs in HE-36 (Figure 16) give clear ideas how to estimate the formation temperature profile of well HE-36 and the initial reservoir pressure can be determined by hydrostatic extrapolation from the measured pivot point pressure measured at 1750 m in December 2007 and March 2008, using the program “PREDYP”. The formation temperature and the initial reservoir pressure are shown in figure 18. The data points to be used in the BERGHITI programme were selected from the temperature logs at 1450 and 2125 m depth. Their formation temperature at these depths was determined with the Horner plot method in BERGHITI using data from the logs during heating. The results are shown as dark circles in Figure 18 and line connecting the points were drawn. Together with selected logs during heat-up, monitoring and after production. The estimated formation temperature for HE-36 is shown in figure 18. It is only 20-30°C down to about 400 m, as seen in temperature logs. Below 400 m the temperature rises rapidly with depth through the cap rock of the geothermal reservoir reaching boiling temperature ~285°C at about 800 m depth. The formation temperature profile follows the boiling point curve in the zone from 800 m to 1200 m depth, as seen in the logs, indicating boiling conditions in the reservoir with a maximum temperature of 302°C at 1200 m. Below 1700 m, there is an inversion in the formation temperature which starts increasing below 1800 m. Below 1800 m the formation temperature rises gradually reaching 280°C, at bottom. The cause for this inversion could be a cold water inflow into the system. The formation temperature profile is straight like linear

between the zones of boiling and temperature inversion. This shows convective heat flow in the zone is present due to the cross flow between the feed zones. The recent logs tend to follow the estimated formation temperature, suggesting that the well's temperature has reached equilibrium (Figure 18).

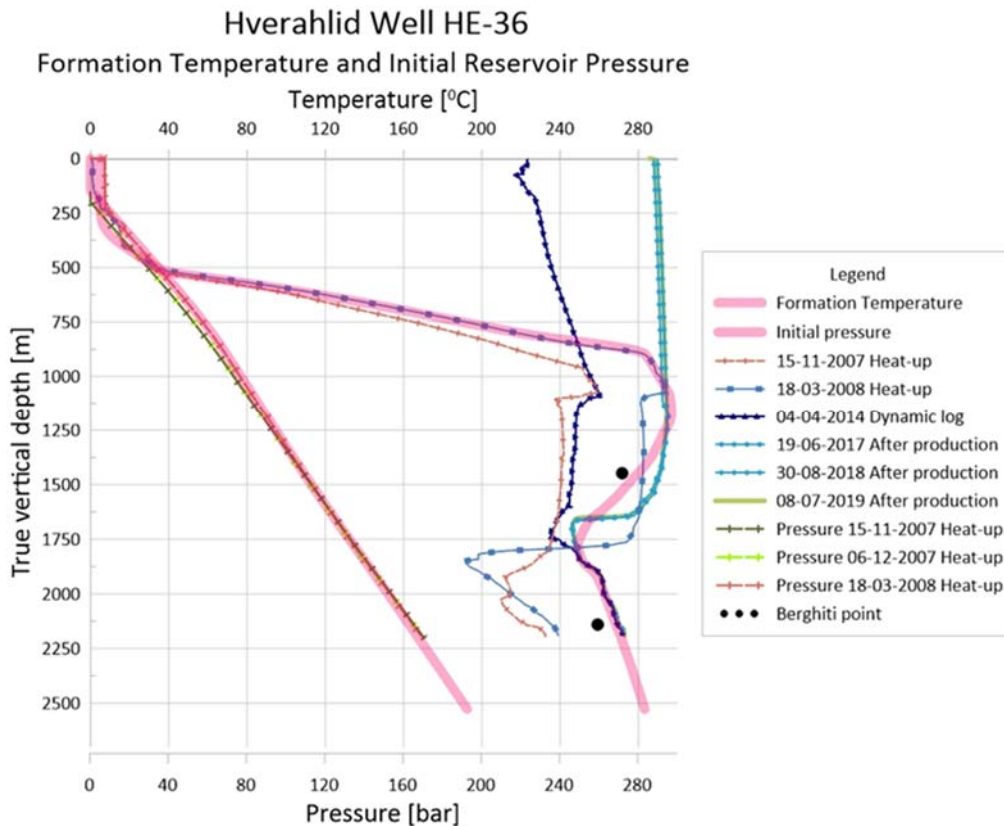


FIGURE 18. Estimated formation temperature and initial (2007/8) reservoir pressure for HE-36 and selected T&P logs.

To estimate the initial reservoir pressure, the estimated formation temperature from Figure 18 was used as input to the PREDYP program. The water level was adjusted in the calculations until the calculated profile matched the pivot point pressure, 135 bar at 1750 m. The hydrostatic pressure profile, calculated with PREDYP, that matched the pivot point pressure had water level at approximately 140 m depth. This is the initial (2007) pressure profile shown in Figure 17.

4.2 Analysis of T and P logs in well HE-53

The location of well HE-53 is shown in Figure 9 and the casing program of the well is shown in Table 6. Drilling of well HE-53 started in April 2009 and completed in June 16th, when injection into the well was stopped and heat up after drilling started as the rig was moved of the well. Two T&P logs were performed during the heating period on July 2nd, after 17 days of heating and on July 29th, after heating for 44 days.

Selected temperature logs from HE-53 are plotted against the true vertical depth and shown on figure 19 together with a boiling point depth (BPD) curve and figure 20 shows the

corresponding pressure logs. The temperature profile during injection on June 13th shows two main feed zones at around 1120-1250 m and at 2150-2200 m. Injection and heating logs suggests that the main feed zones are estimated to be at 1100-1300m, 1400-1500m, 1600-1700m and at 2180 m depth respectively. The well was opened to flow on June 30th, 2009 and discharged for the next few months. When the well was closed in November, the wellhead pressure rose to 100 bar. To reduce the pressure, bleeding of the gas was performed but the bleeding was unsuccessful and the pressure did not decline. Cold water was then injected into the well in order to kill the well but that was also unsuccessful. Temperature log showed high anomaly at 300 m depth due to leaking of hot fluid from damaged casing. This anomaly was seen in temperature logs in well HE-36, few tens of meters away from HE-53 as a 100 m wide temperature spike reaching 200°C at about 240 m -340 m depth in HE-36 (see Figure 16 in previous chapter). For a safety reason, it was decided to plug the well with cement to the bottom of the production casing (959 m). The operation was successfully completed. The cement was drilled out and 7" casing run to 607 m and cemented. After heating up after the repair, well HE-53 has been discharging most of the time and the few logs available are dynamic logs.

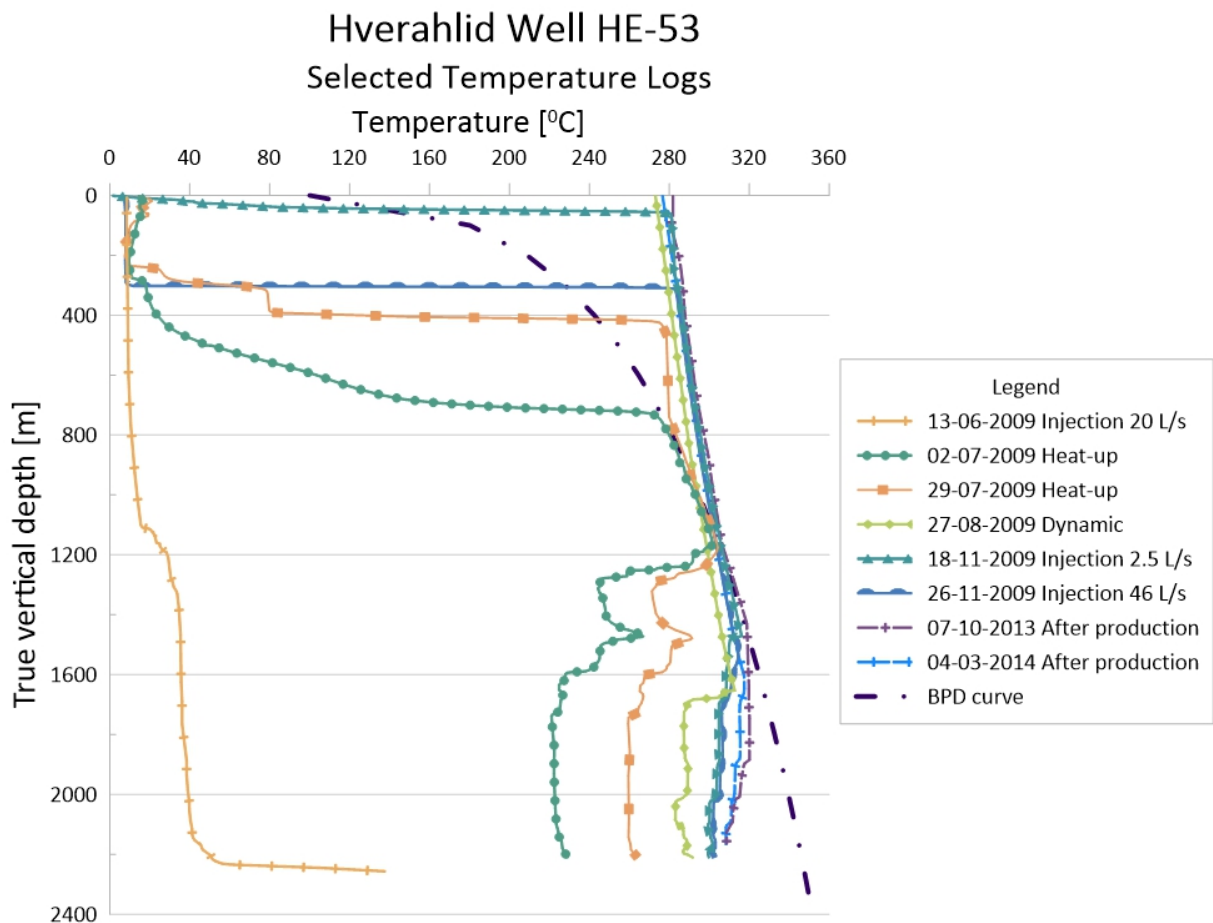


FIGURE 19. Well HE-53. Temperature logs during injection, heat-up, after a period of production.

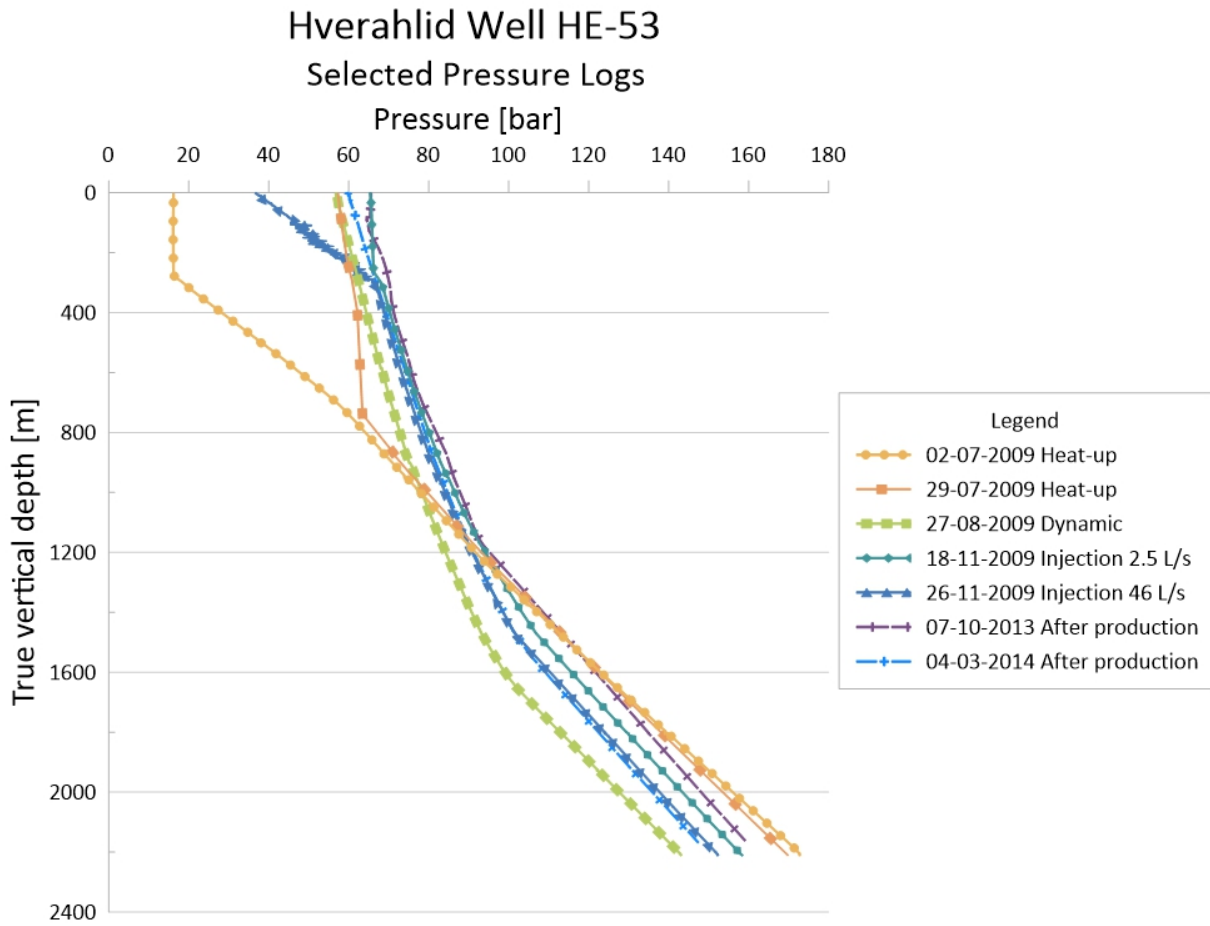


FIGURE 20. Well HE-53. Pressure logs during injection, heat-up, after a period of production.

The temperature logs on figure 19 show in the logs from 2013 and 2014 stabilized temperatures following the BPD curve from some 800 m down to about 1500 m where the temperature is 320°C. The temperature is slightly reversed below 1500 and to bottom where it is 300°C. The temperatures above 800 are in most logs controlled by boiling up flow of steam. The first log during the heat up (July 2nd, 2009) shows, however, the groundwater temperatures in the uppermost 400 m similar to what we saw in well HE-36 (Figure 16).

The pressure logs on figure 20 give information on the pressure in the reservoir since the drilling of the well in 2009. The pressure log during the heat-up in July 2009 show a pivot point at 1500 m depth. This suggest that the best feed zone of the well is close to 1500 m. The pivot point pressure value, 118 bar, defines the initial (2009) reservoir pressure at 1500 m depth. Later pressure logs are disturbed by injection and production and can't be used to determine accurately reservoir conditions at the time.

Formation temperature of HE-53 and reservoir pressure in 2009

The data points to be used in the BERGHITI programme were selected from the temperature logs at 1200 m, 1500 m and 2180 m depth. Their formation temperature at these depths was determined with the Horner plot method in BERGHITI using data from the logs during

heating. The results are shown as dark circles in Figure 21 and line connecting the points were drawn. An estimated formation temperature profile for HE-53 is shown in Figure 21 it starts out similar to well HE-36 with ground water temperatures (20-30°C down to 400 m, where the temperature rises fast through the cap rock of the geothermal system reaching boiling temperature of 280°, at 700 m depth. The formation temperature profile seems to be higher than the boiling point curve at a depth of 800-1600 m, indicating steam dominated conditions in the zone with a temperature in the range of 280-320°C. The estimated formation temperature at bottom of the well is about 312°C. The estimated formation temperature tends to follow the most recent logs as it is assumed that the well has reached equilibrium with the geothermal reservoir.

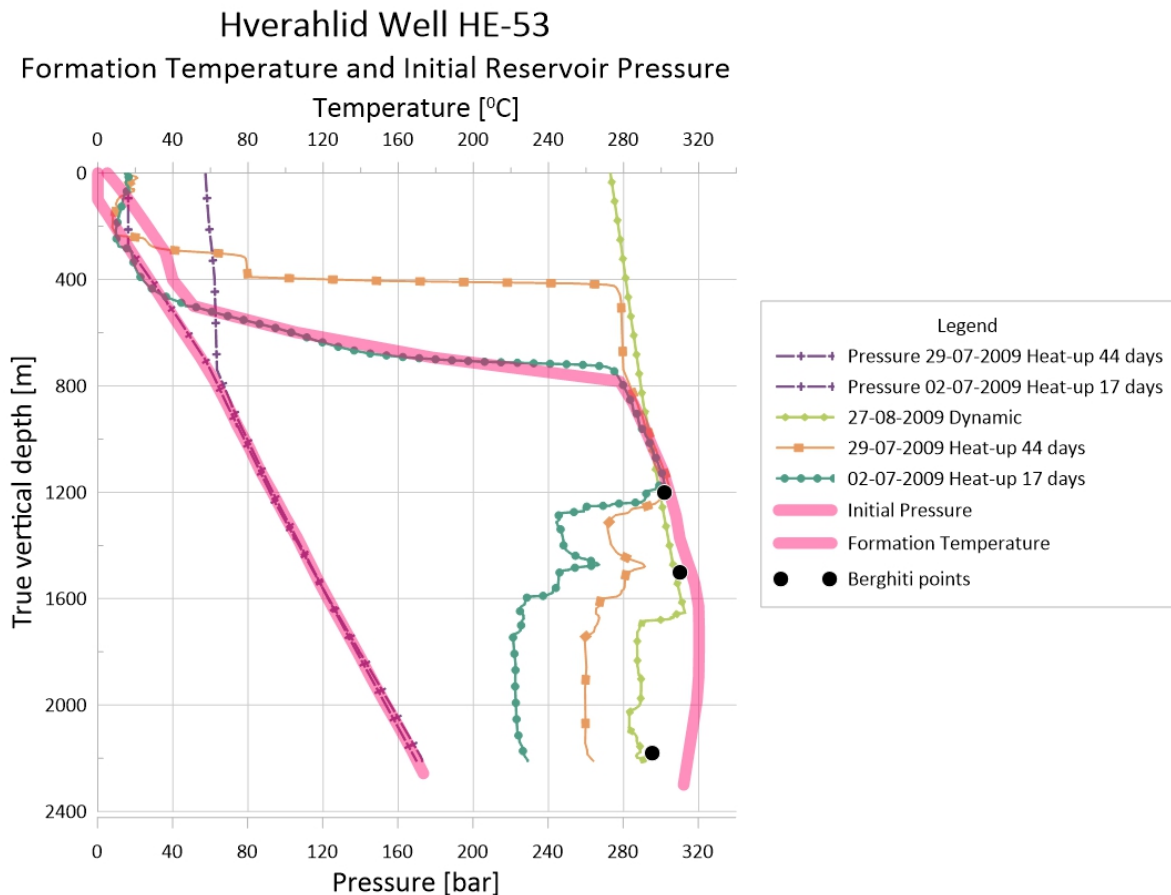


FIGURE 21. Estimated formation temperature and initial (2009) reservoir pressure for HE-53 and selected T&P logs.

To estimate the initial reservoir pressure, the estimated formation temperature from Figure 21 was used as input to the PREDYP program. The water level was adjusted in the calculations until the calculated profile matched the pivot point pressure i.e. 118 bar at 1500 m. The hydrostatic pressure profile, calculated with PREDYP, that matched the pivot point pressure had water level at approximately 100 m depth. This is the initial (2009) pressure profile shown in Figure 21.

4.3 Analysis of T and P logs in well HE-61

The location of well HE-61 is shown in Figure 9 and the casing program in Table 11. Drilling of well HE-61 started on February 1st, 2018 and was completed on April 19th, 2018. Several T&P logs were carried out during the heating period of HE-61, on June 25th only 3 hours after the injection was stopped, and then on June 28th, July 3rd, July 12th, and the last on July 23rd. The well was opened for flow shortly after the last heat-up log was measured and has been in production since then.

The temperature and pressure logs during the heat-up are plotted against the true vertical depth in Figure 22 and Figure 23. The results of the logs during injection show feed zones at 1020 m, 1252 m, and 1333 m depth. The temperature logs during heating up show multiple inflows zones at 1020, 1130, 1177, 1211, and 1252 and even at 1272 m but then outflow at 1333 m depth. The temperature log from April 18th, shows a similar result as of April 15th, however, the inflow at 1272 m is more evident than in the older measurement. In a period of four weeks heating after injection was stopped, the well heats to a maximum temperature of 302°C at a depth of 1200 m. The heat-up temperature logs tend to follow the boiling point curve at 400-1200 m depth.

The pressure logs on figure 23 give information on the pressure in the reservoir in July 2018. The logs show a pivot point at 1140 m depth. This suggests that the best feed zones of the well are those at 1130 and 1177 m. The pivot point pressure value is 85 bar, which defines the initial (2018) reservoir pressure at 1140 m depth.

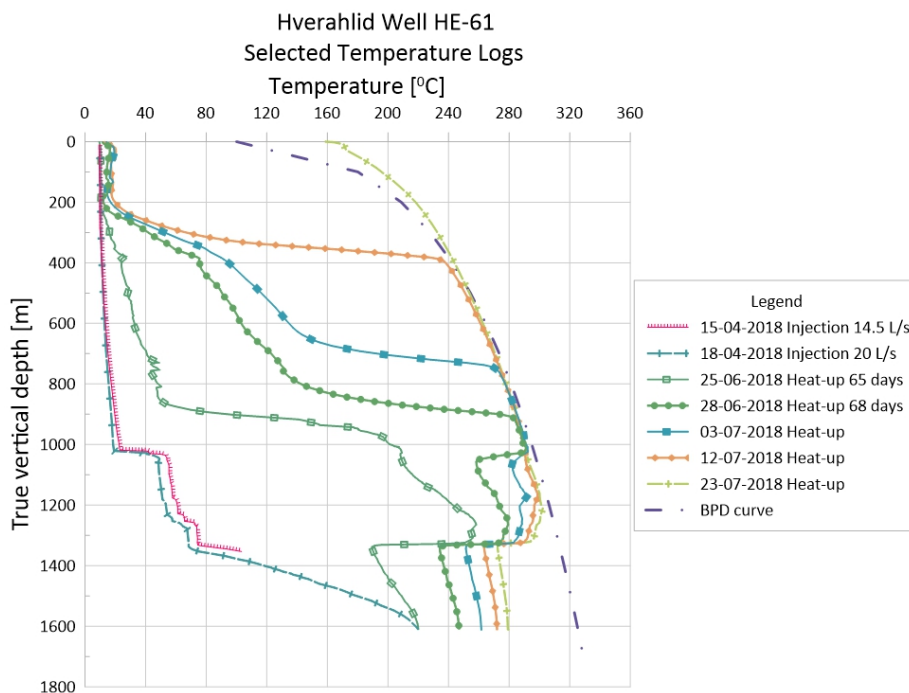


FIGURE 22. Well HE-61. Temperature logs during injection and heat-up. BPD-curve for reference.

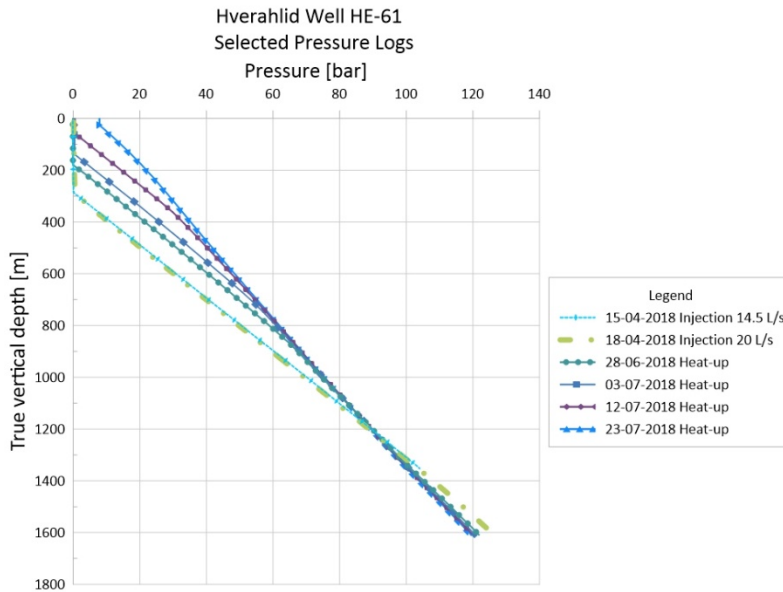


FIGURE 23. Well HE-61. Pressure logs during injection and heat-up.

Formation temperature of HE-61 and reservoir pressure in 2018

The data points to be used in the BERGHITI programme were selected from the temperature logs at 1100m and 1550 m depth. Their formation temperature at these depths was determined with the Horner plot method in BERGHITI using data from the logs during heating. The results are shown as dark circles in Figure 24 and line connecting the points was drawn. The formation temperature for HE-61 in figure 24 shows conduction in the casing. The formation temperature profile follows the boiling point curve in the zone from 400 m to 1250 m depth indicating steam dominated condition in the well with a maximum formation temperature of 310°C. Below 1250 m, the formation temperature and other temperature logs are below the boiling point curve indicating a liquid dominated reservoir at this depth with a maximum formation temperature of 280°C at the bottom. The recent logs tend to follow the estimated formation temperature, suggesting that the well's temperature has reached equilibrium. The formation temperature at bottom is about 280°C.

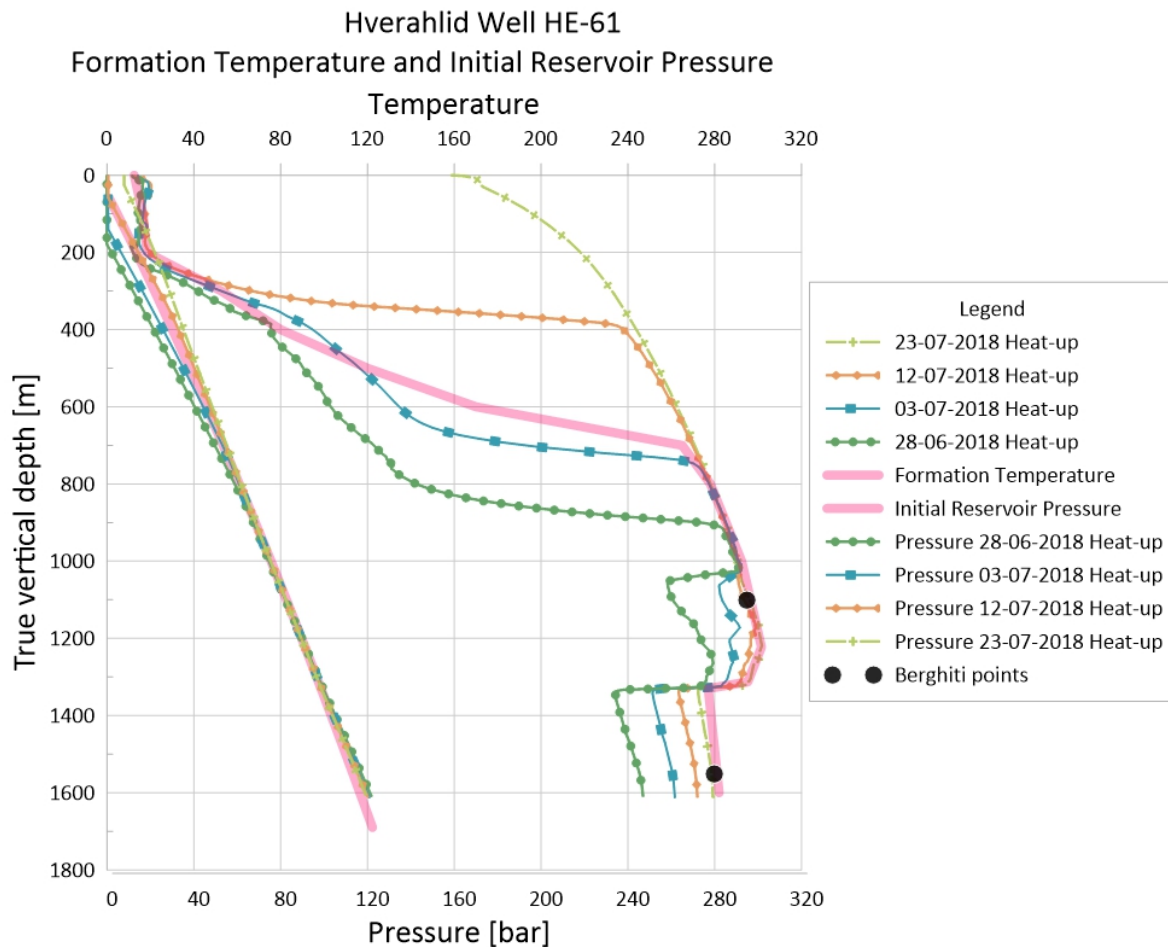


FIGURE 24 Estimated formation temperature and initial (2018) reservoir pressure for HE-61 and selected T&P logs

To estimate the initial reservoir pressure, the estimated formation temperature from Figure 24 was used as input to the PREDYP program. The water level was adjusted in the calculations until the calculated profile matched the pivot point pressure, 85 bar at 1140 m. The hydrostatic pressure profile, calculated with PREDYP, that matched the pivot point pressure had water level at approximately 50 m depth. This is the initial (2018) pressure profile shown in Figure 24.

5 Analysis of Discharge Testing

Upon completion of drilling of a geothermal well, the well is given a certain period to warm up and recover its temperature, after the cooling of the well during drilling. As temperature of fluid increases during the warm up period, the water level in the well rises and if boiling occurs below the water level, a wellhead pressure builds up. In many cases, the wells build up sufficient pressure at the wellhead to start well flowing to the surface, and sustain the flow (Grant and Bixley, 2011).

After the well has started to flow continuously, a discharge test is carried out with the main aim of getting information on the well's productivity and flow characteristics. Downhole measurements are also done where temperature and pressure (sometimes spinner as well) logging tools are lowered down to the bottom of the well and retrieved back to the surface. Equipment selection in terms of size and type is based on availability, accuracy and expected production rate, pressure and fluid type (steam/water ratio). A short time vertical discharge together with the James lip pressure method can be used to determine the suitable equipment for long time testing as well as to estimate the production rate.

For the James Lip pressure method, the liquid flow is measured in a V-notch weir while the vapor is allowed to escape into the atmosphere. In the long term testing we use RJ-pipe, silencer and weir box and we measure the critical pressure and water height in the weir box to calculate flow rate and enthalpy.

5.1 James lip pressure method

The lip pressure method is commonly used to measure the flow from geothermal wells. It is based on an empirical equation developed by Russell James (1966) and is considered the most versatile method for testing all geothermal wells. For medium enthalpy wells, we can use P_c , the pressure at the end of a straight pipe (James tube) and silica temperature to calculate the flow using the Russel James formula, but for high enthalpy wells we use P_c and water flow in the weir box. For steam wells, we use P_c and the enthalpy of the steam, which is determined from the wellhead temperature and pressure (steam tables).

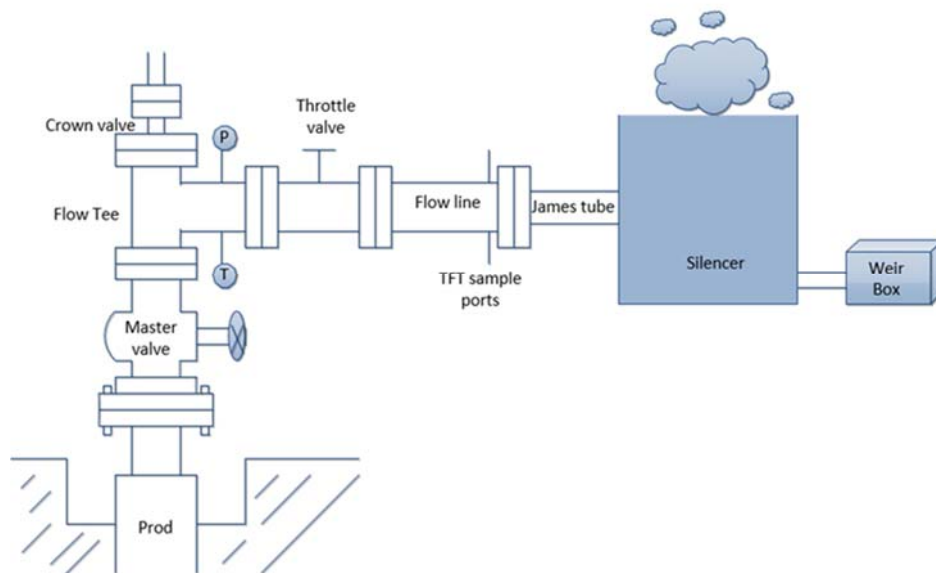


FIGURE 25. Schematic representation of the Russel-James lip pressure method.

To use this approach for the flow testing, the two-phase fluid is discharged through an orifice, flow line and a James tube into a silencer to separate the steam and water phases at atmospheric pressure (Figure 32). The lip pressure is measured at the extreme end of the

James tube using a liquid-filled gauge to damp out pressure fluctuations. Water flow from the silencer is measured using weir box near the silencer outlet (Grant and Bixley, 2011)

James's equation, which was tested for an enthalpy range of 400 – 2800 kJ/kg, links mass flow, m (kg/s), discharge pipe (James tube) area, A (m²), discharge enthalpy, H_t (kJ/kg), and lip pressure, P_{lip} (bar):

$$m = \frac{184 * P_{lip}^{0.96} * A}{H_t^{1.102}} \quad (27)$$

When the flow is measured in tonnes per hour the following equation is used:

$$m = \frac{663 * P_{lip}^{0.96} * A}{H_t^{1.102}} \quad (28)$$

The total mass flow rate obtained from lip pressure measurement can be related to water flow rate measured in the weir box after separation in the silencer (at atmospheric pressure):

$$m = \frac{H_s - H_w}{H_s - H_t} m_w \quad (29)$$

Where H_w is enthalpy of water and H_s is the enthalpy of steam.

By combining equations (27) and (29) we obtain:

$$\frac{m_w}{AP^{0.96}} = \frac{184}{H_t^{1.102}} \frac{H_s - H_t}{H_s - H_w} \quad (30)$$

The steam mass fraction, x can be calculated as:

$$x = \frac{H_t - H_w}{H_s - H_w} \quad (31)$$

By measuring the lip pressure, water flow, cross sectional area of the pipe, then the total enthalpy can be estimated. The enthalpies of steam and water can be obtained with the help of steam table from their corresponding temperatures and pressures.

With the help of the LIP program from the ICEBOX software package (Kjartan Marteinsson, 2016), the enthalpies and flow rates are calculated considering weir properties corresponding to a standard 90° V-notch weir box and head correction factor (0.00085 cm). Discharge coefficient (0.59) and weir notch angle (1.571 radians) are among the considered ones. For each well, enthalpy and mass flow rate parameters were calculated using the Lip program. The Lip program requires the input of the pipe diameter, the lip pressure (critical pressure) and the water level (height) in the weir box to calculate the mass flow rate and enthalpy.

5.2 Discharge Testing at Hverahlid

Due to the plans of connecting the production wells at Hverahlid to the Hellisheidi geothermal power plant, extensive production testing of the boreholes was performed in the winter of 2013-2014. The tests began on December 11, 2013 with opening of well HE-21 and ended on May 21, 2014 with the closure of well HE-36. The wells had all been flow tested shortly after drilling but for the decision to construct a separator station at Hverahlid and a long high-pressure steam and water pipeline from the separator station to the

Hellisheidi power plant, the productivity of the wells had to be verified by more detailed long term testing than had been done after drilling.

The wells were flow tested at different wellhead pressures to determine their output curves, and the wells were tested in 3 to 4 steps over 69-91 days period. An overview of the test time and the number of the steps is shown in Table 16.

Table 16 Summary of production tests of the Hverahlid wells in 2013-2014.

Well	Period	No. of days	Number of steps
HE-21	13-12-11 to 14-03-12	91	3
HE-36	14-03-12 to 14-05-21	70	4
HE-53	14-01-21 to 14-03-31	69	4

5.3 Discharge testing of well HE-21

Drilling of HE-21 was completed in February 2006. The well was flow tested for three and a half months from May to August 2006. The latest Russel-James flow measurement on August 30, 2006 at 25 bar-g WHP gave a total flow rate of 22.9 kg/s with enthalpy of 1815 kJ/kg. Assuming separation pressure of 17 bar-g the well would produce 11.1 kg/s of steam at these conditions.

Due to the planned connection of the wells at Hverahlid to the Hellisheidi geothermal power plant, well HE-21 was discharge tested again from December 11, 2013 to March 12, 2014 (Table 16). The well was tested in three steps with 100 mm orifice for 69 days from December 11, 2013 to February 18, 2014, with 75 mm orifice for 18 days from February 18, 2014 to March 8, 2014 and finally with 50 mm orifices for 4 days from March 9 to March 12, 2014. A 161 mm Russel James lip pipe was used throughout the test

Figure 26 shows the flow measurement parameters measured during the flow test of HE-21. It shows the wellhead pressure (WHP) pressure, the critical lip pressure (Pc) and the water height (h) in the V-shaped weir box when well HE-21 was discharge tested. While discharging through 100 mm orifice the WHP took less than one week to stabilize (Figure 26) at approximately 14 bar-g and became stable for the 75 and the 50 mm orifices at a pressure of 25 and 38 bar, respectively. While discharging during all the three steps, the water height in the weir box and the critical pressure never reached stabilization (Figure 26).

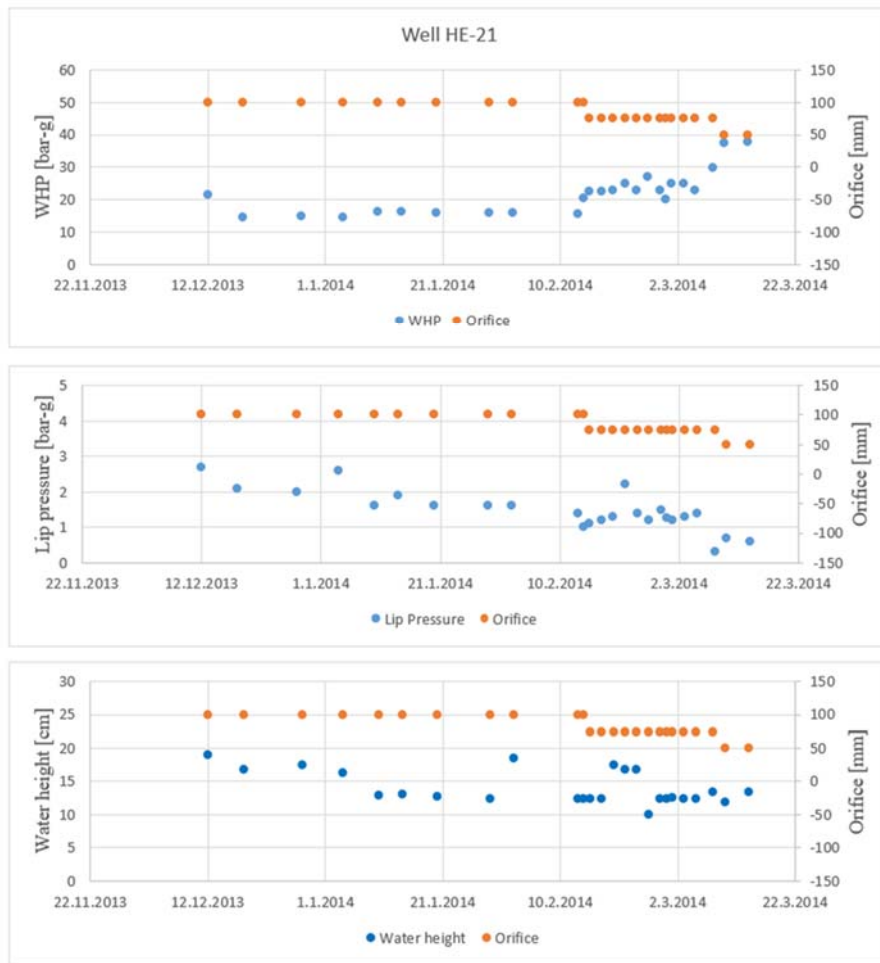


FIGURE 26. Summary of wellhead pressure (WHP), critical lip pressure and water height in the weir box during the discharge testing of well HE-21 in 2013-2014.

The calculated water, steam, total mass flowrate and fluid enthalpy of discharge test of well HE-21 is shown in Figure 27 and in Table 25 in the Appendix. At the beginning of the test and at the time of change of orifice, the flowrate is relatively high just after the well is reopened but the flow stabilizes with time. During the flow test, the total flow rate ranges from 16.3 to 41.2 kg/s and enthalpy ranging from 1340 to 2114 kJ/kg. The WHP ranged from 14.5 to 37.8 bar-g.

The analysis of the measurements during the discharge test of well HE-21 gives an estimate of steam flow in range of 6 – 13 kg/s assuming a separation pressure of 17 bar-g at Hverahlid. This steam flow is equivalent to 3 – 6.5 MW_e of electric power output assuming that 2 kg/s of steam will generate one MW_e. The steam flowrate at wellhead pressure of 14.5 bar-g was 10.4 kg/s, which is equivalent to 5.2 MW_e of electric power.

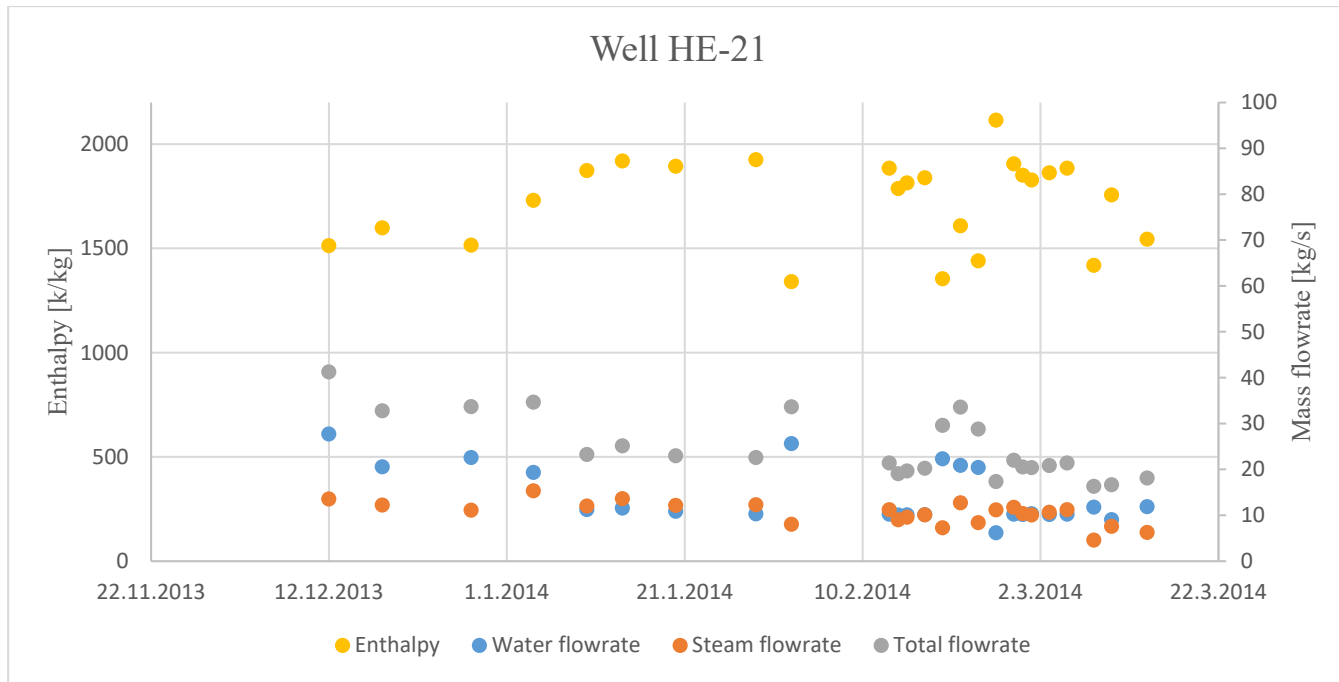


FIGURE 27. Summary of enthalpy and flowrates during the discharge testing of well HE-21 in 2013-2014.

Table 17. Measured and calculated values for well HE-21 by the James lip pressure method assuming a separation pressure of 17 bar-g.

Step No	Date	P ₀	P _c	Orifice	Lip-p	Weir-h	H _t	m _t	m _w	m _s
		bar	bar	mm	mm	cm	kJ/kg	kg/s	kg/s	kg/s
1	14-01-30	11.7	1.53	100	161	12.5	1906	22.2	14.6	7.6
3	14-02-28	21.3	1.05	75	161	13.5	1685	20.7	12	8.7
4	14-03-11	34.3	0.1	50	161	11.4	1574	15.6	10	5.6

The stabilized values in Table 17 are plotted in Figures 32-35. The characteristic curve of well HE-21, which shows the relationship between wellhead pressure and steam, water flow and total mass flow rate were created using relatively stable data at different wellhead pressure. The stabilized wellhead pressure of well HE-21 was 11.7 bar-g while using the 100 mm orifice. It rose up to 21.3 bar-g when the 75 mm orifice was used and 34.3 bar-g when the 50 mm orifice was used. The steam flow rate is about 4-15 kg/s. Well HE-21 fluid enthalpy is in the range of 1576 kJ/kg to 1911 kJ/kg. The curves are though relatively flat which indicates that the total flow rate remains constant for varying wellhead pressure. The curve indicates that the well produces about 27 kg/s of total flow rate at a wellhead pressure of 11.5 bar and produces about 12.4 kg/s at a maximum wellhead pressure of 34.3 bar. Decreasing or increasing the WHP will not have a great effect on the total flow rate.

5.4 Discharge testing of well HE-36

Drilling of HE-36 was completed in October 2007. In the spring of 2008, the well was flow tested for four months from March 16, 2008 to July 10, 2008. The Russel-James flow measurement in July 2008 showed that at 16 bar-g WHP a total flow rate of 59.5 kg/s with enthalpy of 1235 kJ/kg. Assuming separation pressure of 17 bar-g the well would produce 10.9 kg/s of steam, at these conditions.

Due to the planned connection of the wells in Hverahlid to the Hellisheidi geothermal power plant, well HE-36 was discharged during the period from March 12, 2014 to May 21, 2014 (Table 16). The well was tested in four steps with 100 mm for 29 days from March 12, 2014 to April 10, 2014, with 75mm for 8 days from April 10, 2014 to April 18, 2014, with 125 mm orifices for 30 days from April 18 to May 14, 2014 and again with 100 mm orifice for 1 day from May 15 to 16, 2014 as shown in Figure 28. Finally, an attempt was made to test the well with a 50 mm orifice but the well choked and the flow test was stopped on May 21. A 161 mm Russel James lip pipe was used throughout the test.

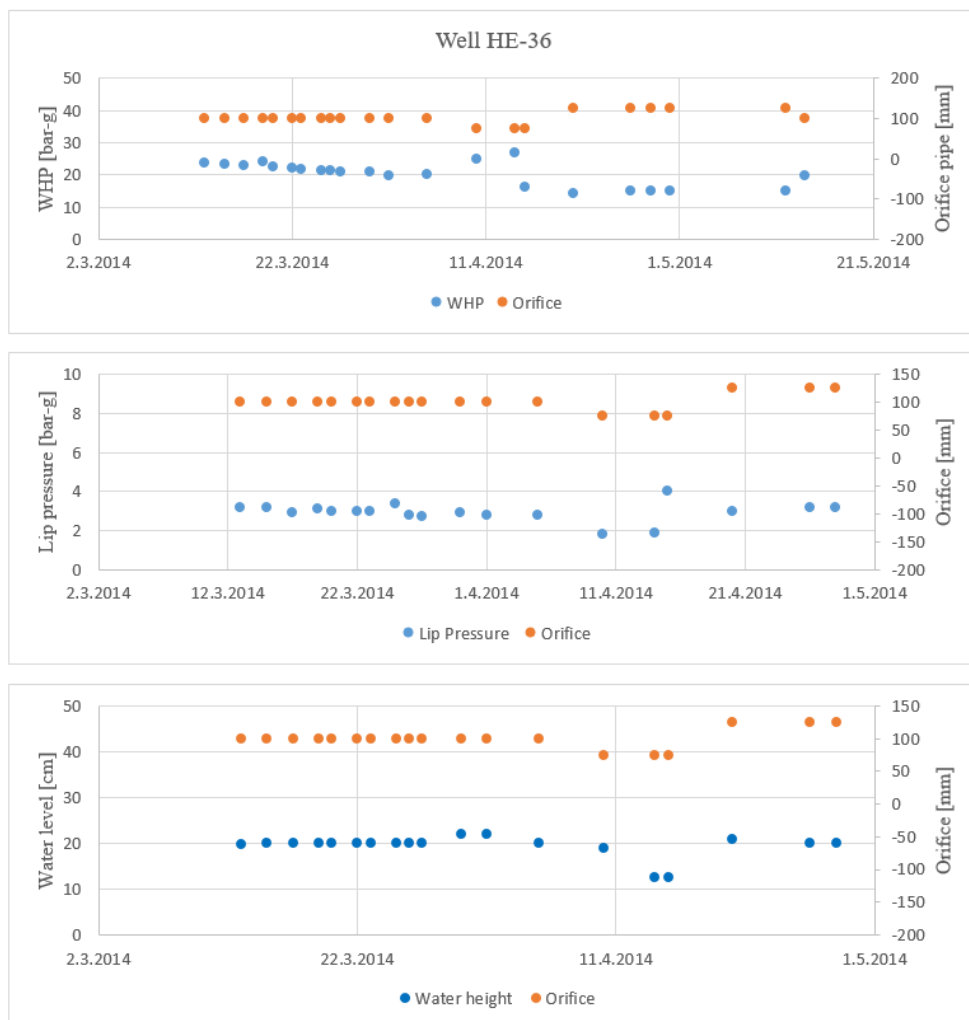


FIGURE 28. Summary of wellhead pressure (WHP), critical lip pressure and water height in the weir box during the discharge testing of well HE-36 in 2014.

The results of the measurements of the wellhead pressure, critical lip pressure and water height in a V-shaped weir box during the discharge test of well HE-36 is shown in Figure 28. During the first step (testing with 100 mm orifice), the well took relatively long time to reach equilibrium, WHP was still decreasing even after three weeks of discharging.

The calculated water, steam, total mass flowrate and fluid enthalpy of discharge test of well HE-36 is summarized in Figure 29 and Table 26 in the Appendix. The analysis of the measurements from the discharge test of well HE-36 gives estimates of steam flow in range of 9 – 15 kg/s at the separation pressure of 17 bar-g, which is equivalent to 4.5 – 7.5 MWe of electric power output, assuming that 2 kg/s of steam will generate one MWe. During the flow test of HE-36, the total flow rate ranges from 12 to 49 kg/s, the enthalpy was ranging from 1330 to 2280 kJ/kg and the WHP ranged from 14 to 26 bar-g.

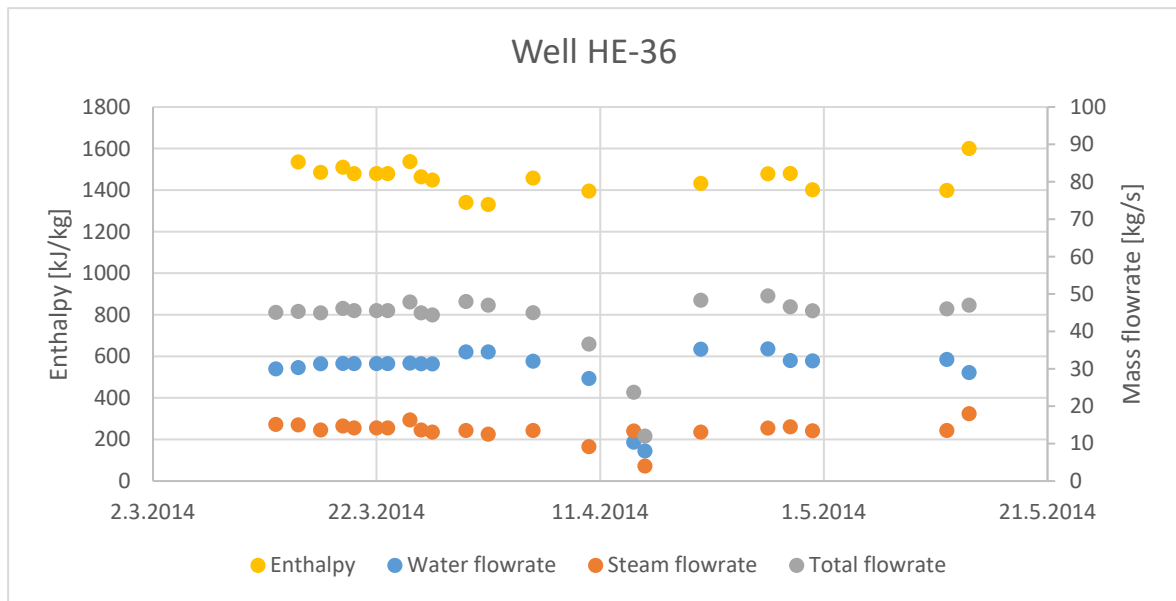


FIGURE 29. Summary of enthalpy and flowrates during the discharge testing of well HE-36 in 2014.

Table 18. Measured and calculated values for well HE-36 by the James lip pressure method with separation pressure of 17 bar-g.

Step No	Date	P0	Pc	Lip	orific	weir-h	H _t	m _t	m _w	m _s
		bar	bar	mm	mm	cm	kJ/kg	kg/s	kg/s	kg/s
1	14-03-27	20.8	1.7	161	100	20	1238	38.2	31.1	7.0
2	14-04-14	26.3	2	161	75	20	1302	41.8	32.7	9.1
3	14-05-06	15.6	1.7	161	125	19	1330	55	32.8	22.2
4	14-05-20	19.5	2.7	161	100	21	1357	56.5	36.5	20

The well characteristic curve of well HE-36 is shown in Figure 32-35. It shows the relationship between wellhead pressure and steam, water, total mass flow rate, and is based on the relatively stable data at different wellhead pressure shown in Table 18. The wellhead pressure of well HE-36 was 19.5 bar-g while using the 100 mm orifice. It rose up to 26.3 bar-g when the 75 mm orifice was used and fell to 15.6 when 125 mm orifice was used. The steam flow rate is around 7-11.4 kg/s. The output measurement at 19.5 bar-g WHP gives a total flow rate of 46.8 kg/s of which 11.4 kg/s is steam with enthalpy of 1352 kJ/kg. The steam flowrate at this wellhead pressure was 11.4 kg/s which is equivalent to 5.7 MW_e of electric power.

5.5 Discharge testing of well HE-53

Drilling of HE-53 was completed in June 2009. The well was flow tested twice in 2009 and 2010. The first test was conducted in the fall of 2009 for about two months; the result gave a total flow rate of 90.7 kg/s at wellhead pressure of 26-bar-g and 38.5 kg/s of steam assuming a separation pressure of 17 bar-g. The second test was performed in 2010 after repairing the casing damage at around 300 m depth as described in the previous chapter. The test was done for four months in the winter of 2010-2011, which resulted in a total flow rate of 46.5 kg/s at wellhead pressure of 35 bar-g and 26.8 kg/s of steam assuming 17 bar-g separation pressure.

Due to the planned connection of the wells in Hverahlid to the Hellisheidi geothermal power plant, well HE-53 was discharged during the period from January 21 to March 31, 2014, tested for two and half months. The well was tested in four stages with 100 mm orifice for 21 days from January 21, 2014 to February 11, 2014, with 125 mm orifice for 16 days from February 11, 2014 to February 27, 2014, with 50 mm orifice for 13 days from February 27, 2014 to March 12, 2014 and finally with 75 mm orifice for 19 days from March 12, 2014 to March 31, 2014 as shown in Figure 30. The figure shows the results of the measurements of wellhead pressure, critical pressure and water level in a V-shaped weir box during the discharge test of well HE-53 in 2014.

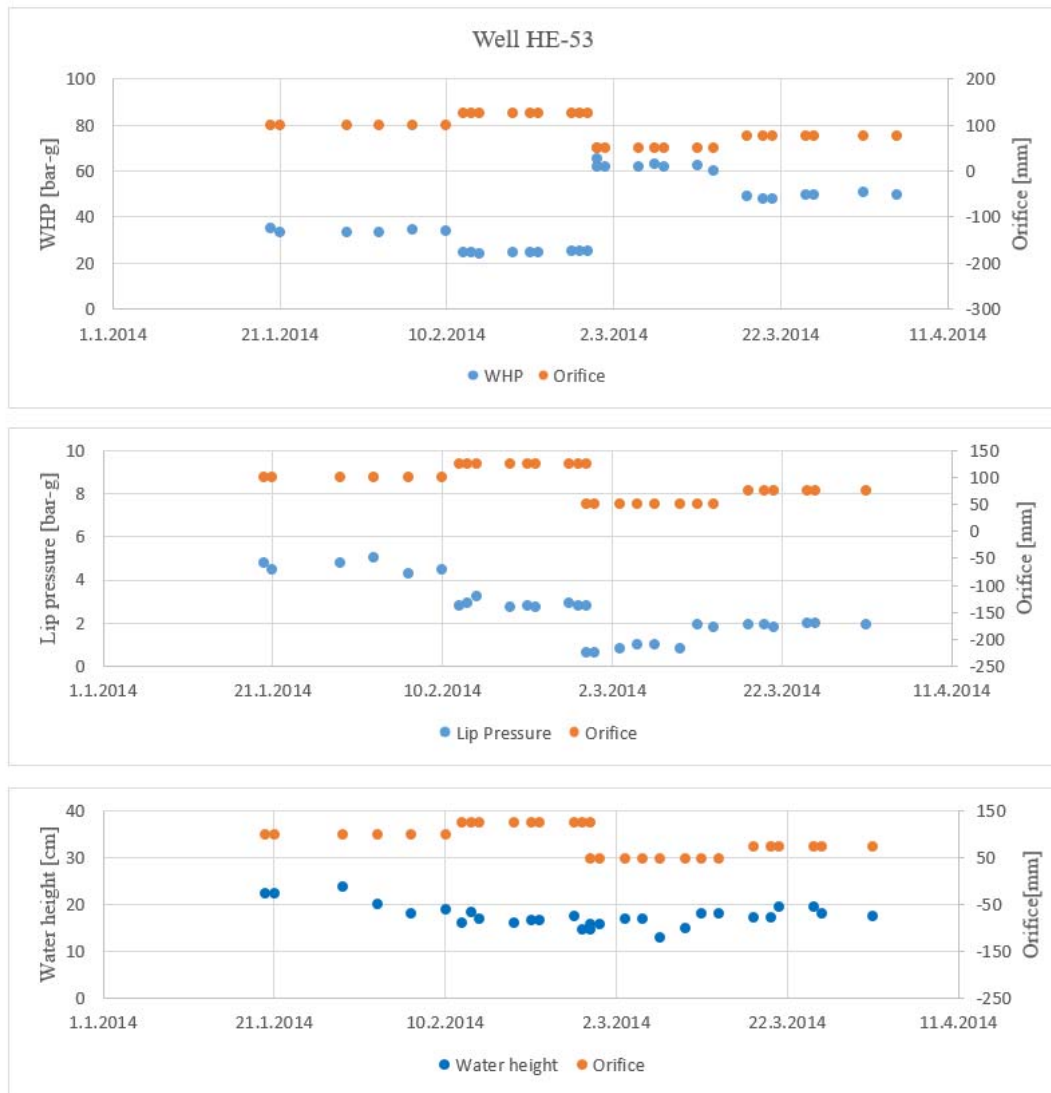


FIGURE 30. Summary of wellhead pressure (WHP) pressure, critical lip pressure and water height in the weir box during the discharge testing of well HE-53 in 2014.

The calculated water, steam, total mass flowrate and fluid enthalpy of discharge test of well HE-53 is shown in Figure 31 and Table 27 in Appendix. The analysis of the measurements from the discharge test of well HE-53 in 2014 gives an estimates of steam flow in range of 11 – 29 kg/s at the separation pressure of 17 bar-g which is equivalent to 5.5 – 14.5 MW_e of electric power output assuming that 2 kg/s of steam will generate one MW_e. The steam flowrate at the wellhead of 33.2 bar-g was 24.8 kg/s, which is equivalent to 12.41 MW_e of electric power. During the flow test, the total flow rate was ranging from 28 to 67 kg/s and the enthalpy was ranging from 1423 to 2134 kJ/kg, WHP was ranging from 23 to 65 bar-g.

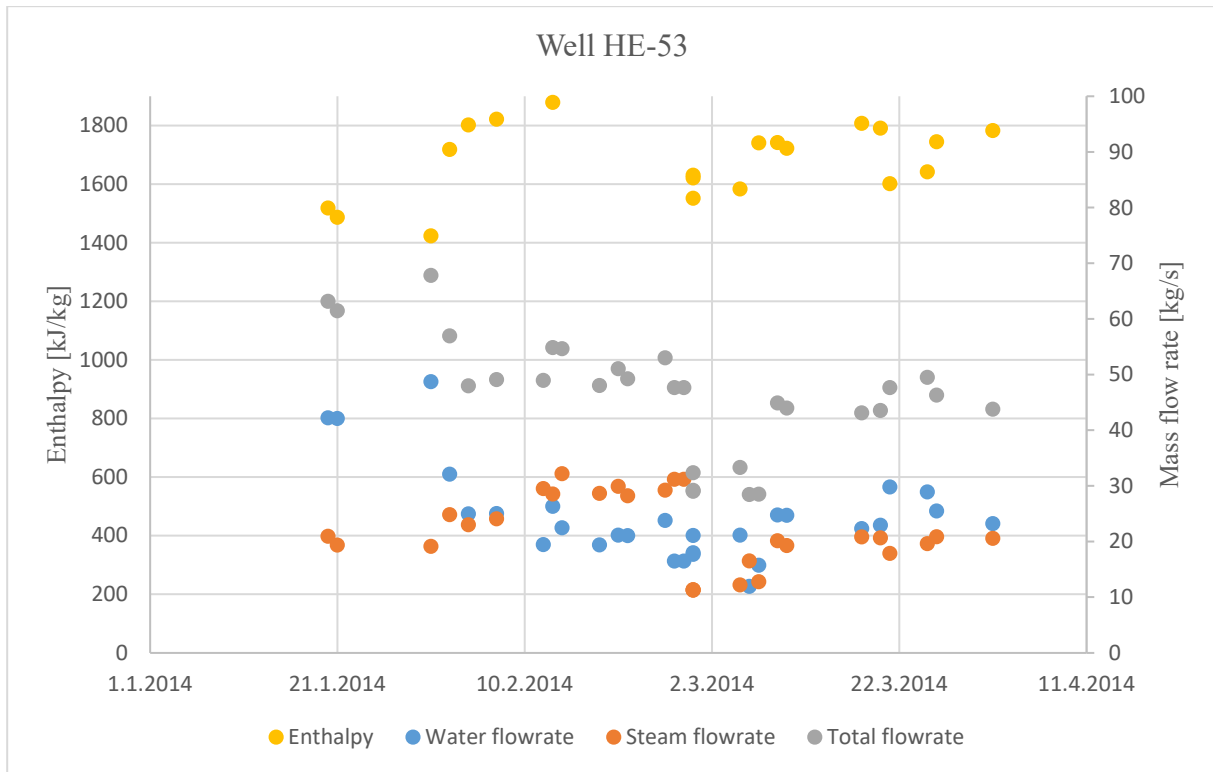


FIGURE 31. Summary of enthalpy and flowrates during the discharge testing of well HE-53 in 2014.

Table 19. Measured and calculated values for well HE-53 by the James lip pressure method with separation pressure of atmospheric pressure.

Step No	Date	P_0	P_c	Lip-p	orific	Weir-h	H_t	m_t	m_w	m_s
		bar	bar	mm	mm	cm	kJ/kg	kg/s	kg/s	kg/s
1	14-02-07	33.5	4.5	161	100	22.5	1602	61.9	23.2	38.7
2	14-02-25	24.3	2.9	204	125	18.3	1613	58.6	22.3	36.3
3	14-03-05	60	1.8	204	50	18	1493	28.9	9.2	19.7
4	14-03-27	49.3	1.8	204	75	19.5	1606	46.9	17.7	29.2

The well characteristic curve of well HE-53 is shown in Figure 32-35. It shows the relationship between wellhead pressure and steam, water, total mass flow rate and is based on relatively stable data at different wellhead pressure shown in Table 19. The wellhead pressure of well HE-53 was 33.5 bar-g while using the 100 mm orifice but fell to 24.3 bar for the 125 mm orifice. It rose up to 60 bar-g when the 50 mm orifice was used and fell to 49.3 bar for the 75 mm orifice. The steam flow rate at 17 bar separation pressure ranges from

17.9 to 28.6 kg/s, equivalent of some 9 to 14 MW_e. Well HE-53 fluid enthalpy ranges from 1485 kJ/kg to 1876 kJ/kg with increasing flowrate, but this is the result of steam flowrate increasing almost linearly with decreasing wellhead pressure but the curves are relatively flat.

The output measurement at 24.3 bar-g WHP gives a total flow rate of 55.1 kg/s of which 28.6 kg/s is steam with enthalpy of 1876 kJ/kg. The steam flowrate at this wellhead pressure is equivalent to 14.3 MW_e of electric power assuming 2 kg /s of steam will generate one MW of electric power.

5.6 Summary of selected discharge measurements

Figures 32 to 35 summarize the output characteristics of wells HE-21, HE-36 and HE-53 at Hverahlid where enthalpy, total flow, steam and water flow is plotted against the well head pressure (WHP) by picking stable values for each flow test step (the different orifices) during the flow testing of the well in 2013-2014. One of the main result from the flow test is that these wells can produce a cumulative total of 129.5 kg/s of steam and water or for all 3 wells:

HE-21: The flow test measurements show that at 21.3 bar-g well head pressure the total flow is 20.9 kg/s of which 8.7 kg/s is steam at a separation pressure of 17 bar-g with enthalpy of 1684 kJ/kg.

HE-36: The flow test measurements show that at 19.5 bar-g well head pressure the total flow is about 46.8 kg/s and with enthalpy of 1352 kJ/kg at a separation pressure of 17 bar-g, which gives a steam flow rate of 11.4 kg/s and water flow rate of about 35.4 kg/s.

HE-53: The flow test measurements show that at 33.5 bar-g well head pressure the total flow is 61.7 kg/s (1485 kJ/kg), of which 19.4 kg/s is steam at separation pressure of 17 bar-g.

The conclusion is that wells HE-21, HE-36 and HE-53 can cumulatively produce 129.5 kg/s of water and steam. If separated at 17 bar-g 39.5 kg/s of high pressure steam is produced. This is equivalent to about 19.75 MW_e of electricity, assuming that 2 kg/s of steam is needed to generate 1 MW_e.

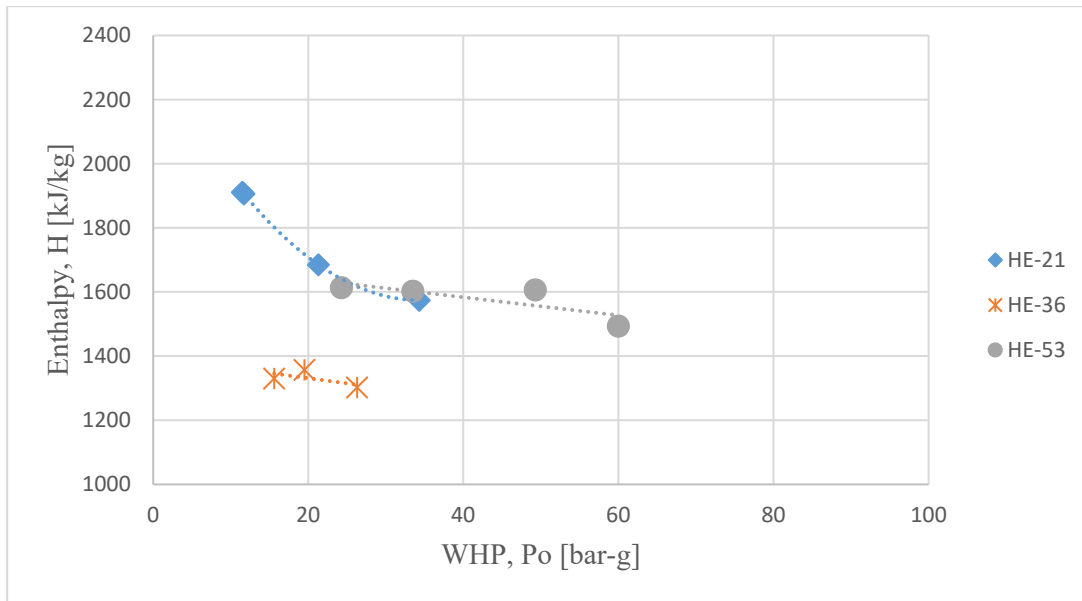


FIGURE 32. Comparison of the enthalpy of wells HE-21, 36 and 53 at Hverahlid at different WHP during the flow test in 2013-2014.

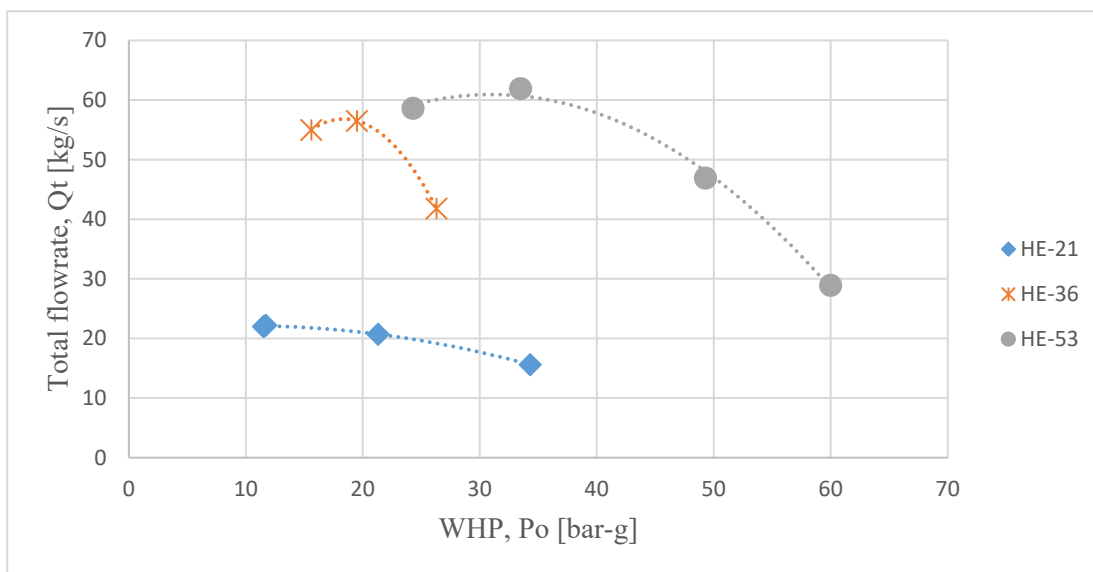


FIGURE 33. Comparison of the output curves (total flow steam+water) for wells HE-21, HE-36 and HE-53 at Hverahlid at different WHP during the flow test in 2013-2014.

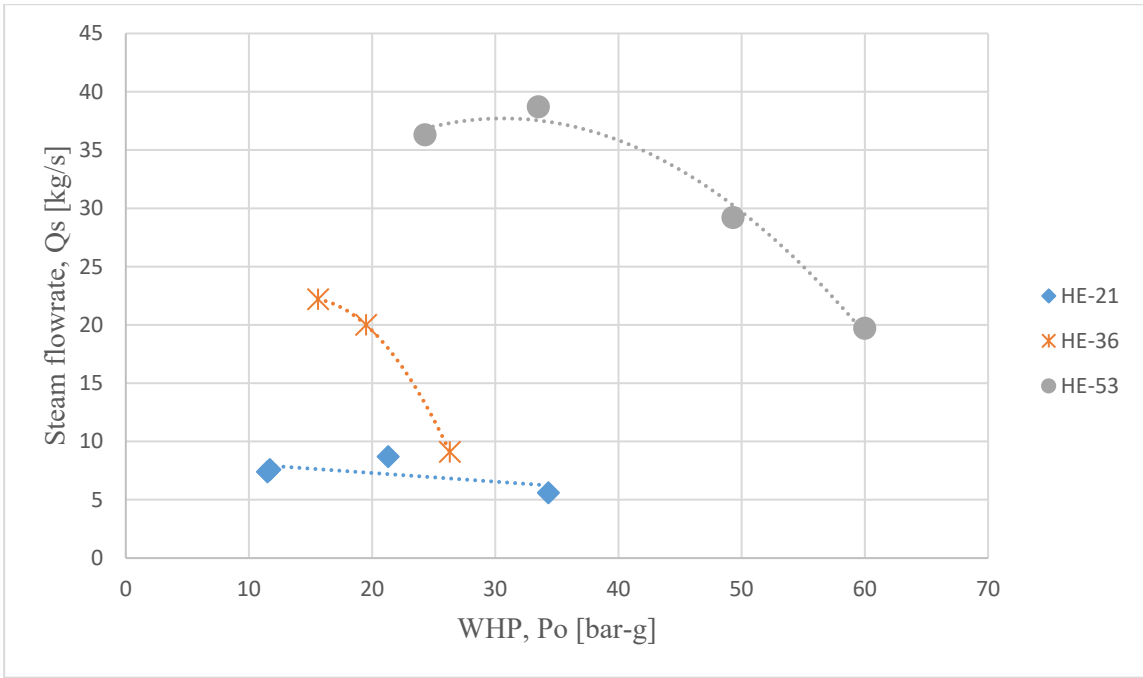


FIGURE 34. Comparison of steam flow at 17 bar-g separation pressure from wells HE-21, HE-36 and HE-53 at Hverahlid at different WHP during the flow test in 2013-2014.

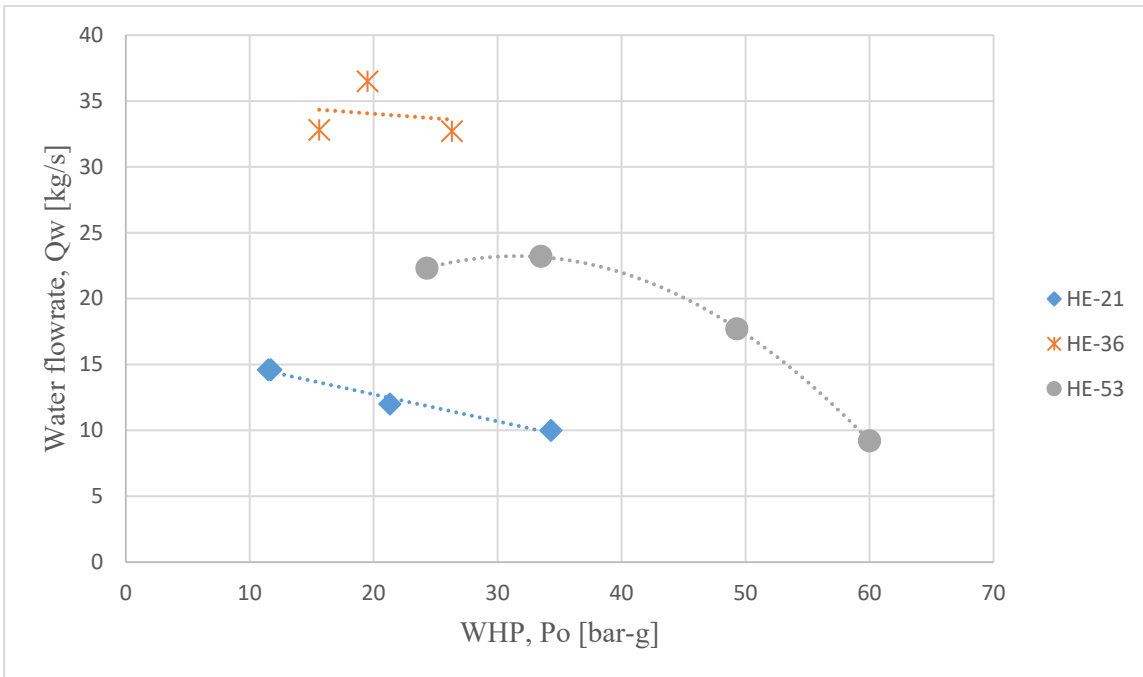


FIGURE 35. Comparison of water flow at 17 bar-g separation pressure from wells HE-21, HE-36 and HE-53 at Hverahlid at different WHP during the flow test in 2013-2014.

6 Power plants scenarios

Geothermal power plants can be categorized into two main groups. Steam cycle plants, which are used at higher well enthalpies, and binary cycle plants used for low enthalpy wells. The steam cycle allows the fluid to boil, and then the steam is separated from the brine and expanded in a turbine. The brine is either rejected to the environment or flashed again at lower pressure.

A binary cycle uses a secondary working fluid in a closed power generation cycle. A heat exchanger is used to transfer heat from the brine to the working fluid and the cooled brine is then rejected to the environment or re-injected.

To evaluate the geothermal electrical power potential of the Hverahlid system, three thermodynamic models were developed, single flash (SF), Double flash (DF) and combined single flash with ORC binary. The thermodynamic models of the geothermal power plants developed in this analysis are based on the lecture notes of the course Geothermal Power Plant Design at the University of Iceland (2018).

Designing process has been done for each of single flash, double flash and binary cycle. The waste heat from single flash cycle was also assumed to be used for combined single flash with ORC binary cycle case. The Engineering Equations Solver (EES) program was used to perform the calculations. Calculations for single and double flash cycles have been done by assuming a separator pressure or wellhead pressure. After calculation of all parameters, optimization to find separator pressure, which gives the most efficient cycle, in connection with steam quality, has been done.

6.1 Single flash power plant

The terminology single-flash system indicates that the geo-fluid has undergone a single flashing process, i.e., a process of transitioning from a pressurized liquid to a mixture of liquid and vapor, as a result of lowering the geo-fluid pressure below the saturation pressure corresponding to the fluid temperature. The process of flashing may occur in different places: (1) in the reservoir as the fluid flows through the porous formation along with a pressure drop; (2) in the production well anywhere from the bottom to the wellhead as a result of pressure drop due to friction and gravity head; or (3) in the separator as a result of a throttling process caused by a control valve or an orifice plate. In a newly developed geothermal field, flashing may occur in the wellbore initially, then with time as the field undergoes exploitation and the reservoir pressure drops, the flash point may move down and enter the formation.

A single flash process flow diagram (PFD) is shown in Figure 36. The flow sheet shows the most important equipment that affects the thermodynamics of the energy conversion process. The geothermal fluid enters the well at the source inlet temperature, point 1. Due to the well pressure loss, the fluid has started to boil at point 2, when it enters the separator. The brine from the separator is at point 7, and is re-injected. The steam from the separator is at point 4, where the steam enters the turbine. The steam is then expanded through the turbine thereby providing a mechanical force that rotates the turbine. The turbine is connected to a generator by a shaft that eventually generates electricity as the steam expands through the turbine.

After expanding through the turbine down to point 5, the steam is either released into the atmosphere in a back-pressure type power plant or the steam is sent to a cooling tower in a condensing type power plant, in this case condensing type is used. The condensate water is then either used as a make-up water in the power plant cooling system or re-injected with the separated brine at station 4. A typical thermodynamic process for a single flash cycle is shown in a Temperature-entropy (T-s) diagram (Figure 37).

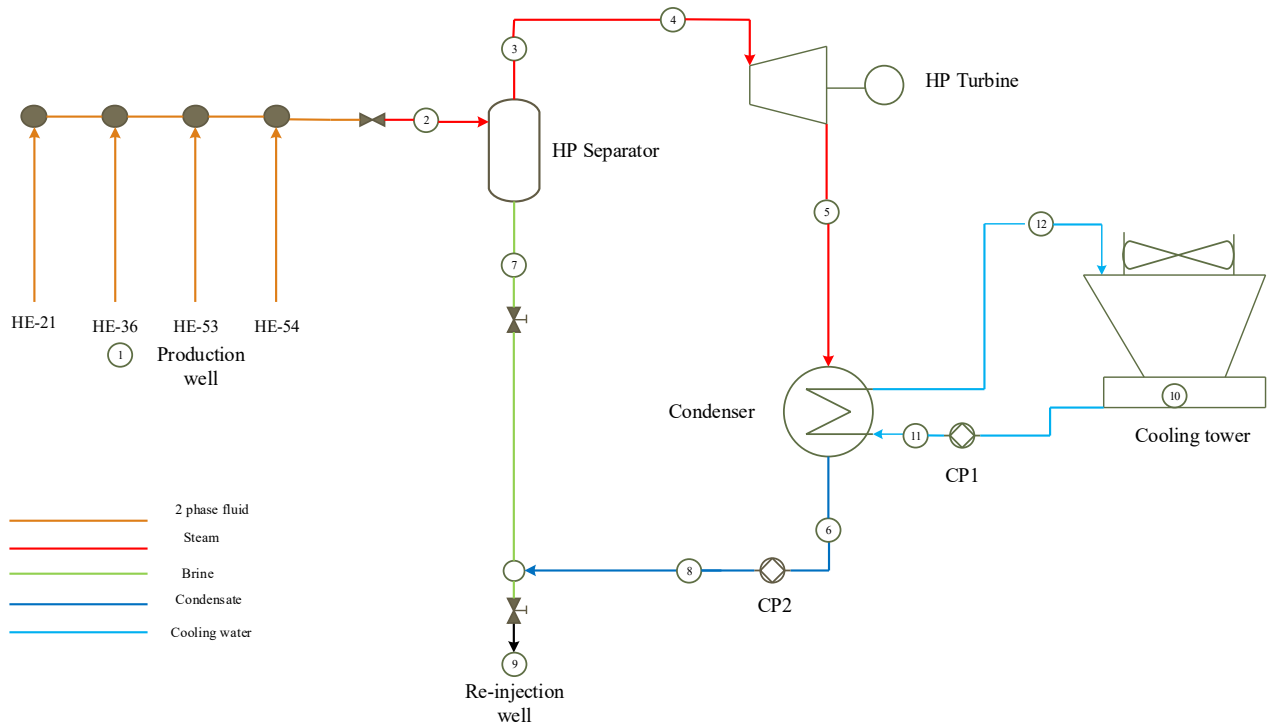


FIGURE 36. Process flow diagram (PFD) of single flash power plant.

$$x_2 = \frac{h_2 - h_7}{h_3 - h_7} \quad (35)$$

where $h_3 = h_4$

The mass flow rate of the steam is given by:

$$m_3 = m_2 x_2 \quad (36)$$

A steam turbine is a device that converts thermal energy from pressurized steam into useful mechanical work. The isentropic efficiency for a geothermal steam turbine is typically 81-85% and the mechanical efficiency of the turbine generator is about 96.3% (Dickson and Fanelli, 2005). Due to pressure drops across the steam turbine, the steam quality decreases and can form small droplets that can damage the turbine blades. Due to this reason, the pressure drop across the turbine is limited to produce no less than 85% quality of steam at the turbine outlet.

In an ideal turbine, the entropy is assumed constant from inlet at point 4 to the ideal exit at point 5s. The isentropic enthalpy at 5s is then calculated from the pressure at point 5 and the entropy at point 4. The work produced by the turbine per unit mass of steam flowing through is given by

$$w_t = h_4 - h_5 \quad (37)$$

Heat loss from the turbine and changes in kinetic and potential energy of the geothermal fluid entering and leaving the turbine is neglected.

If the turbine operated adiabatically and reversibly, maximum work would be generated at constant entropy. The isentropic turbine efficiency, η_t , as the ratio of the actual work to the isentropic work is defined as

$$\eta_t = \frac{h_4 - h_5}{h_4 - h_{5s}} \quad (38)$$

The power output or the gross mechanical power developed by the turbine is given by

$$W_t = m_s w_t = m_s (h_4 - h_5) = \eta_t m_s (h_4 - h_{5s}) \quad (39)$$

The gross electrical power is given by equation (40)

$$W_e = \eta_g W_t \quad (40)$$

The purpose of the condenser is to condense the spent steam flowing from the turbine. There are two methods to perform condensation. The first is to mix the cooling water and the steam (direct contact) and the second is to cool the steam without mixing (shell-tube type condenser). In a water-cooled condenser, the cooling water flows through a shell-tube heat exchanger and removes heat from the steam. The heat exchangers in the condensing cycle in this study were assumed to be shell-tube type condenser. Energy balance equation for the heat exchanger is given as

$$m_5 (h_5 - h_6) = m_{11} (h_{12} - h_{11}) \quad (41)$$

The cooling tower must accommodate the heat load from the condensing steam. The steam condensate is sprayed into the cooling tower where it falls through an air stream drawn into the tower by a motor driven fan at the top of the tower. The ambient air contains some amount of water vapor when it enters and absorbs more water vapor as the condensate evaporates partially. The evaporation process requires heat that comes from the water itself, thereby reducing its temperature. As shown in Figure 39, the cooling water is pumped from the pond to the condenser at station 11, and warm water at station 12 is cooled by being sprayed into the tower.

6.2 Double flash power plant

The double-flash plant is an improvement of the single flash design in that it can produce 15-25% additional power output for the same geothermal fluid conditions, where the geothermal brine from the separator is flashed in a throttling process that decreases the pressure of the brine and allows it to boil to produce additional steam that can drive a low-pressure turbine (DiPippo, 2005). A flow sheet for the double flash cycle is shown in Figure 38. The process for the high pressure part is explained in the previous section. The brine from the separator is at point 7, and is throttled down to a lower pressure level at point 8. The separated fluid (brine) is then led to a low-pressure separator, where the steam is expanded to a low-pressure turbine at point 9. The brine from the low-pressure separator is at point 12 and is then re-injected to the reservoir and the cooling tower for the low pressure is not shown here.

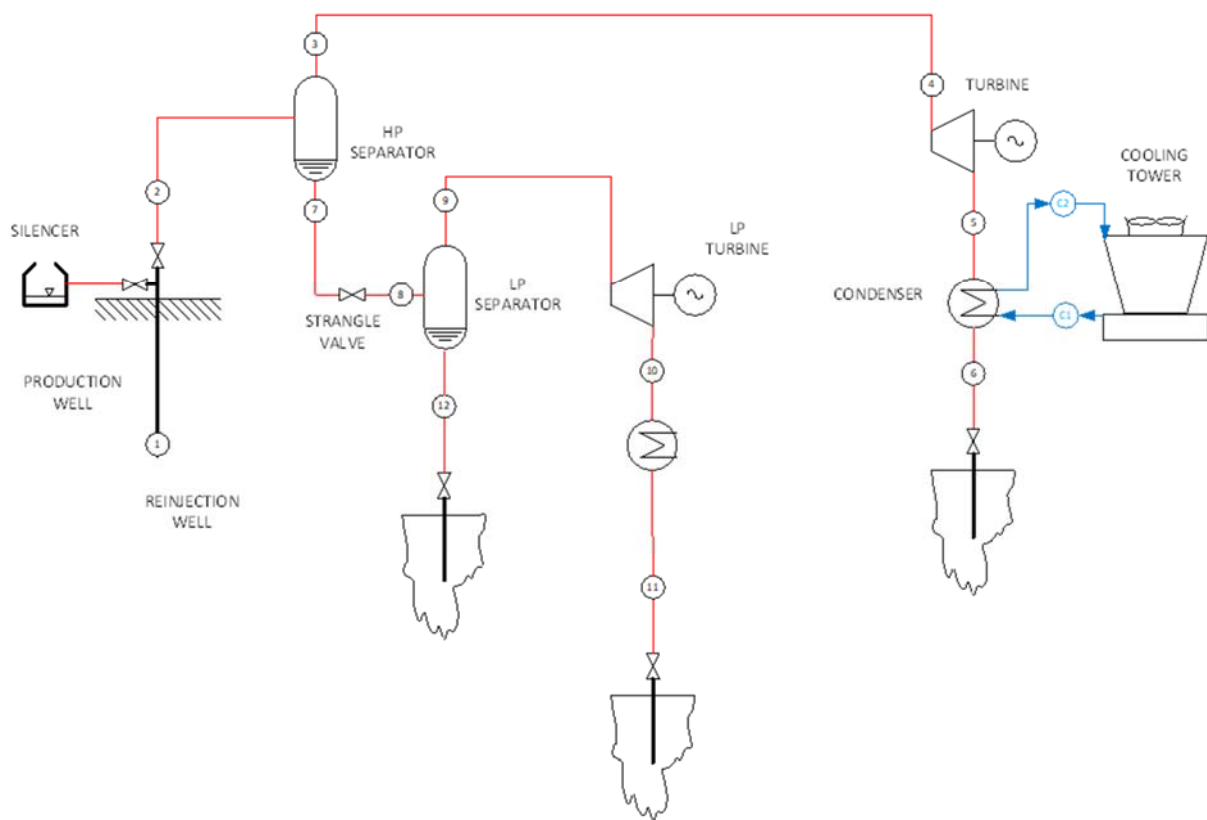


FIGURE 38. Double flash energy conversion system.

The flashing process is isenthalpic:

$$h_7 = h_8 \quad (42)$$

LP separator mass and heat balance is given by

$$m_8 = m_9 + m_{12} \quad (43)$$

$$m_8 h_8 = m_9 h_9 + m_{12} h_{12} \quad (44)$$

And the steam mass fraction is given by

$$x_8 = \frac{h_8 - h_{12}}{h_9 - h_{12}} \quad (45)$$

The work produced by the turbine per unit mass of steam flowing through it is given by

$$W_{LPT} = m_9(h_9 - h_{10}) \quad (46)$$

The net power output of a double flash system is calculated by summing up the power output of the turbines (HP and LP turbine) and the auxiliary power consumptions are neglected. The thermodynamic process is shown in T-s diagram (Figure 39).

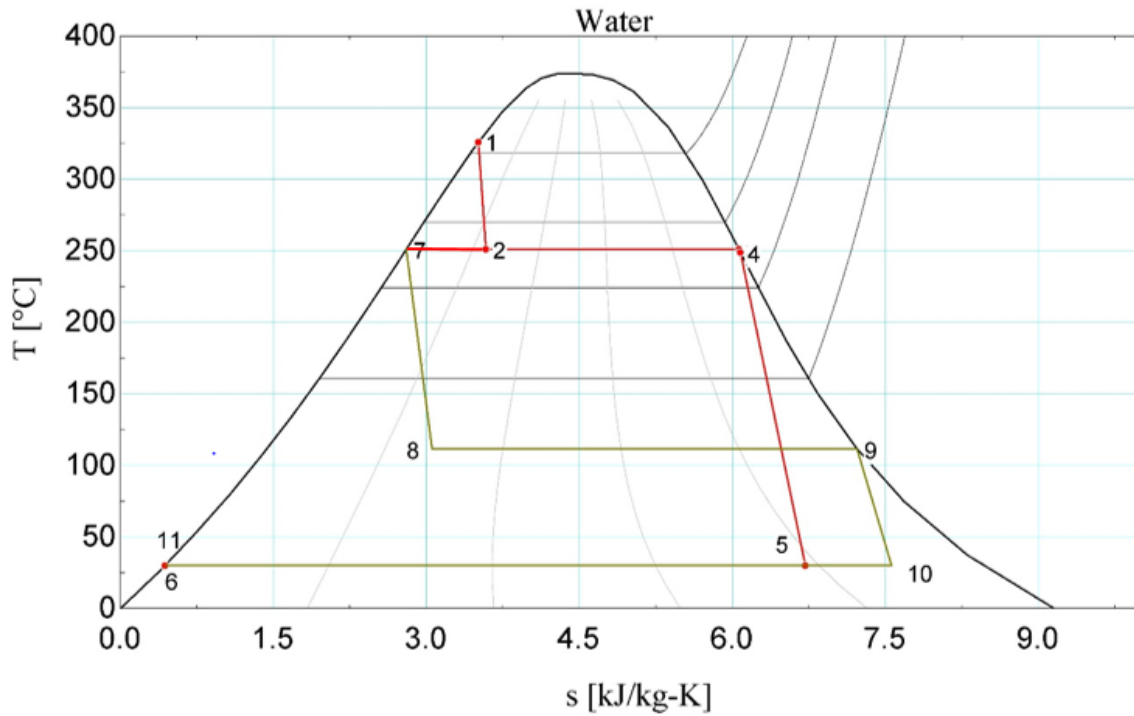


FIGURE 39. *T-s diagram for double flash cycle.*

6.3 Binary cycle power plant

Binary geothermal power plants are similar to conventional fossil or nuclear plants in terms of thermodynamic principle in that the working fluid is kept in a closed cycle. Technically an organic Rankine cycle can be divided into three subsystems: (1) brine (the geothermal fluid), (2) power conversion cycle and (3) the cooling system for the removal of heat (Frick et al., 2015). The working fluid selected for its proper thermodynamic properties, accepts heat from brine, evaporates, expands through a turbine, condenses and is returned to the evaporator by means of a pump. The ORC uses secondary fluid (organic working fluid) to produce power. According to Palsson et al. (2010) the shape of the curve leads to ensuring the dryness of the steam at the turbine outlet at low condenser pressures since the fluid becomes superheated at the outlet of the turbine. The secondary working fluids typically have lower boiling temperatures than water, making them well suitable for utilizing lower temperature geothermal brine for power production (Palsson et al., 2010). For modelling a bottoming binary cycle, ORC was coupled in parallel to the single flash cycle as shown in Figure 40.

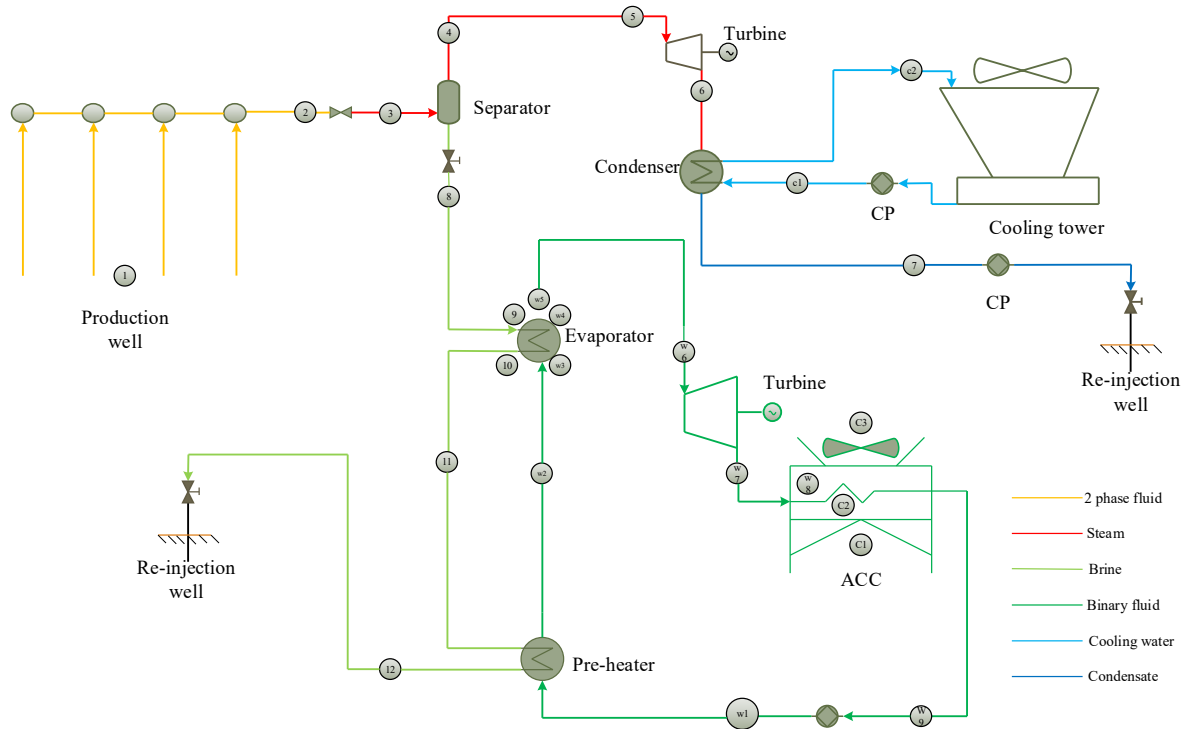


FIGURE 40. Flow diagram for ORC cycle.

The thermodynamic analysis of the cycle is similar with that of steam turbines.

With assumptions of negligible potential and kinetic energy terms together with steady, adiabatic operation, the power is found from

$$W_t = m_{wf}(h_{w6} - h_{w7}) \quad (47)$$

The heat that must be rejected from the working fluid to the cooling medium is given by

$$Q_c = m_{wf}(h_{w7} - h_{w9}) \quad (48)$$

The flow rates of the working fluid and the cooling water is related as:

$$(m_{cw}(h_{c3} - h_{c1})) = m_{wf}(h_{w7} - h_{w9}) \quad (49)$$

The power imparted to the working fluid from the feed pump is given

$$W_p = m_{wf}(h_{w1} - h_{w9}) \quad (50)$$

$$W_{pump} = \frac{v_{w1} * (P_{w1} - P_{w9}) * m_{w1}}{\eta_{fan} * \eta_{motor}} \quad (51)$$

Power of motor fan in air cooling condenser

The air-cooled type uses electrical fans to cool the working fluid and is dependent on the environmental temperature for its efficiency. The power of the fan can be calculated as

$$W_{fan} = \frac{v_{c3} \Delta P_{fan} m_{c1}}{\eta_{fan} \eta_{motor}} \quad (52)$$

ΔP_{fan} is the pressure drop in pa with an assumption of 120 millibar and v_{c3} is the specific volume of air in m^3/s . In addition, the following is assumed:

$$\eta_{fan} = 0.65 \text{ and } \eta_{motor} = 0.75$$

Heat exchanger parameters

A heat exchanger is a system used to transfer heat between two or more fluids and used in both cooling and heating processes. A solid wall to prevent mixing may separate the fluids or they may be in direct contact. The working fluid must have a margin to the boiling point when entering the binary vaporizer. If this is not obeyed, boiling may happen in the preheater, which has difficulties in dealing with vapor bubbles in the flow.

Mass and heat balance for the Pre-heaters (PH)

To establish thermodynamic relationship between the brine and the working fluid, steady-state operating conditions are assumed and that the differences in entering and leaving potential energy and kinetic energy are negligible. In order to make the heat transfer between the brine and the working fluid, we assume that the heat exchangers are well insulated. The total amount of heat added to the working fluid is equal to the heat extracted from the brine. This is described in the equations of the preheater and vaporizer.

Pre-heater heat balance:

$$m_{11} * (h_{11} - h_{12}) = m_{w1} * (h_{w1} - h_{w2}) \quad (53)$$

Mass and heat balance for the Vaporizers

Heat balance for brine heated vaporizer is given by:

$$m_8 * (h_8 - h_{11}) = m_{w2} * (h_{w2} - h_{w5}) \quad (54)$$

6.4 Result and discussion for the scenarios

After drilling and testing geothermal wells, then we want to know how much power output can be generated from the tested wells. Furthermore, we want to know what kind of energy conversion system can produce the optimum power output, using the energy in the fluid as much as possible. Single flash, double flash and combined single flash and binary systems are among the energy conversion systems. The main question is which of the conversion technologies can generate an optimum power output based on a given enthalpy of the geothermal fluid.

Single flash power plants are the most common type of plants installed in the liquid dominated reservoirs. Once the geothermal fluid is separated from the steam, the steam drives a turbine and the waste liquid is either re-injected or used in binary system or used in second flash power plants to produce additional power output.

In general, the project involves the preliminary design of geothermal power plants according to given information in Table 20 from the results of discharge testing of well HE-21, HE-36, HE-53, which is based on the testing results for the Hverahlid wells presented previously in this thesis.

Table 20. Input Data from wells.

Well	Date	WHP	Orifice	m_t	H_t	$m_s@17 \text{ barg}$	$m_w@17 \text{ barg}$
		bar-g	mm	kg/s	kJ/kg	kg/s	kg/s
HE-21	28.2.2014	21.3	75	20.7	1685	8.7	12
HE-36	20.5.2014	19.5	100	56.5	1357	13.9	42.6
HE-53	7.2.2014	33.5	100	61.9	1602	23.2	38.7
HE-54	25.3.2014	43.8	100	73.0	2008	42.9	30.1
Sum/average				202	1667	84.7	123.4

Optimization to find wellhead pressure (separator pressure) and high side pressure in binary cycle, which gives the most power production, also has been done for all cycles considered.

The design process involves:

1. Design of a single flash power cycle with a condenser pressure of 0.1235 bar or condenser temperature of 50 °C and turbine efficiency of 0.81-0.85 and finding the separator pressure which gives the most efficient cycle, but does not exceed the minimum value of turbine outlet quality which is 0.85
2. Design of a double flash power cycle

- Design of an optimal ORC power cycle, which function as a bottoming plant added to the single flash power plant. Different working fluids are compared and the fluid that gives the optimum output, is selected.

Table 21. Optimization variables and limitations for each power cycle.

Scenarios	Optimization variables	Limitations
Single flash	P_2	$x_5 \geq 0.85$
Double flash	P_2, P_6	$x_5 \ \& \ x_{10} \geq 0.85$
Single flash with bottoming ORC plant	P_1, P_{11}	$x_3 \geq 0.85$

6.4.1 Wellhead pressure

The wellhead pressure directly affects the mass flow from a well. A productivity curve for wells in Hverahlid producing two-phase fluid is shown in Figure 41. As the pressure increases, the mass flow produced by a well will eventually decrease to a point that the well is completely closed and no mass flow is produced. It is assumed that the pressure drop in pipelines are negligible. It is also assumed that the pressure of the wellhead can be controlled by means of a throttle valve. Then the well productivity can be approximated as an a polynomial for the mass flow rate as function of the wellhead pressure. In Figure 41, the mass flowrate is plotted with the corresponding wellhead pressure. The total flow rate for the figure in Figure 44 is approximated using:

$$Q_{total} = ax^2 + bx + c, x = P_0 \quad (55)$$

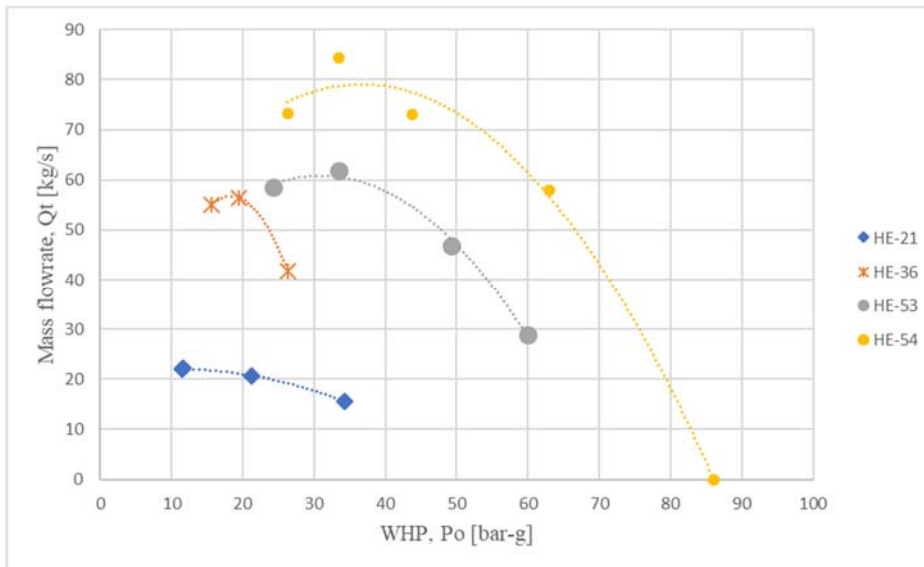


FIGURE 41. Production curves of wells in Hverahlid and can also be seen in Figures 32-35.

6.4.2 Assumptions

The following values are assumed for the power plants analysed in the following power production scenarios.

Steam turbine isentropic efficiency

The steam turbine isentropic efficiency can be assumed to be from 81% to say 85%. A turbine with fewer stages such as a back-pressure turbine will have lower efficiency than a large turbine with more stages. Condensing steam turbine isentropic efficiency is assumed 81% here (Dickson and Fanelli, 2005).

Condenser hot well temperature

The condensation is calculated assuming negligible non-condensable (NCG) gas content. The assumed hot well temperature is then equal to the temperature at which the steam condenses in the condenser. The condensation temperature is assumed 50 °C (Valdimarsson, 2018).

No pressure loss is assumed in the calculations, while binary turbine isentropic efficiency is assumed 85%.

The binary working fluid circulation pump is assumed to have 75% isentropic efficiency, including the motor efficiency. Cooling water and condensate pumps are assumed to be with slightly lower efficiency or 65% (Valdimarsson, 2018).

Binary condenser hot well temperature

A binary condenser operates without non-condensable gas contamination. The pressure in a binary system is normally above atmospheric pressure (exception is a high molecular weight working fluid at low ambient temperature), so there is no likelihood of air leakage into the system. As the working fluid is in a closed loop system there will not be any ingress of non-condensable gas into the system (exception is possible seal gas leakage for some types of dry gas turbine seals). The condensation temperature in a binary condenser can therefore be considerably lower than for a steam condenser, and is assumed here to be 25 °C (Valdimarsson, 2018).

The cooling air fan efficiency is assumed 65% (Valdimarsson, 2018).

Heat exchanger parameters

The preheater is in counter-flow, which is the best way to operate a heat exchanger for liquid to liquid heat transfer, where no latent heat is involved. Typically, a binary plant is designed for a “boiling margin” at the vaporizer entry of 2 °C (Valdimarsson, 2018).

6.4.3 Scenario 1: Single flash power plant

Optimization of the power output of the single flash is based on selecting the optimum wellhead or separator pressure that gives the maximum power output for the cycle with limitation of steam quality at the turbine outlet. The optimization routine is relatively simple

since there is only one optimization variable and it can be determined from varying the value of the separator pressure to locate the power output maximum. The steam quality at the outlet of turbine is the only limit in the optimization problem, as the quality may not go below 0.85 and that limits the maximum wellhead pressure allowed. The results of the optimization process are presented in Figure 42 and 43 as the optimum power output and specific power output as a function of the separator pressure.

The power output increases for a separator pressure of 1 to 10 bar, while the steam quality at the turbine outlet is above 0.85. At separation pressure of 10 bar, the power output is about 49.0 MW_e, while the steam quality is over 0.85 and above 10 bar, the power output increases with the steam quality falling below 85%.

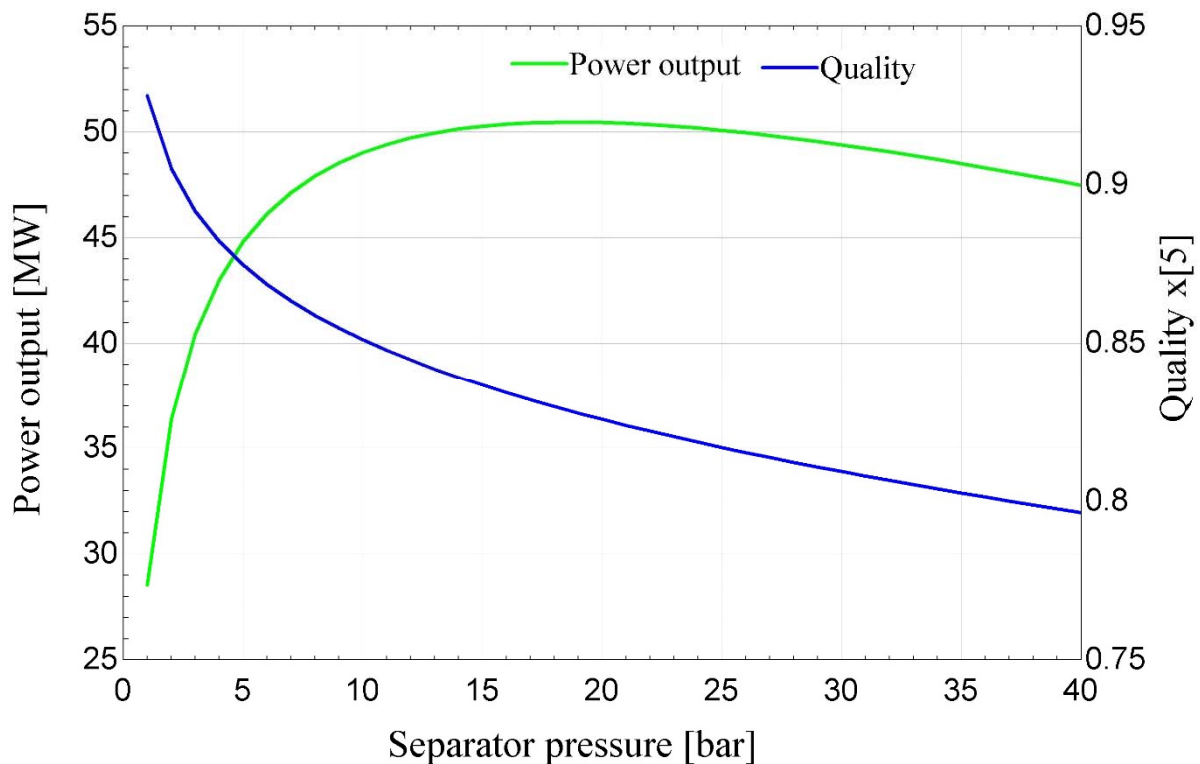


FIGURE 42. Modelled power plant output and steam quality vs. separator pressure

The specific steam consumption, SSC, is defined as the mass of geothermal steam needed to generate 1 kWh of electricity or equivalently, the mass flow rate of geothermal steam needed to generate one kilowatt of net electric power (DiPippo, 2005). The specific steam consumption as well as the specific well fluid consumption is now known and specific steam consumption is plotted as a function of separator pressure (Figure 43).

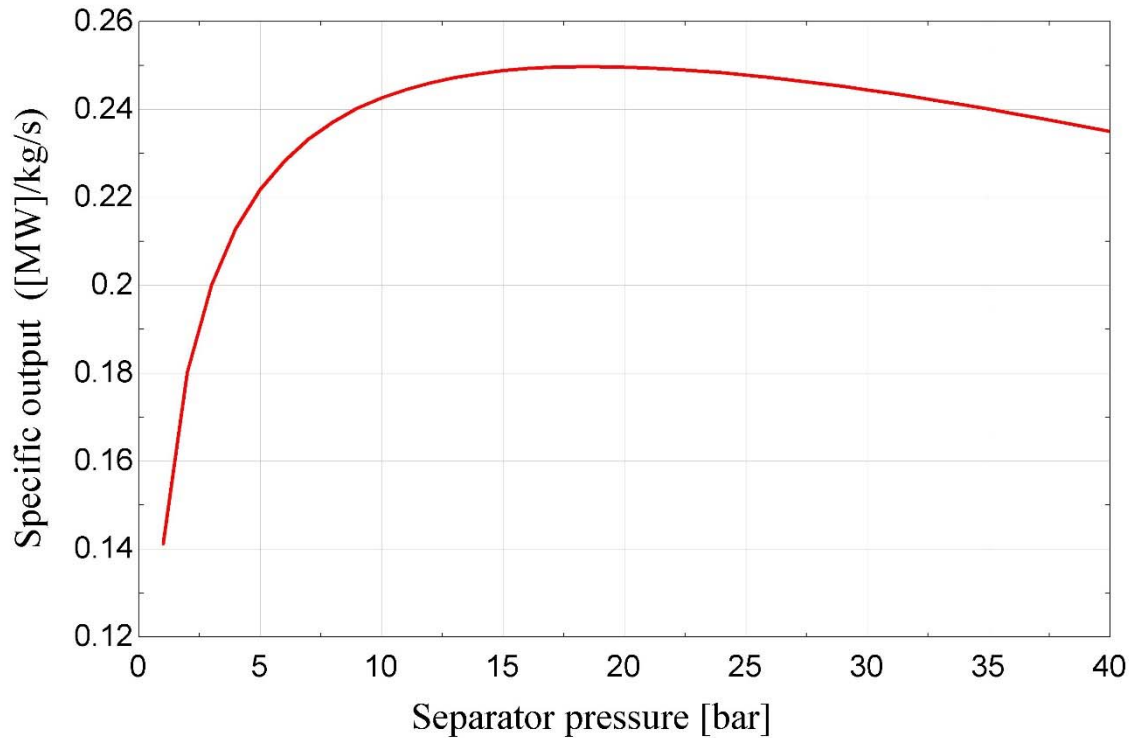


FIGURE 43. Scenario I specific power output vs. separator pressure.

The plant design parameters have been selected at a condenser temperature of 50 °C (0.1235 bar) and at 10 bar-a separator pressure. It can be seen that the maximum specific power occurs at a separator pressure of 10 bar-a with constraint of quality at turbine outlet. The optimum specific power is about 241 kW for each kg/s of total flow from the wells.

The separator pressure determines the brine temperature from the separator. The separator pressure is set by a fixed pressure loss and is estimated to be 10 bar-a. Plant return temperature as a function of separator pressure is shown in Figure 44 and the return brine at this pressure is about 185 °C.

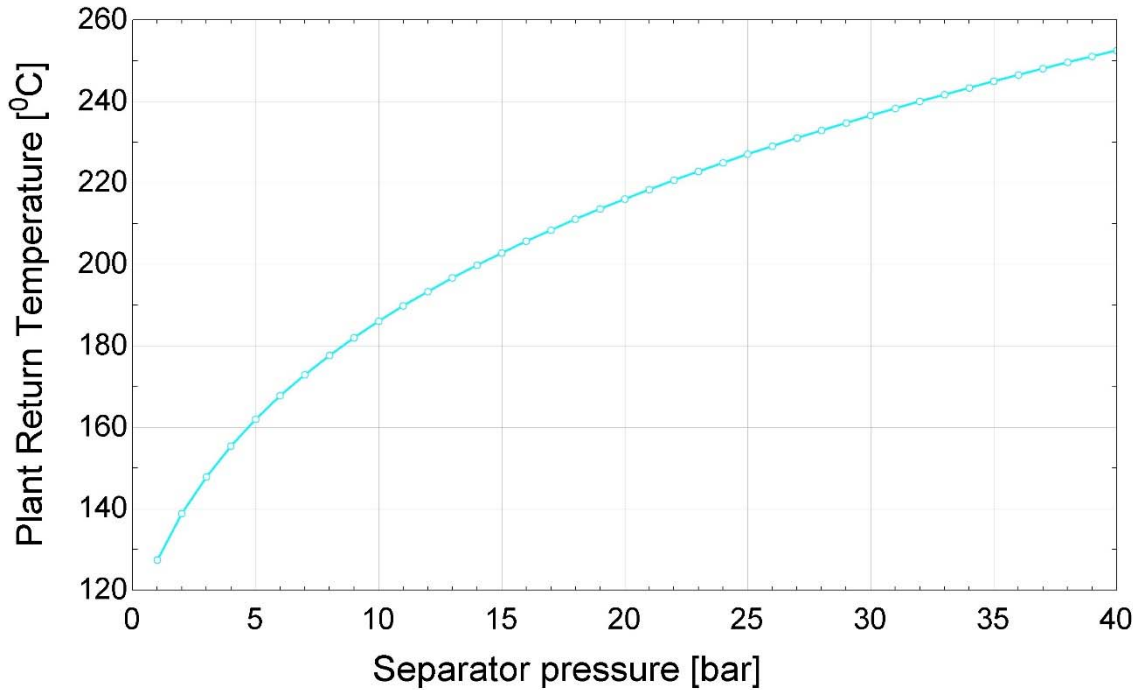


FIGURE 44. Plant return temperature vs. separator pressure.

The PFD of the plant at the baseline condition is shown on Figure 45 with the baseline single flash plant data:

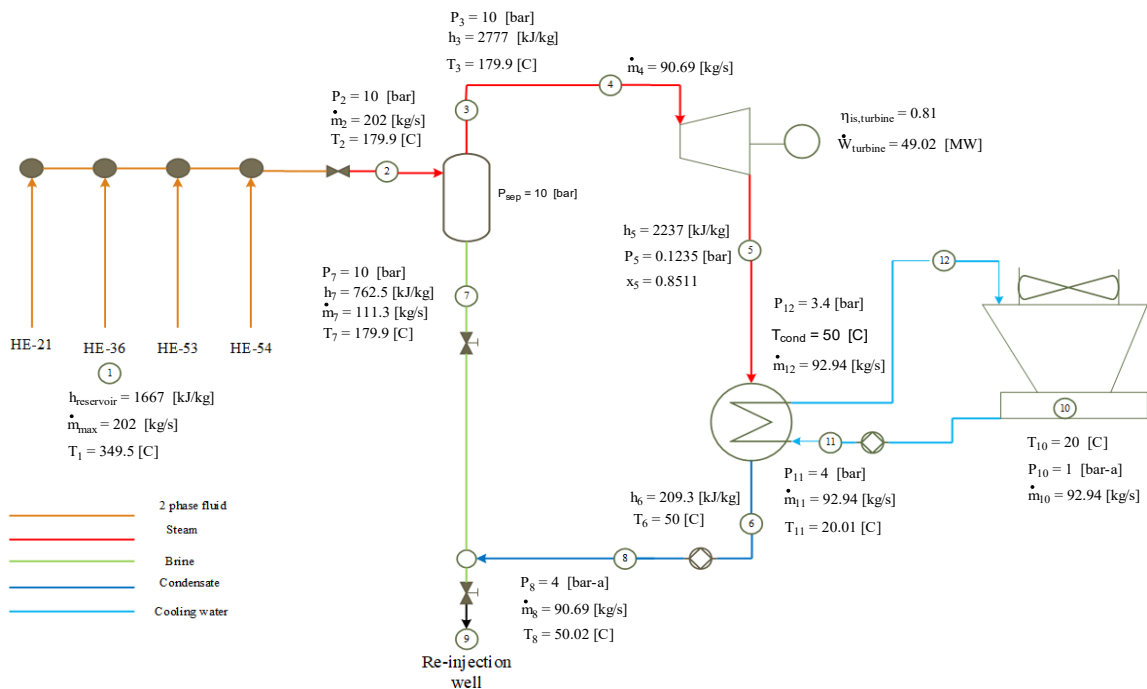


FIGURE 45. Scenario I plant PFD at baseline condition.

The conclusion for this scenario is that a separator pressure of 10 bar and condenser temperature of 50°C (0.1235 bar) seems to be the best selection, producing a net power of 49.0 MWe.

6.4.4 Scenario 2: Double flash power plant

To optimize the power output of the double flash cycle, two optimum pressure states, P_2 and P_6 , need to be found. Compared to the single flash, an extra parameter is added to the optimization routine, which makes it more complicated. For each value of operating pressure of the high-pressure separator, an optimum pressure value can be found for the low-pressure separator. The limitation in the optimization process is similar to the single flash power plant, i.e. the steam quality at the outlet of each turbine, at station 5, x_5 and station 10, x_{10} . The optimization method for the high-pressure steam turbine, separator pressure is similar with single flash discussed in scenario I. Figure 46 shows the optimization of power output of double flash power plant and quality at the low-pressure turbine outlet for different separator pressure. The optimized power output for the low-pressure turbine occurs at a separation pressure of 2 bar yielding about 4.45 MWe, steam quality in range.

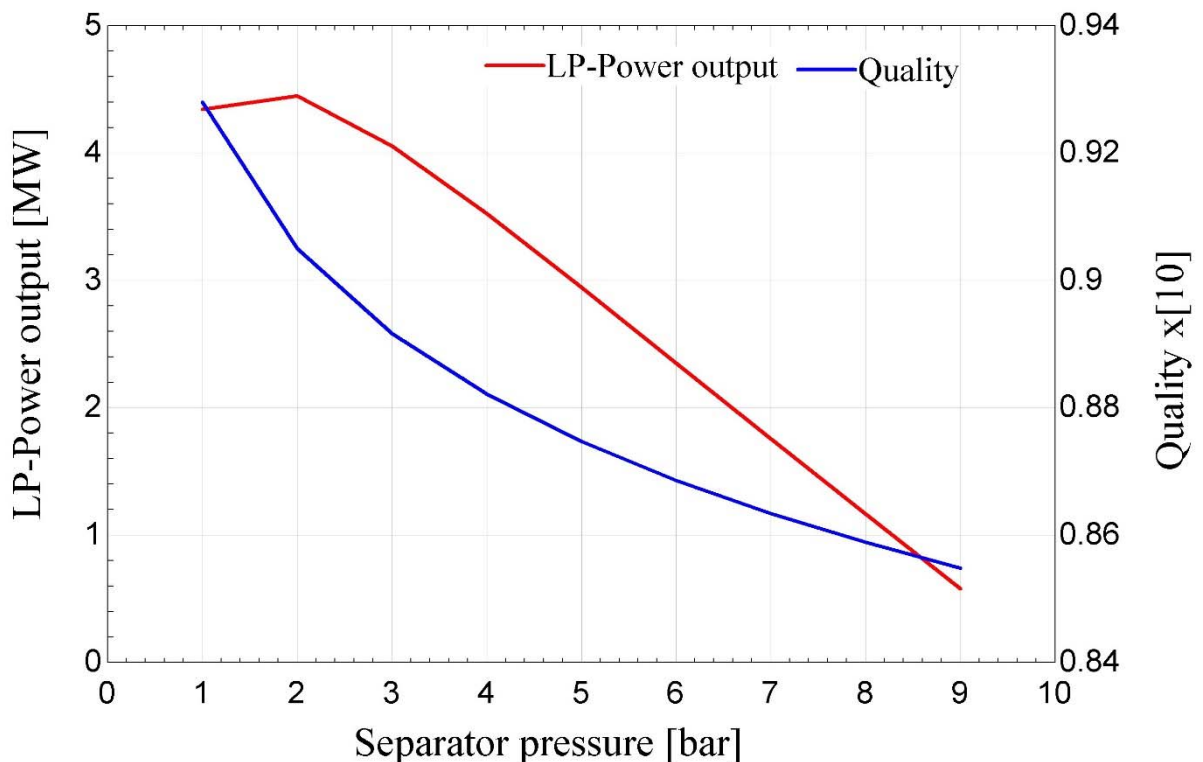


FIGURE 46. Optimized power output and steam quality for a low pressure steam turbine.

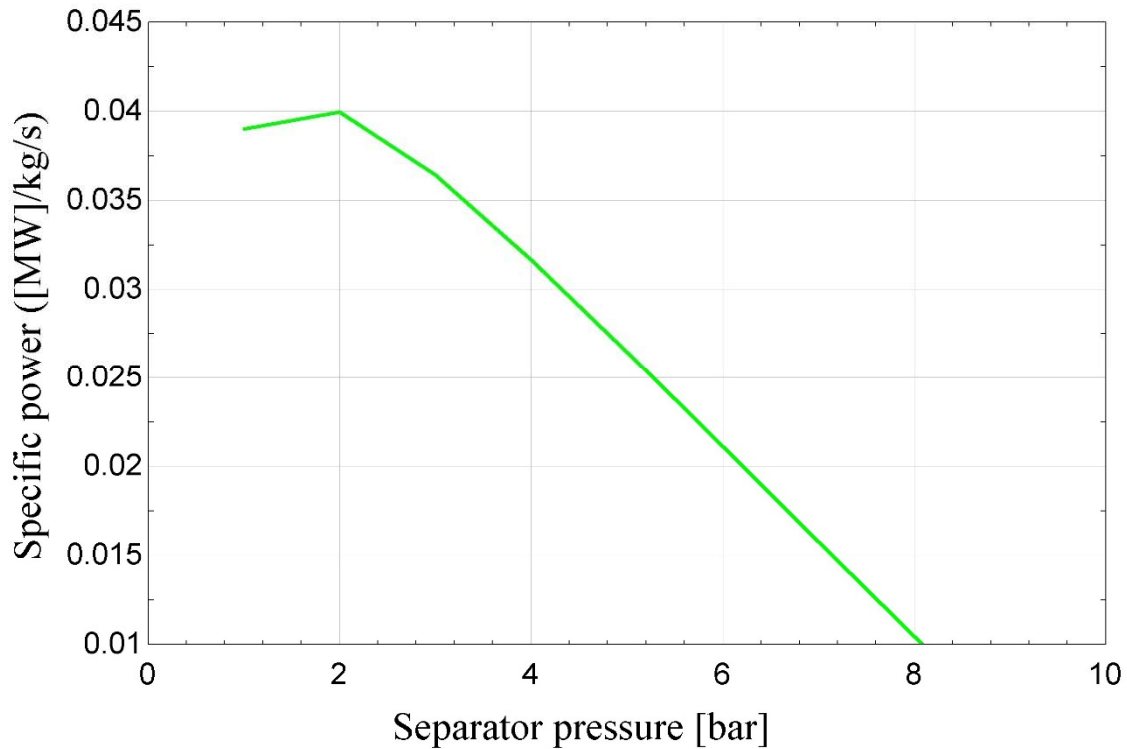


FIGURE 47. Specific output of the low-pressure steam turbine.

It can be seen that the maximum specific power occurs at a separator pressure of 2 bar-a, for the low-pressure steam turbine with constraint of steam quality at turbine outlet. The optimum specific power is about 39 kW for each kg/s of total flow from the low-pressure separator (Figure 47).

The double flash power plant totally produces about 53.5 MW_e power (Figure 48). Compared to the single flash power plant, this scenario produces additional 4.5 MW_e. Power production of double flash is increased by about 8% when compared with the single flash power plant.

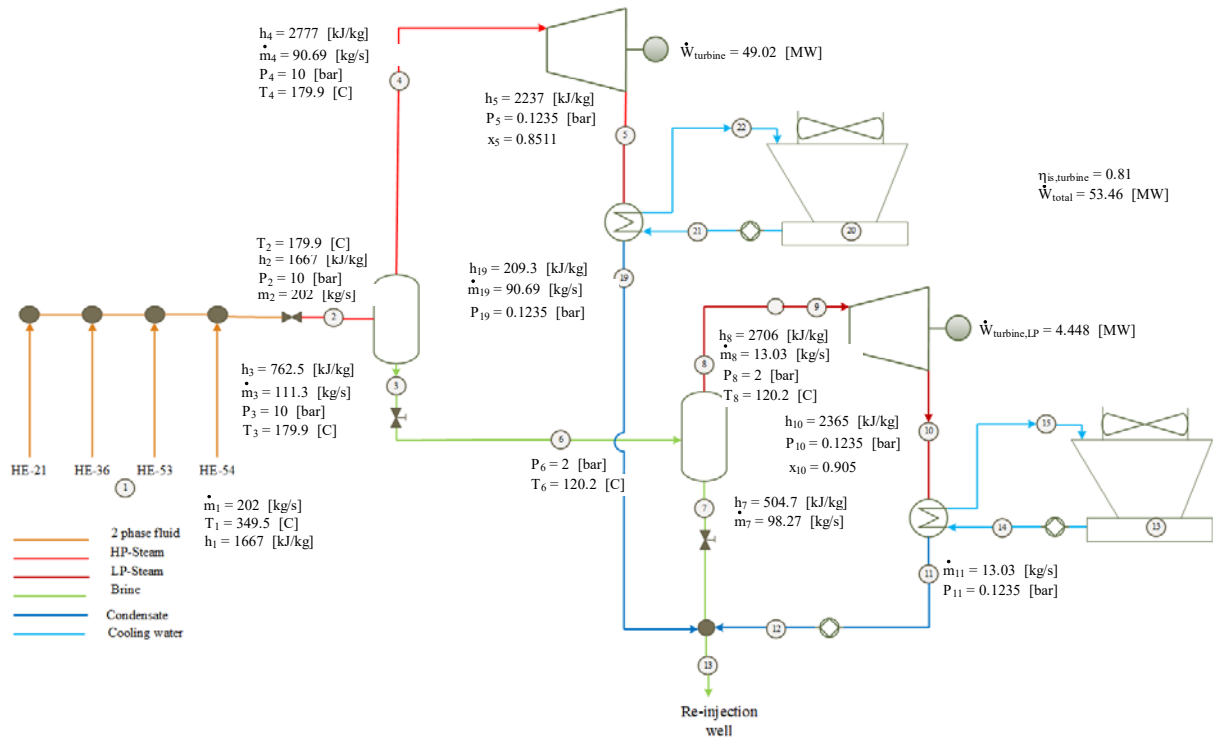


FIGURE 48. PFD result for the double flash power plant.

6.4.5 Scenario 3: Single flash with bottoming ORC plant

The single flash combined with a binary system that was proposed in this study uses geothermal fluid from the separator (Figure 49). Then the geothermal fluid flows directly to a heat exchanger system, enters the vaporizer at point 6 and leaves the pre-heater at station 8. The process of the binary cycle starts from the brine that heats and evaporates the working fluid in the heat exchanger. The saturated vapor of the working fluid flows to the turbine at point 13 and generates electricity. The working fluid is then condensed in air-cooled condenser, enters the ACC (Air Cooled Condenser) at point 14 and leaves at point 10 and flows back to the heat exchanger using a pump at point 11 (Figure 49). The binary plant has then to be designed according to the properties of the brine input stream and the desired plant return or re-injection temperature.

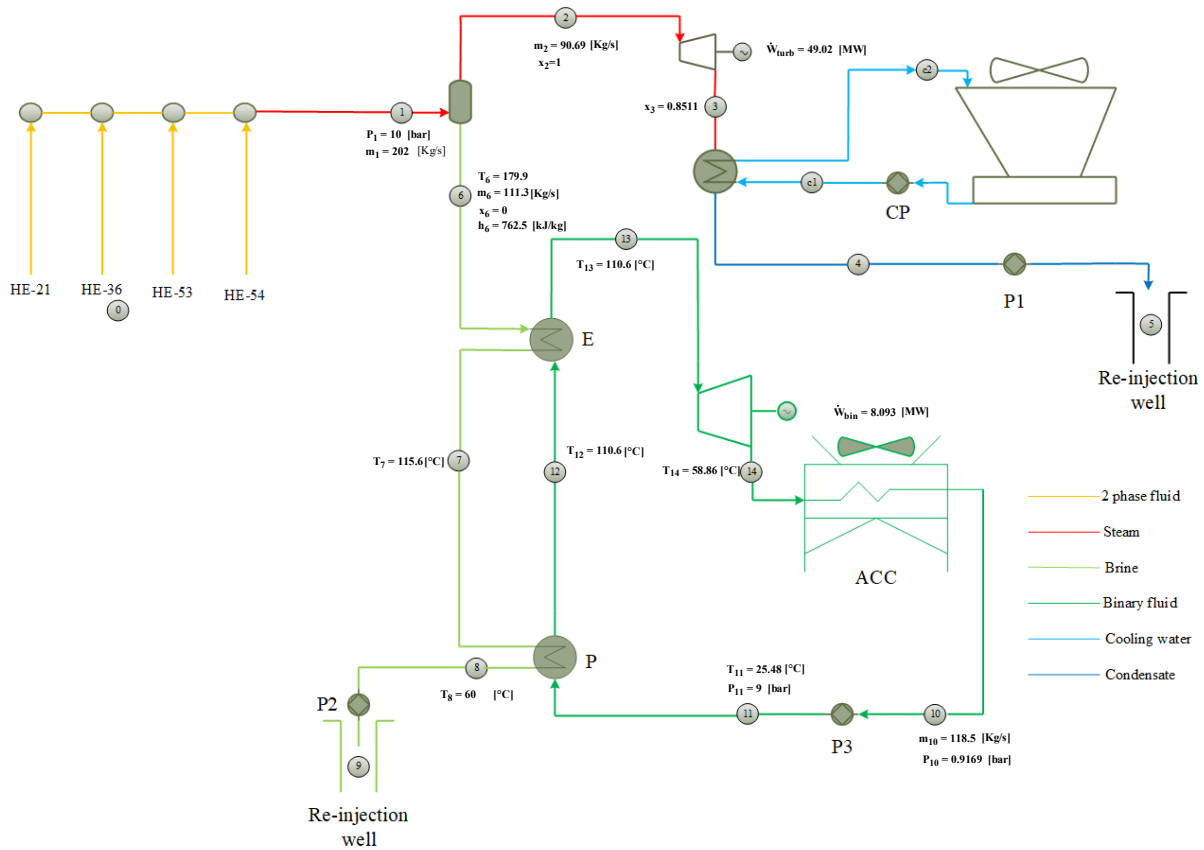


FIGURE 49. PFD results for single flash with ORC bottoming binary plant.

There are two optimization variables for the single flash cycle with the ORC bottoming plant. First, the separator pressure as a function of the wellhead pressure must be optimized similar to scenario I and II. Second, the pressure (Vaporizer) in the organic Rankine cycle needs to be optimized. For this cycle, only the steam quality at the outlet of the steam turbine becomes a limitation due to the fact that the binary fluid at the outlet of the binary turbine is superheated and thus, no moisture is present.

Separator pressure

Optimization method for the single flash and double flash is discussed in the previous sections. In the combined flash binary cycle, changes in separator pressure would also alter the temperature and flow rate of the geo-fluid into the binary evaporator. Higher separator pressure would result in lower steam flow rate into the steam turbine, but the steam would be at higher temperature and possess more workability. Similarly, the brine flow rate and temperature into the binary cycle would be higher. Lowering the separator pressure, would result in higher steam flow rate into the steam turbine but possess less workability, also the temperature and mass flow rate into the binary cycle would be lower. For each case, the separator pressure value should be selected in a manner that yields highest power output with limitation of the steam quality at the steam turbine outlet.

Binary fluid selection

There are many candidate fluids for a binary plant. Five fluids are tested, all having sufficiently high critical point to be operated with a sub-critical ORC cycle. Table 22 presents the list of candidate ORC working fluids with their critical temperatures and pressures.

Table 22. The main characteristics of working fluids. Water is referred to for comparison.

Fluid	Formula	Critical Temperature [°C]	Critical pressure MPa	Toxicity	Flammability
Isobutane	(CH ₃) ₃ CH	135	3.7	Low	Very high
Isopentane	C ₅ H ₁₂	187.2	3.38	Low	Very high
n-pentane	C ₅ H ₁₂	193.9	3.24	Low	Very high
Propane	C ₃ H ₈	96.6	4.24	Low	Very high
R-134a	CF ₃ -CH ₂ F	101	4.06	Low	No
Water	H ₂ O	374.1	22.01	No	No

The power produced for these five fluids is shown in Figure 50 as a function of plant return temperature. The plant return temperature influences the power of the binary plant. The steam turbine power is not influenced. Lowering of the plant return temperature from 80 °C to 50 °C will increase the binary power but this has to be determined according to the scaling properties of the fluid.

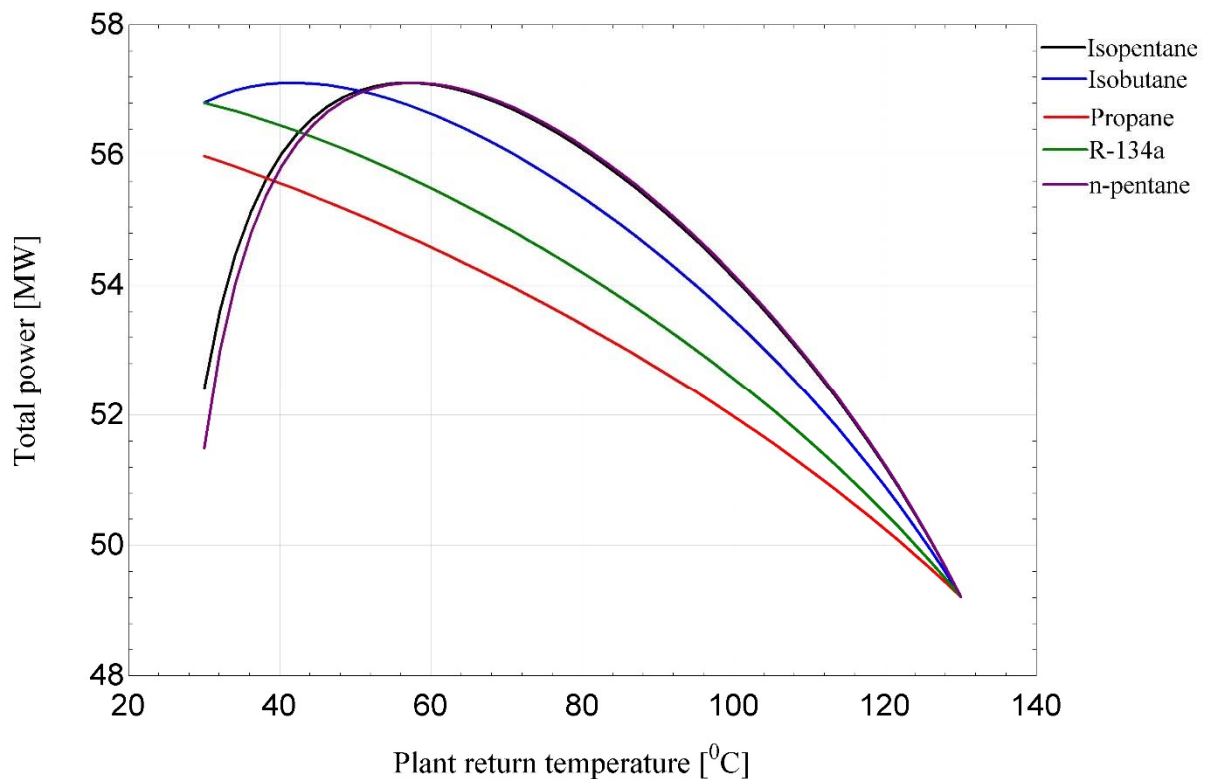


FIGURE 50. Total power output as function of plant return temperature.

The best fluid is Isopentane with a vaporizer pressure of 9 bar-a (Figure 51), with an optimum plant return temperature close to 60 °C and with binary power of 8.01 MWe. The binary power is just an addition to the single flash steam plant power from Scenario I.

Table 23. Power output for different fluids.

Fluid	W_total	W_dot_SF	W_dot_binary
	MWe	MWe	MWe
Isobutane	54.581	49.02	5.561
R134fa	54.2	49.02	3.2
Isopentane	57.03	49.02	8.01
n-pentane	56.72	49.02	7.7

Where W_total is the total power output, W_dot_SF is the single flash power output and W_dot_binary is the binary power output.

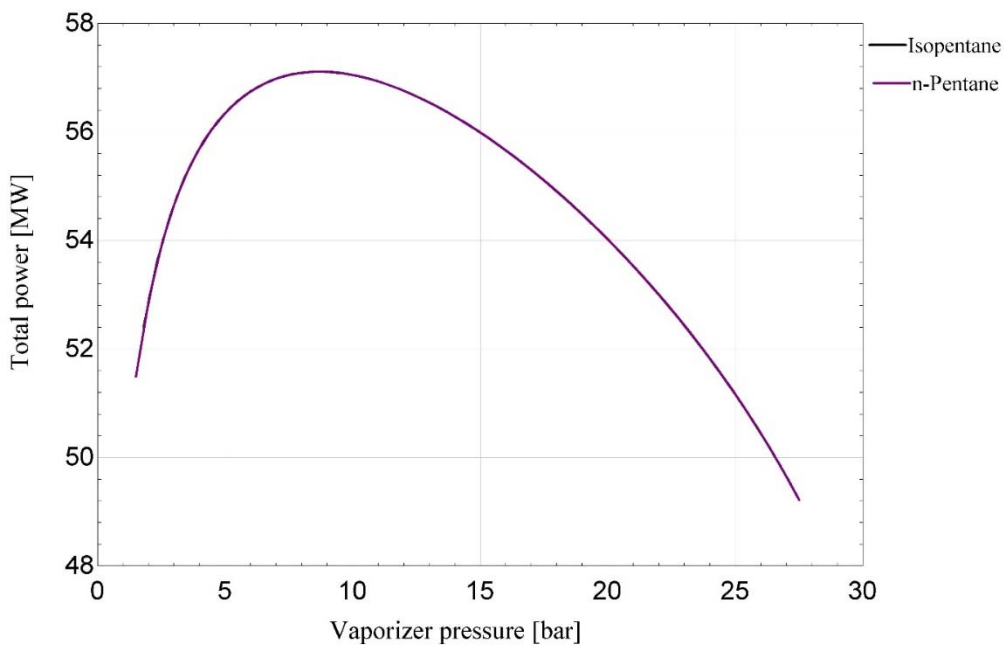


FIGURE 51. Total power as function of vaporizer pressure.

Both the steam flash plant and the binary plant are plotted against the separator pressure Figure 52.

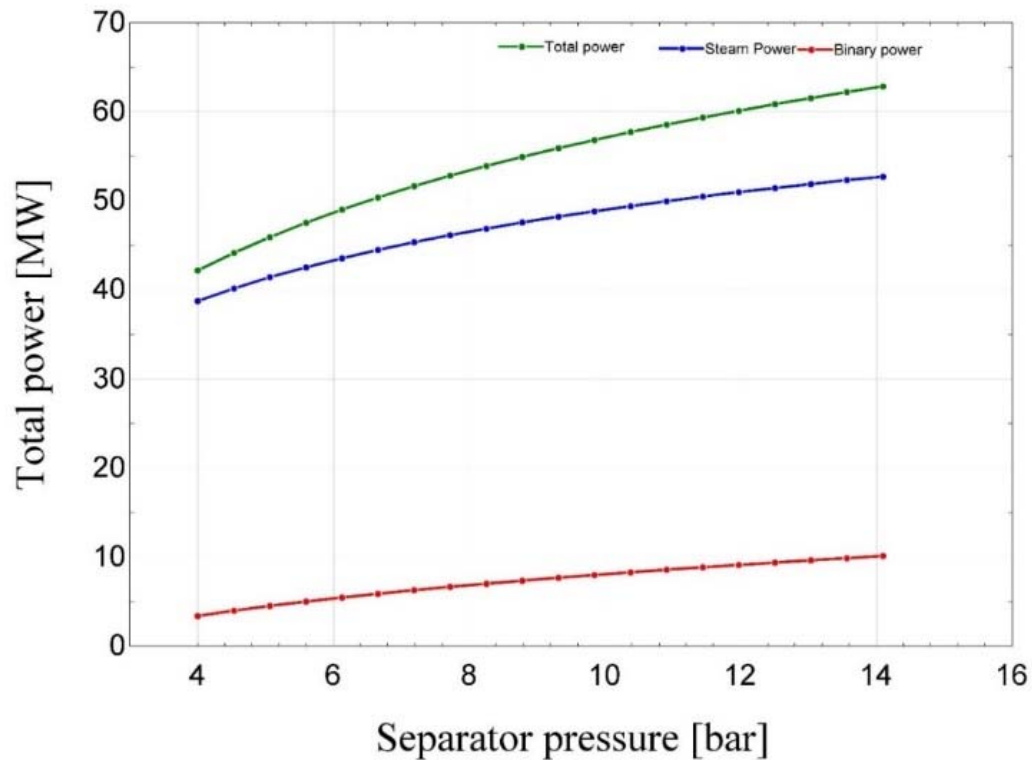


FIGURE 52. Total, binary and steam power output as a function of separator pressure.

The best separator pressure of 10 bar-a is evident here, with limitations of quality at the turbine outlet and produces about 57.0 MW_e in total using Isopentane as a binary fluid.

Comparison of the scenarios

The optimized power production from each of the scenarios discussed is shown in Table 24. The single flash power plant, where the geothermal fluid is reinjected after separator, has the lowest power production of all the scenarios. The hybrid flash-binary scenario that uses an organic Rankine cycle as a bottoming unit in connection to the single flash cycle gives the best result for the maximum power production.

Table 24 Comparison of the scenarios

Scenarios	Output power [MW _e]
Single flash	49.0
Double flash	53.5
Single flash with bottoming ORC	57.0

7 Discussion and Conclusions

The aim of this study was to discuss the role of well testing in evaluating geothermal resources and evaluate how different well testing methods give information that can increase understanding of the Hverahlid geothermal system in SW-Iceland. A significant amount of information that characterizes the reservoir only becomes available during and after drilling completion. Injection tests are designed to provide estimates of reservoir parameters such as permeability and injectivity index that characterize the reservoir in question as well as a particular well.

The results of well testing, including injection testing, along with estimates of reservoir temperature and pressure and discharge test results, can be used to develop a conceptual model of the geothermal system by joining the results with geochemical, geophysical and geological data. Moreover, well testing and temperature/pressure logging can be used to monitor production output and the reservoir response during exploitation. Additionally, the results of well testing can also be used when designing a power plant by constructing thermodynamic models of different power cycles. In this study, three such power cycle models were developed for the Hverahlid field.

The models selected for simulating the injection step tests in wells HE-36, HE-53 and HE-61 assume a homogenous reservoir and constant pressure boundary. The Hverahlid geothermal system is mainly composed of hyaloclastite formations (sub-glacial) characterized by uniform fissures and fractures. In Iceland, comparable formations provide the main aquifers of many geothermal systems. Juliusson et al. (2008) stated that for Icelandic geothermal reservoirs the transmissivity T is of the order of $10^{-8} \text{ m}^3/(\text{Pa}\cdot\text{s})$. The results of this study give transmissivity estimates of the wells studied well as $4.9 \cdot 10^{-8} \text{ m}^3/(\text{Pa}\cdot\text{s})$ for well HE-36, $4.2 \cdot 10^{-8} \text{ m}^3/(\text{Pa}\cdot\text{s})$ for HE-53, and $1.8 \cdot 10^{-7} \text{ m}^3/(\text{Pa}\cdot\text{s})$ for HE-61, respectively. All the estimated transmissivity values are comparable and similar to expected values for Icelandic geothermal wells.

The results for HE-36, gave a storage coefficient estimate of $2.4 \cdot 10^{-8} \text{ m/Pa}$, $9.6 \cdot 10^{-8} \text{ m/Pa}$ for well HE-53, and $6.0 \cdot 10^{-7} \text{ m/Pa}$ for HE-61, respectively. Therefore, it can be said that all the wells reflect liquid-dominated reservoir conditions, even though two-phase effects may influence the higher values to some extent.

The injection test analysis for Hverahlid shows that the reservoir is characterized by good transmissivity values for wells HE-36 and HE-53 and a high value for HE-61. Above average estimates of the injectivity index is also estimated for well HE-61. The pressure response observed during the tests is small, even at high pumping rates. This indicates that the reservoir system is open and that good permeability controls the flow.

The skin factor for geothermal wells in Iceland is commonly negative, around -1 to -2, although values may range from about -5 to 20. In the three wells at Hverahlid that were studied, the skin factor values were within the range of -5.5 and -1.6; the values were negative which means that the wells are stimulated and in good connection with the reservoir.

Comparing the injectivity indices (68 and 64 (l/s)/bar) and permeability (5 and $2.8 \cdot 10^{-14}$) estimated from the two injection tests (15-16 and 18th April 2018) conducted in well HE-61,

suggests that the well was more open during the 1st test. For well HE-53, comparing the injectivity indices (12, 7 and 8 (l/s)/bar) and permeability (4, 1.7 and $2.8 \cdot 10^{-14}$) estimated from the single test, suggests that the well was more open during the 1st step. For well HE-36 comparing the injectivity indices (4 and 5 (l/s)/bar) and permeability (9.6 and $27 \cdot 10^{-14}$) estimated from the single test, suggests that the well was more open during the 2nd step.

Well HE-36 has major feed zones at depth of 1100 m, 1900 m and at 2050 m where almost all water enters or exits the well. Two main feed zones are located in well HE-53 at 1120-1250 m and 2150-2200 m. The main feed-zones are at 1020 m, 1252 m and 1333 m depth for well HE-61.

The estimated formation temperature for wells HE-36, HE-53 and HE-61 gave an estimation in the range of 270-320°C. The initial reservoir pressure is about 132 bar at 1750 m depth in HE-36 (in 2008), 118 bar at 1500 m depth in HE-53 (in 2009) and 85 bar at 1140 m depth in HE-61 (in 2018). So, the Hverahlid geothermal system is a high temperature geothermal field with estimated formation temperature of greater 300°C.

The analysis of the measurements during the discharge tests of wells HE-21, HE-53 and HE-61 in 2013-2014 gives an estimate of steam flow in range of 6 – 13 kg/s, 9-15 kg/s and 11-29 kg/s assuming a separation pressure of 17 bar-g at Hverahlid. This steam flow is equivalent to 3 – 6.5 MW_e (HE-36), 4.5-7.5 MW_e (HE-53) and 5.5-14.5 MW_e of electric power output, respectively, assuming that 2 kg/s of steam will generate one MW_e. The present discharge measurement gave a total cumulative flow of 129.5 kg/s excluding well HE-54. Of these 39.5 kg/s is steam and 90 kg/s brine at separation pressure of 17 bar-g. The analysis of the measurements from these wells gave a steam flow of 39.5 kg/s at the separation pressure of 17 bar-g, which is equivalent to 19.75 MW_e of electric power output assuming 2 kg/s of steam flow convert to 1 MW_e.

The single flash power plant (scenario 1), where the geothermal fluid is reinjected after separator, has the lowest power production of all the scenarios generating about 49 MW_e. Scenario 2, which is a double flash power plant, which adds a low-pressure unit to the Scenario 1. Therefore, Scenario 2 generates power output of 53.5 MW_e. Scenario 3 is a hybrid flash-binary scenario that uses an organic Rankine cycle as a bottoming unit in connection to the single flash cycle. Scenario 3 generates about 57 MW_e. Scenario 3 proves to be the most feasible scenario in terms of generating power. It has also the benefit of being an addition to Scenario 1, which can be made at any.

References

- Alfredsson, H.A., Hardarson, B.S., Franzson, H. and Gislason, S.R (2008): CO₂ sequestration in basaltic rock at the Hellisheidi site in SWIceland: stratigraphy and chemical composition of the rocks at the injection site. *Mineralogical Magazine*, vol. 72 (1) 1-5.
- Árnason, K., and Magnússon, I.Th., (2001): Geothermal activity in the Hengill area. Results from resistivity mapping. Orkustofnun, Reykjavík, report OS-2001/091 (in Icelandic with English abstract), 250 pp.
- Arason, Th., Björnsson, G., Axelsson, G., Bjarnason, J.Ö., and Helgason, P., (2004): The geothermal reservoir engineering software package ICEBOX, user's manual. Iceland GeoSurvey - ÍSOR, Reykjavík, report ISOR-2004/014, 80 pp.
- Arnórsson, S., Steingrímsson, B., and Hersir, G., (2009): EXPLORATION AND DEVELOPMENT OF THE HENGILL GEOTHERMAL FIELD. Presented at "Short Course on Surface Exploration for Geothermal Resources", organized by UNU-GTP and LaGeo, in Ahuachapan and Santa Tecla, El Salvador, 17-30 October 2009.
- Axelsson, G., (2012): The physics of geothermal energy. In: Saying, A., (ed.), *Comprehensive Renewable Energy*, 7, 3-50.
- Biru Fekadu, M., (2016) Analysis of Welltesting, Temperature and Pressure in high-temperature wells of Aluto-Langano, Ethiopia. UNU-GTP, report 13.
- Bjornsson, G., (2007). Endurskodad hugmyndalíkan af Jarðhitakerfum í Hengli og einfalt mat á vinnslugetu nýrra borsvaeda. Reykjavík Energy, report 10, 93.
- Bödvarsson, G.S., and Witherspoon, P.A., (1989): Geothermal reservoir engineering, part 1. *Geotherm. Scie & Tech*, 2-1, 1-68.
- Bourdet, D. (2002). Well test analysis: the use of advanced interpretation models. *Handbook of Petroleum Exploration and Production*. Elsevier, Amsterdam.
- Dickson, M. H., & Fanelli, M. (2005). *Geothermal Energy - Utilization and Technology*. Earthscan.
- DiPippo, R. (2005). *Geothermal Power Plants - Principles, Applications and Case Studies*. Elsevier.
- Earlougher, R.C. (1977). Advances in well test analysis. *Soc. Petr. Eng., Monograph 5*, pp.264
- Franzson, H., Kristjánsson, B.R., Gunnarsson, G., Björnsson, G., Hjartarson, A., Steingrímsson, B., Gunnlaugsson, E. and Gislason, G., (2005): The Hengill-Hellisheidi geothermal field. Development of a conceptual geothermal model. *Proceedings of the World Geothermal Congress 2005, Antalya, Turkey*, 7 pp.
- Franzson H., Gunnlaugsson E., Arnason K., Saemundsson K., Steingrímsson B. and Hardarson B.S., (2010): The Hengill geothermal system, conceptual model and thermal evolution. *Proceedings of the World Geothermal Congress 2010, Bali, Indonesia*, 9 pp

Franzson, H., Árnason, K., Saemundsson, K. and Gunnlaugsson E., (2010a): The Hengill geothermal system, Proceedings of the World Geothermal Congress 2010, Bali, Indonesia, 9 pp.

Grant, M.A., and Bixley, P.F., (2011): Geothermal reservoir engineering (2nd ed.). Academic Press, Burlington, USA, 359 pp.

University of Iceland, (2018). Geothermal Power Plant Design lecture notes. University of Iceland, Faculty of Industrial Engineering, Mechanical Engineering and Computer Science, Reykjavik.

Haraldsdóttir, S.H., Franzson, H., and Árnason, K., (2012): Preliminary study of down-hole resistivity from 72 boreholes in the Hengill geothermal field, SW-Iceland, with respect to surface resistivity data and alteration minerals proceedings, Thirty-Seventh Workshop on Geothermal Reservoir Engineering Stanford University, Stanford, California, January 30 - February 1, 2012 SGP-TR-194

Haraldsdóttir S.H., (2016): *Well testing theory - injection*. UNU-GTP Iceland, unpublished lecture notes.

Hardarson, B.S., (2014): Geothermal exploration of the Hengill high temperature area. Presented at Short course IX on exploration for geothermal resources 2014, organized by UNU-GTP, KenGen and GDC, Naivasha, Kenya, UNU-GTP SC-19, 9 pp.

Helgadóttir, H.M., Snaebjörnsdóttir, S.A., Nielsson, S., Gunnarsdóttir, S.H., Matthíasdóttir, T., Hardarson, B.S., Einarsson, G.E., and Franzson, H., (2010): Geology and hydrothermal alteration in the reservoir of the Hellisheidi high temperature system, SW-Iceland. Proceedings of the World Geothermal Congress 2010, Bali, Indonesia, 10 pp.

Helgason, P., (1993): Step by step, guide to BERGHITI. User's guide. In: Arason, Th., Björnsson, G., Axelsson, G., Bjarnason, J.Ö., and Helgason, P., 2004: ICEBOX – Geothermal reservoir engineering software for Windows, a user's manual. Iceland GeoSurvey - ÍSOR, Reykjavík, report ISOR-2004/014, 80 pp.

Hersir, G.P., Árnason, K., and Steingrímsson, B., (2009): Exploration and development of the Hengill geothermal field. Presented at "Short Course on Surface Exploration for Geothermal Resources", organized by UNU-GTP and LaGeo, in Ahuachapan and Santa Tecla, El Salvador, 12 pp.

Horne, R.N., (1995): Modern well test analysis, a computer aided approach (2nd ed.). Petroway Inc., USA, 257 pp.

Idnadarraduneytid, (1994). Innlendar Orkulindir til Vinnslu Raforku, Idnadarraduneytid.

Ívarsson, G., (1998): Fumaroles gas geochemistry in estimating subsurface temperatures at Hengill in southwestern Iceland. Proceedings of the 9th Symposium on Water-Rock Interaction, Taupo, New Zealand, 459-462.

James, C.R., (1966): Measurement of steam – water mixtures discharging at the speed of sound to the atmosphere. New Zealand Engineering 21-10.

James R., (1970): Factors controlling borehole performance. *Geothermics, Sp. issue, 2-2*, 1502-1515.

- Júliússon, E., Gretarsson, G.J., and Jónsson, P., (2008): WellTester 1.0b, user's guide. Iceland GeoSurvey - ÍSOR, Reykjavík, 27 pp.
- Kjarran, S.P., & Eliasson, J. (1983). Geothermal reservoir engineering lecture notes. UNU G.T.P., report 2, Iceland, pp 250.
- Larsson, D., Grönvold K., Oskarsson, N. and Gunnlaugsson E. (2002): Hydrothermal alteration of plagioclase and growth of secondary feldspar in the Hengill Volcanic Centre, SW Iceland. *Journal of Volcanology and Geothermal Research*, vol. 114., 275-290.
- Palsson, H., Karlsdóttir, M.R., and Palsson, O.P., (2010): Comparison of Methods for Utilization of Geothermal Brine for Power Production. *Proceedings of the World Geothermal Congress 2010, Bali, Indonesia*, 12 pp.
- Marteinsson, K., (2016): Well Tester User Manual. Version 2. ÍSOR-. – Iceland GeoSurvey, Reykjavík, report in publication.
- Reykjavik Energy (OR)., (2007): Geothermal power plants, pp 7.
- Saemundsson, K., (1995a). Hengill. Geological map (bedrock) 1:5000. Published by Iceland GeoSurvey.
- Schlumberger, (1998): *Introduction to Well Testing*. Bath, England pp 309
- Stefánsson, V., and Steingrímsson, B., (1980): *Geothermal Logging I – An introduction to techniques and interpretation*. Orkustofnun, Reykjavík, report OS-89917/JHD-09, 117 pp.
- Steingrímsson, B., (2013): Geothermal well logging: Temperature and pressure logs. Paper presented at “Short Course V on Conceptual Modelling of Geothermal Systems”, UNU-GTP and LaGeo, Santa Tecla, El Salvador, UNU-GTP, SC-17, 16 pp.
- Stewart, G., (2011): *Well test design and analysis*. PennWell Corporation., Tulsa, Oklahoma, USA, 1545 pp.
- Tryggvason, H., Steingrímsson, B., and Egilson. P., (2018): *Monitoring logging in Hverahlid. – Annual report*. Iceland GeoSurvey, report ISOR-2018/077. .
- VSO, (2007): *Bitruvirkjun, allt að 135 MWe Jarðvarmavirkjun*. Frummatsskýrsla. VSO for OR.
- VSO, (2007): *Hverahlidavirkjun, allt að 90 MWe Jarðvarmavirkjun*. Frummatsskýrsla. VSO for OR.

Appendix A

Tables 25-27 contain the discharge test step data and the overall estimates of the flow rate and enthalpy for wells HE-21, HE-36 and HE-53.

Table 25. Well HE-21.

Date	WHP	Lip-P	orifice	weir-H	m _w	m _s	m _t	H _t
12.12.2013	21.5	2.7	100	19	27.69	13.54	41.24	1512.55
18.12.2013	14.5	2.1	100	16.8	20.54	12.23	32.77	1598.09
28.12.2013	14.7	2	100	17.5	22.57	11.11	33.68	1515.12
4.1.2014	14.5	2.6	100	16.3	19.32	15.32	34.64	1730.12
10.1.2014	16.1	1.6	100	13	11.23	12.02	23.25	1872.98
14.1.2014	16.3	1.9	100	13.1	11.54	13.6	25.13	1918.76
20.1.2014	15.8	1.6	100	12.8	10.84	12.13	22.97	1893.83
29.1.2014	16	1.6	100	12.5	10.28	12.28	22.56	1925.12
2.2.2014	16	1.6	100	18.5	25.6	8.02	33.62	1340.54
13.2.2014	15.7	1.4	100	12.5	10.21	11.19	21.4	1884.36
14.2.2014	20.5	1	100	12.5	10.06	9	19.06	1787.27
15.2.2014	22.5	1.1	75	12.5	10.1	9.55	19.65	1813.8
17.2.2014	22.6	1.2	75	12.5	10.13	10.1	20.23	1838.73
19.2.2014	22.7	1.3	75	17.5	22.31	7.26	29.58	1354.04
21.2.2014	25	2.2	75	16.9	20.86	12.69	33.56	1607.71
23.2.2014	22.9	1.4	75	16.85	20.43	8.36	28.79	1439.82
25.2.2014	27	1.2	75	10	6.18	11.16	17.34	2114.55
27.2.2014	22.8	1.5	75	12.5	10.24	11.74	21.98	1905.3
28.2.2014	20	1.25	75	12.5	10.15	10.37	20.53	1850.64

1.3.2014	25	1.2	75	12.6	10.32	10.05	20.37	1827.66
3.3.2014	25	1.3	75	12.5	10.17	10.65	20.82	1862.21
5.3.2014	22.7	1.4	75	12.5	10.21	11.19	21.4	1884.36
8.3.2014	29.8	0.3	75	13.5	11.75	4.56	16.31	1418.74
10.3.2014	37.5	0.7	50	12	9.05	7.59	16.64	1756.26
14.3.2014	37.8	0.6	50	13.5	11.87	6.24	18.11	1543.6

Table 26 Well HE-36

Date	WHP	Lip-P	orifice	weir-H	m _w	m _s	m _t	H _t
13.3.2014	23.7	3.2	100	19.9	29.95	15.11	45.06	1545.6
15.3.2014	23.4	3.2	100	20	30.31	15.01	45.32	1535
17.3.2014	23	2.9	100	20	31.34	13.62	44.96	1485
19.3.2014	24	3.1	100	20	31.42	14.7	46.12	1510
20.3.2014	22.5	3	100	20	31.38	14.16	45.54	1479.0
22.3.2014	22	3	100	20	31.38	14.16	45.54	1479.0
23.3.2014	21.8	3	100	20	31.38	14.16	45.54	1479.0
25.3.2014	21.5	3.4	100	20	31.52	16.31	47.84	1536.5
26.3.2014	21.4	2.8	100	20	31.34	13.62	44.96	1463.7
27.3.2014	21	2.7	100	20	31.31	13.08	44.39	1447.9
30.3.2014	21	2.9	100	22	34.5	13.5	48	1340
1.4.2014	19.6	2.8	100	22	34.5	12.5	47	1330
5.4.2014	20.2	2.8	100	20	32	13.5	45	1457
10.4.2014	25	1.8	75	19	27.4	9.19	36.59	1394.7
14.4.2014	27	1.9	75	12.5	10.35	13.37	23.72	2050
15.4.2014	16	4	75	12.5	8	4	12	2280
20.4.2014	14	3	125	21	35.24	13.07	48.31	1431.6

26.4.2014	15	3.2	125	20	35.31	14.15	49.46	1478.3
28.4.2014	15	3.2	125	20	32.17	14.49	46.55	1479.8
30.4.2014	15	2.8	125	21	32.09	13.41	45.5	1401.2
12.5.2014	15	4	125	21	32.5	13.5	46	1398
14.5.2014	19.8	2.8	100	20	29	18	47	1600

Table 27 Well HE-53

Date	WHP	Lip-P	orifice	weir-H	m _w	m _s	m _t	H _t
20.1.2014	35	4.8	100	22.5	42.21	20.93	63.14	1518.4
21.1.2014	33	4.5	100	22.5	42.1	19.34	61.44	1486.3
29.1.2014	33	4.8	100	23.9	48.7	19.1	67.81	1423.2
2.2.2014	33.1	5	100	20	32.09	24.82	56.92	1718.2
6.2.2014	34.1	4.3	100	18	24.95	23.01	47.97	1801.7
10.2.2014	34	4.5	100	19	25.02	24.07	49.09	1821.8
12.2.2014	24.3	2.8	125	16	19.44	29.49	48.93	2036.6
13.2.2014	24.2	2.9	125	18.3	26.31	28.52	54.82	1878.9
14.2.2014	23.9	3.2	125	17	22.46	32.17	54.63	2010.1
18.2.2014	24.4	2.7	125	16	19.38	28.63	48.02	2024.4
20.2.2014	24.2	2.9	125	16.6	21.14	29.91	51.05	2004.4
21.2.2014	24.2	2.7	125	16.6	21.03	28.19	49.22	1979.4
25.2.2014	25.1	2.9	125	17.5	23.78	29.2	52.98	1938.0
26.2.2014	25.1	2.9	125	14.8	16.48	31.15	47.63	2134.8
27.2.2014	25.1	2.8	125	14.8	16.48	31.15	47.63	2134.8
28.2.2014	65	0.7	50	15.9	17.95	11.24	29.19	1620.8
28.2.2014	62	0.7	50	15.8	17.69	11.32	29	1630.4
1.3.2014	62	0.8	50	17	21.06	11.28	32.35	1551.4

5.3.2014	62	1	50	17	21.12	12.17	33.3	1583.5
7.3.2014	63	1	50	13	11.93	16.49	28.42	1993.6
8.3.2014	62	0.8	50	15	15.73	12.76	28.49	1740.7
12.3.2014	62.5	1.9	50	18	24.76	20.13	44.89	1741.8
14.3.2014	60	1.8	50	18	24.7	19.26	43.96	1722.0
18.3.2014	49	1.9	75	17.2	22.3	20.8	43.11	1807.1
20.3.2014	48	1.9	75	17.4	22.9	20.64	43.54	1790.7
21.3.2014	48	1.8	75	19.5	29.77	17.86	47.63	1601.3
25.3.2014	49.7	2	75	19.5	28.89	19.6	49.49	1641.8
26.3.2014	49.7	2	75	18.2	25.46	20.83	46.29	1744.7
1.4.2014	50.8	1.9	75	17.5	23.2	20.56	43.76	1782.5